DEVELOPMENT, VALIDATION, AND USE OF A SEMI-QUANTITATIVE HISTOPATHOLOGIC SCORING SYSTEM FOR ASSESSMENT OF PULMONARY PATHOLOGY IN RHESUS MACAQUES EXPERIMENTALLY INFECTED WITH *MYCOBACTERIUM TUBERCULOSIS*

AN ABSTRACT

SUBMITTED ON THE NINTH DAY OF NOVEMBER, 2018

TO THE GRADUATE PROGRAM IN BIOMEDICAL SCIENCES

IN PARTIAL FULFILLMENT OF THE REQUIREMENTS

OF THE SCHOOL OF MEDICINE OF TULANE UNIVERSITY

FOR THE DEGREE OF DOCTOR OF PHILOSOPHY BY:

Denae N. LoBato

APPROVED:

Deepak Kaushal, Ph.D.

Robert Blair, Ph.D.

Smriti Mehra, Ph.D.

Chad Roy, Ph.D.

Ronald Veazey, Ph.D.

ABSTRACT

Mycobacterium tuberculosis (*Mtb*) remains the single largest infectious disease killer of man worldwide. The non-human primate (NHP) model, including the Indian Rhesus macaque, is particularly valuable for the study of this disease because they fully recapitulate the pathological and immunological responses, can be co-infected with Simian Immunodeficiency Virus to model lentivirus synergism, and provide ideal candidates to study novel vaccine and drug development. However, while much has been elucidated over the past centuries in regards to host immunity, bacterial responses, and granuloma formation, little remains known about histomorphologic differences between active tuberculosis (ATBI) and latent tuberculosis (ATBI) disease states. Differentiation between these disease states, in humans or in NHPs, is based on clinical parameters, and there are currently no established methods for detecting morphologic differences between these conditions at the microscopic level. The aim of this study was to develop and validate a novel approach for assessment of pulmonary pathology in Rhesus macaques experimentally-infected with *M. tuberculosis* alone or in the setting of SIV co-infection. Archival lung samples from experimentally-infected macaques were assessed by blinded pathologists to determine differences in a series of pathological parameters based on previous experiments. Interobserver agreement and repeatability was good between pathologists. Significant differences were observed in several pathology categories, with ATBI animals having a greater likelihood of increased alveolar macropahges, type II pneumocyte hyperplasia,

perivasculitis, vasculitis/lymphangitis, and consolidation in comparison to LTBI animals. SIV co-infection increased the likelihood of perivasculitis and lymphangitis/vasculitis in both ATBI and LTBI animals. SIV co-infection also increased alveolar macrophages and type II pneumocyte hyperplasia in LTBI animals. Immunofluorescence was used to confirm the presence of *Mtb* bacilli within the perivascular inflammation. A similar grading system approach was used in 2 additional studies examining reactivation of ATBI in the setting of SIV coinfection unrelated to CD4+ T cell depletion and to evaluate pulmonary pathology changes in the setting of the use of an attenuated vaccine in SIV co-infected animals with similarly significant results. This grading scheme provides a valuable and desperately needed adjunctive assessment tool for evaluation of pulmonary pathology changes in the NHP model of pulmonary tuberculosis.

DEVELOPMENT, VALIDATION, AND USE OF A SEMI-QUANTITATIVE HISTOPATHOLOGIC SCORING SYSTEM FOR ASSESSMENT OF PULMONARY PATHOLOGY IN RHESUS MACAQUES EXPERIMENTALLY INFECTED WITH *MYCOBACTERIUM TUBERCULOSIS*

A DISSERTATION

SUBMITTED ON THE NINTH DAY OF NOVEMBER, 2018

TO THE GRADUATE PROGRAM IN BIOMEDICAL SCIENCES

IN PARTIAL FULFILLMENT OF THE REQUIREMENTS

OF THE SCHOOL OF MEDICINE OF TULANE UNIVERSITY

FOR THE DEGREE OF DOCTOR OF PHILOSOPHY BY:

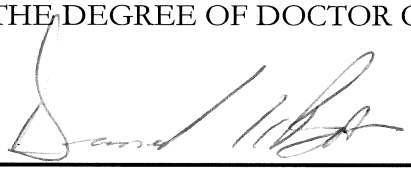

Denae N. LoBato

APPROVED:

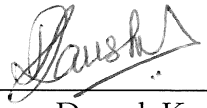

Deepak Kaushal, Ph.D.

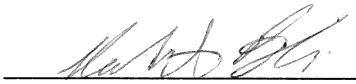

Robert Blair, Ph.D.

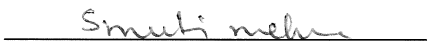

Smriti Mehra, Ph.D.

Chad Roy, Ph.D.

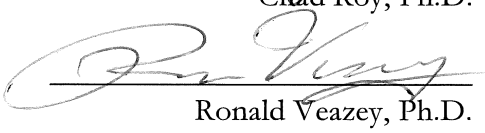

Ronald Veazey, Ph.D.

ACKNOWLEDGEMENTS

My list of individuals, like many who have come before me, is long, and will invariably be incomplete.

I would first like to thank the NIH T32 program, and the coordinators of this fellowship at the TNPRC and within the Tulane BMS department for supporting this program. I believe that it provides a valuable service in support of research training for veterinarians, like myself, who could not have afforded the time or financial sacrifice necessary to pursue graduate research training in a more traditional setting despite a longstanding desire to do so. I think that our training and backgrounds do offer a unique perspective that, if supported, could lead to significant advances in biomedical research; thank you for believing that too.

In that vein, I want to express my utmost gratitude to Dr. Andrew Lackner, who is the man who brought me to the Tulane Primate Center. His mentorship, guidance, and approach to research, leadership, pathology, and life really inspired me and will never be forgotten, despite the unfortunately short time I got to spend with him. I continue to miss him. Thank you, Andrew, for everything.

Thank you to Dr. Deepak Kaushal for offering me a number of fantastic opportunities to use my training in pathology to contribute in real and meaningful ways to ask my own questions to advance the study of primate TB. You have made me a better scientist, and have allowed me the flexibility to do so unconventionally in order to meet the

professional demands before me. Thank you for working with me to turn out a project we can both, I hope, be proud of. I have learned so much from our time together, and I wish you the best in your future endeavors.

Thank you to all the members of my committee for their flexibility, too, in accommodating my need to finish my dissertation while working as a junior faculty member at a different institution. Your support means so much.

Thank you, thank you, thank you to Dr. Robert Blair. You have been my lifeline in so many ways throughout this process. You've been my pathology buddy, my scientific support, and have become one of my truly great friends. I love ya, man. And Dr. Mee Ja Sula. What I must owe you for scoring and re-scoring a million monkey TB slides. That's what you get for being nice to the third year resident.

Thank you to Nadia Golden for always keeping the ship running smoothly even in the stormiest of seas. And for tracking down samples and slides for me from afar. None of this would be possible without you. But you must know that. Thank you to Dr. Allison Buçsan. You made the sciencing much more fun. I'm so proud of you, and so happy to have worked with you. You are going to continue to do amazing things, and I want to know all about it.

I must mention Dr. Becky Smith whose truly excellent statistical support made all of our hard work mean something tangible. Your encouragement kept me going.

Thank you to my mentors, past and present, for encouraging me along this path—from Dr. Morgan Wilson and Dr. Renee Godard at Hollins University who first encouraged me to pursue research and showed me how much I would love it; to Dr. Ben Brainard, the beloved and late Dr. Steeve Giguiere, Dr. Buffy Howerth, and Dr. David Hurley who I

worked with at UGA; Dr. Linden Craig, Dr. Bob Donnell, and Dr. Kim Newkirk at UT for encouraging me to pursue this PhD—and especially Kim for making me finish it, whatever it took. May I have a similar impact on my students, for what a legacy that would be.

Many thanks to my coworkers at UofI, especially my director, Dr. Rick Fredrickson, for giving me support to finish this even while working full-time. Hopefully I'll be better rested now.

But mostly, thank you to Darrel Hale for standing by my side through what has been an incredibly tumultuous ride. Who knew when you said you wanted someone with a graduate degree you'd be signing up for someone who'd have to finish a residency, study for boards, do a PhD, write and defend a dissertation, and start a faculty position. Worth it? I sure hope so. Love you, dear. And finally, to my mom, Denise Morris. I love you, and I promise I'm *finally* done with school.

For a while at least.

TABLE OF CONTENTS

CHAPTER 1: INTRODUCTION

Despite advances in antibiotic therapy and epidemiological control since Robert Koch first identified *Mycobacterium tuberculosis* (*Mtb*) as the causative agent of tuberculosis (TB) in the 1800's, *Mtb* continues to be responsible for the largest number of human deaths from a single infectious agent worldwide (Brosch et al., 2002; WHO, 2017). Tuberculosis is typically classified into 1 of 2 clinical states: 1. Latent tuberculosis (LTBI), during which the bacilli are not actively replicating, the host immune system maintains the disease in a quiescent state, and the disease is not considered transmissible, or 2. Active tuberculosis (ATBI) when bacilli are actively replicating and disseminating, have evaded host immune control, and can be transmitted to others(Kaushal et al., 2012; Sakamoto, 2012; Scanga and Flynn, 2014). At some point, however, we know that the distinction between these two clinical states exists along a spectrum, and when that transition from latent disease to active disease occurs from a pathophysiologic and immunologic standpoint remains poorly understood. While individuals latently infected with TB generally have a low risk of progression from LTBI to ATBI, several factors can increase risk of progression. Notably, infection with the lentivirus Human immunodeficiency virus (HIV)—the retrovirus responsible for progression to Acquired Immunodeficiency Syndrome (AIDS) in humans, increases the risk for progression from LTBI to ATBI from 5-10% over the course of an infected individual's lifetime to 5-15% over the course of a year (Aaron et al., 2004; Pawlowski et al., 2012). Additional factors such as diabetes mellitus, smoking, intravenous

drug use, and alcohol use have also been shown to increase risk of Mtb infection and disease progression (Altet-Gómez et al., 2005; Boon et al., 2005; Davies et al., 2006; van Crevel and Dockrell, 2014; Deiss et al., 2009; Dooley and Chaisson, 2009; Imtiaz et al., 2017; Lönnroth et al., 2014; The Lancet Diabetes & Endocrinology, 2014).

Since the beginning of biomedical research in this area, animal models have been used to study TB in the hope of being able to better understand and intervene in this disease process. Several animal models have been used over time, with the most commonly used animal models today including the mouse, guinea pig, rabbit, zebrafish, and macaque. The non-human primate (NHP) model remains the gold-standard animal model for translational studies of TB, and offers several unique advantages over other commonly used animal models including mice, guinea pigs, rabbits, and zebrafish. Rhesus macaques (*Macaca mulatta*) and Cynomolgus macaques (*Macaca fasicularis*) are currently the most commonly used NHP in translational studies of TB(Altet-Gómez et al., 2005; Davies et al., 2006; Foreman et al., 2017). These two old world primate species are particularly valuable in the study of TB for several reasons. For one, they fully recapitulate the spectrum of clinical and pathological disease observed in human TB. This includes the development of naturally occurring latent and active disease states with similar rates of reactivation, the formation of true well-structured caseous granulomas as seen in humans, and clinical changes indicative of ATBI as seen in humans including elevated serum C reactive protein, dyspnea, pyrexia, anorexia and cachexia, presence of pulmonary inflammation on thoracic radiographs, presence of acid fast bacilli within sputum samples, and positive PPD and IGRA responses following infection (Foreman et al., 2017a; Kaushal et al., 2012; Mehra et al., 2013). The patterns of pathology seen in mice, guinea pigs, rabbits, and zebra fish differ from those seen in both humans and macaques with TB (Palmer, 2018; Sakamoto, 2012). The most commonly used laboratory

mouse strains infected with *Mtb* generally display poorly organized lymphohistiocytic inflammation; the Kramnik or C3HeB/FeJ mouse has been useful for the study of *Mtb* infection because unlike most strains (i.e. C57/BL6 mice), they will develop necrotic granulomas, though these granulomas still differ from those seen in NHP and humans, and their relative resistance requires high infecting dosages of *Mtb* to be administered for infection (Driver et al., 2012; Kramnik and Beamer, 2016). Guinea pigs have been valuable animal models for the study of aerosol infection for several decades. Unlike the mouse model of TB, guinea pigs are exquisitely sensitive to infection with *Mtb*, and are in fact more susceptible to infection than any other animal model, including macaques (and humans) (Clark et al., 2015; Smith and Harding, 1977). This enhanced susceptibility can hamper application of certain results to human medicine. While guinea pigs do form necrotizing granulomas, they fail to form granulomas that undergo cavitation as is sometimes seen in human and NHP TB (Basaraba, 2008; Basaraba et al., 2006; Palanisamy et al., 2008; Smith and Harding, 1977; Turner et al., 2003). Additionally, the primary method of *Mtb* spread in Guinea pigs is via the hematogenous, rather than aerogenous route, which makes translation to human medicine difficult. Furthermore, their granulocytic response consists of heterophils, rather than neutrophils as in humans and NHPs, and there is controversy over whether or not these heterophils produce myeloperoxidase (as do human neutrophils) though previous studies have demonstrated an ability of these heterophils to have antifungal activity agains *Candida* spp. (Lehrer et al., 1975). Rabbits have also been used as a model for *Mtb* infection, because unlike mice or Guinea pigs, they do form true cavitating granulomas, and can be used as an excellent model of latent infection and of meningeal tuberculosis (Arthur M. Dannenberg, 1994; Manabe et al., 2008; O'Toole, 2010). However, they are the most resistant of the conventional laboratory species, and outbred laboratory rabbits can

often naturally clear *Mtb* infection within 4-6 months of infection without additional treatment, unlike humans (Arthur M. Dannenberg, 1994; Manabe et al., 2008, 2008). Furthermore, rabbits possess heterophils rather than neutrophils, like Guinea pigs, and the same debate over whether or not these heterophils produce myeloperoxidase and thus have similar oxidative activity to human neutrophils, which play a major role in immune responses to tuberculosis, remains (Lehrer et al., 1975). Zebrafish have recently emerged as a useful non-mammalian laboratory species for the study of mycobacterial diseases, and much useful information has been gained through their use in regards to these conditions. However, in this animal model, *Mycobacterium marinum* must be the infecting bacterium, which differs in many respects from *Mycobacterium tuberculosis*. The nature of their aquatic environment changes the parameters of the infecting condition, altering the infection from one of a primary aerogenous spread, to one of primary environmental contamination and hematogenosu spread. Mycobacterial diseases in fish, as well as in amphibians, tend to be rapidly progressive diseases characterized by numerous bacterial organisms, unlike the relatively paucibacillary, slowly progressive diseases they cause in mammals(Palmer, 2018). By virtue of the fact that fish do not, in fact have lungs, it inhibits their use as an animal model for the study of a primary pulmonary disease, though they still provide truly valuable animal models for gaining better understanding of what is happening at the level of the pathogen and host immune response. Indeed, there has been much truly excellent work elucidating mechanisms involved at the intersection of bacterial and granuloma responses that has emerged from their use (van Crevel and Dockrell, 2014; Cronan and Tobin, 2014; van Leeuwen et al., 2015) Conversely, NHPs demonstrate a susceptibility to infection similar to humans, and display the full spectrum of granuloma subtypes seen in human disease,

including solid type granulomas, caseating and neutrophilic granulomas (with hypoxic centers and sometimes central mineralization), and cavitating granulomas .

Additionally, because macaques are so evolutionarily similar to humans, their immunological responses closely mirror those seen in humans with TB, and many of the reagents developed to assay human immunological responses work in these species (Gardner and Luciw, 2008). Their similar physiology and relatively large size makes them superior candidates for the testing of novel drug, treatment, and vaccine strategies that may have applications to human medicine, in comparison to other animal models. Unlike mice, which are relatively resistant to infection with *Mtb*, macaques demonstrate a susceptibility to infection similar to humans (Basaraba, 2008; Foreman et al., 2017a; Gardner and Luciw, 2008; Kaushal et al., 2012; O'Toole, 2010). Different species of NHPs display varying susceptibilities to the disease, which may complicate translation of findings to humans. There is a difference in disease susceptibility between Rhesus and Cynomolgus macaques, which makes them valuable models for studying varying outcomes of natural infection in humans (Gardner and Luciw, 2008; Kaushal et al., 2012). Cynomolgous macaques are relatively more resistant to the disease than Indian Rhesus macaques, and at low infectious doses of *Mtb*, Rhesus macaques tend to show more susceptibility to infection with more rapid disease progression than Cynomologus macaques (Sharpe et al., 2016). Thus, it may be necessary to compare these two models to study both early or rapidly progressing tuberculosis versus the host's response to longer-term infection. Both macaque species, however, have been shown to develop true latent TB infection which can be reactivated either naturally or with the use of SIV co-infection (Foreman et al., 2016; Mehra et al., 2011). Thus, macaques ultimately provide a superior animal model for the study of human TB in several important ways: 1. They fully recapitulate the spectrum of gross and histopathologic

lesions seen in human disease, 1. They can be co-infected with Simian Immunodeficiency Virus (SIV) as an analogue for HIV co-infection, and 3. They naturally develop LTBI and will spontaneously reactivate to ATBI at similar rates to that seen in humans (Capuano et al., 2003; Gardner and Luciw, 2008; Scanga and Flynn, 2014).

However, despite significant advancements in the understanding of TB from numerous scientific approaches—including advanced imaging, the use of ever-sophisticated immunologic assays, and the advent of molecular techniques that have elucidated activities at the genetic level of both the host and bacterium—much of our understanding of the pathologic differences between disease states in tuberculosis remains unknown, and inhibits our ability to best diagnose these conditions and intervene when the bacteria may be most susceptible to treatment. ATBI and LTBI are still distinguished on the basis of clinical parameters. In humans, LTBI is most often presumptively diagnosed on the basis of a positive tuberculin skin test (TST) and/or positive interferon gamma release assay (IGRA)—both of which are methods of assessing a delayed type IV hypersensitivity reaction to previous *Mtb* infection—in the absence of current clinical symptoms of ATBI infection.(LoBue and Mermin, 2017). Diagnosis of ATBI is generally based on the presence of positive TST and/or IGRA in addition to clinical symptoms or signs of infection generally including the presence of acid fast bacilli within sputum or gastric aspirates (then confirmed with positive culture as the gold standard), sustained elevated serum C-reactive protein levels above values shown to be correlated with ATBI, hyperthermia, weight loss and inappetance, positive *Mtb* specific IFN-gamma in peripheral blood mononuclear cells, positive agar gel immundiffusion testing, coughing, dyspnea, and the presence of pulmonary granulomas on thoracic radiographs (Mayo Clinic, 2017; Kaushal et al., 2012; Lin et al., 2009a; Scanga and Flynn, 2014). Recent studies have been investigating the validity of

looking for components of the Mycobacterial wall or specific associated cytokines associated with infection to be used as more sensitive biomarkers to support a more rapid diagnosis of infection to prevent the need to wait for culture confirmation; however, even if these tests can be validated, they still will not help to differentiate between ATBI and LTBI. Previous studies have shown the ability to detect overall differences in gross pathology as a total score at necropsy in ATBI and LTBI infected cynomolgous macaques (Lin et al., 2009a). The use of advanced imaging, including MRI and PET CT has also been used to attempt to determine disease burden and classify disease status with some success (Sharpe et al., 2009). However, these methods typically rely on macroscopically visible lesions, and no reports have been able to definitively distinguish between ATBI and LTBI histologically (Lin et al., 2009, Sharpe et al., 2009).

The histopathologic hallmark of TB has long been considered the formation of caseous granulomas, most commonly within the lungs, though other tissues can be similarly affected in cases of disseminated TB. These granulomas are characterized by a central coagulum of caseous necrosis with neutrophilic infiltration (in which the highest concentration of acid fast bacilli will be observed), surrounded by concentric layers of epithelioid macrophages and Langhans-type multinucleated giant cells, surrounded in turn by concentric layers of lymphocytes, plasma cells, and fibrosis (Kumar et al., 2015; Martinot, 2018; Sakamoto, 2012). Historically, much of the focus in TB-related pathology has been on the granuloma itself. Recently, many of the molecular, cellular, and immunological mechanisms involved at the granuloma level have become better elucidated. The formation of tuberculous granulomas begins with the inhalation of *Mtb* bacilli with subsequent engulfment by and replication within macrophages. The bacilli facilitate phagocytic engulfment via receptors present on the macrophages, including CR3 and mannose binding

lectin (Palmer, 2018; Kumar et al., 2015). Following phagocytosis, *Mtb* inhibits phagosome-lysosome fusion, and undergoes replication within the phagocytic vesicle. Infected macrophages can rupture, leading to infection of adjacent alveolar macrophages, and spread to additional sites within the lungs as well as dissemination to other organs. Immunity to *Mtb* and formation of the granuloma is primarily mediated through a delayed T_H1 response (Sakamoto, 2012; Kumar et al., 2015). This T_H1 response, mediated by T-helper cells and IL-12 from dendritic cells, is mounted approximately 3 weeks post-infection and activates IFN-γ production resulting in bactericidal activity within macrophages that enables them to contain the *Mtb* bacilli (Palmer, 2018). IFN-γ has numerous key roles in the TB granuloma, including the production of inducible nitric oxide synthase and subsequently nitric oxide (NO), which becomes crucial for bacterial killing within the granuloma. The T_H1 response also directly stimulates the formation of the caseous granuloma in TB (Martinot, 2018; Mehra et al., 2011; Sakamoto, 2012; Kumar et al., 2015). IFN-γ stimulates macrophage transition to the epithelioid phenotype. Recent work has demonstrated that these macrophages express E-cadherin, an intercellular adhesion molecule most commonly expressed on epithelial cells; it is currently thought that expression of this molecule by epithelioid macrophages in the TB granuloma may help to more effectively "wall-off" the central caseum and *Mtb* bacilli (Cronan and Tobin, 2014; van Leeuwen et al., 2015). Tryptophan expression has also been shown to play crucial roles in TB granuloma organization and structure. Expression of the enzyme indoleamine 2,3-dioxygenase (IDO), which is induced by *Mtb*, catabolizes tryptophan and may prevent lymphocytes from reaching the center of the granuloma to participate in bacterial killing (Gautam et al., 2018).

However, both LTBI and ATBI animals will show a spectrum of granulomas that do not allow distinction between disease states based on these changes alone (Foreman et al., 2016; Lin et al., 2009; Capuano et al., 2003). From the bacterial standpoint, our previous work has demonstrated significant overlap in *Mtb* bacterial gene expression in granulomas dissected from Rhesus macaques with ATBI and LTBI, supporting the notion that these clinical conditions exist along a spectrum (Hudock et al. 2017). A previous study by Lin et al. (2009) in cynomolgus macaques had suggested that the type of granuloma may be associated with disease progression. In this study, it was determined that classic caseous granulomas could be equally found in both LTBI and ATBI macaques, and that solid type granulomas—composed of central aggregates of epithelioid macrophages and multinucleated giant cells with little to no visible necrosis–conversely, were found in greater numbers in ATBI macaques, indicating that they may be associated with poor immune control; fibrotic granulomas—with replacement of the central caseum by fibrous connective tissue—were identified in both ATBI and LTBI (Lin et al., 2009). However, much of the challenge with classifying granuloma type depends on histological section, as the three dimensional nature of granulomas can result in granulomas that may initially appear as solid at one plane of section, but that may display evidence of caseous necrosis on deeper recuts (personal observation). While recent work has elucidated many of the mechanisms involved in the structure and function of the granuloma in TB, little remains known about additional changes and progression of disease both within the lung itself and throughout the body (Martinot, 2018; Palmer, 2018). Little attention has been paid to changes outside of the granuloma in lungs from non-human primates infected with TB.

Additionally, while synergism between lentivirus infection (including HIV and SIV) and *Mtb* has been well described, (Aaron et al., 2004; Foreman et al., 2016; Pawlowski et al.,

2012) many of the mechanisms of that synergism remain largely unknown. While initial work had suggested that peripheral T-cell depletion was responsible for reactivation of TB in SIV-infected macaques, recent advances in the study of *Mtb* infection in Rhesus macaques have shown that CD4+ T-cell depletion is not the primary factor contributing to disease progression in macaques co-infected with SIV (Diedrich et al., 2010). Rather, it appears that B-cells and CD8+ T-cells may play a more prominent role in TB control than has traditionally been thought (Diedrich and Flynn, 2011; Foreman et al., 2016). Additional studies have demonstrated that SIV infection alters cytokine expression by the T_H1 response—namely downregulating IFN-gamma and IL-22 expression—which may facilitate *Mtb* infection (Guo et al., 2017). However, despite much of the advancement in our immunological understanding of SIV and *Mtb* co-infection, histopathological differences that may be associated with and contribute to that synergism have not been well-characterized.

The emergence of multi-drug resistant and extremely-drug resistant strains of *Mtb*, coupled with the lack of a safe and effective vaccine increases the urgency to better understand the pathogenesis of this disease, particularly in the setting of co-infection, and to develop interventional strategies. The currently used Bacillus Calmette Guérin (BCG) vaccine, is a live attenuated vaccine derived from *Mycobacterium bovis*, and has been used for prevention of *Mycobacterium tuberculosis* in TB-endemic areas since the 1920's (Luca and Mihaescu, 2013). While this controversial vaccine confers variable degrees of protection, it remains the only available vaccine on the market, and is still routinely given to infants primarily to prevent meningeal tuberculosis in that age group. However, there are frequent concerns that it may be unsafe in immunocompromised individuals, and its short duration and incomplete protection put susceptible individuals at risk of infection later in life if not boostered. While there are varying rates of protection reported, estimates range anywhere

from 80% protection to 0% (ACET 1998; Clark and Cameron, 2006; Luca and Mihaescu, 2013). Because of the frequent overlap of HIV prevalence in areas with greatest *Mtb* prevalence, there is a particular need for an effective vaccine that will be safe and effective in all groups, including in immunocompromised individuals. Current work has focused on the development and use of attenuated strains of *Mycobacterium tuberculosis* that may prove viable alternatives to BCG vaccination (Larsen et al., 2009). Some of the most promising candidates for these novel vaccine candidates include *Mtb* strains with mutations either in the stress response factor sigmaH (Dutta et al., 2012; Mehra et al., 2012) or in the DosR regulon which is important in controlling the response of *Mtb* to hypoxia, one of the critical stress factors the bacilli face within the granuloma (Leistikow et al., 2010; Mehra et al., 2015). Previous work with *Mtb*ΔsigH in NHP has demonstrated that animals inoculated with the attenuated strain of bacteria demonstrated significantly lower bacterial burden and longer survival times—surviving to the end of the study—whereas animals infected with wild strains succumbed to disease and developed high bacterial burdens (Mehra et al., 2012). Additional work comparing wild type *Mtb* to *Mtb*ΔsigH showed that sigH affects chemokine activity, and suggests that sigH is responsible for modulating crucial interactions between the bacilli and host phagocytes that may lead to persistence of bacilli within the host (Dutta et al., 2012). Vaccination with *Mtb* strains with mutations in the DosR regulon similarly failed to produce disease or persist in the host, but still elicited an adaptive immune response suggesting they could be a good vaccine candidate (Leistikow et al., 2010; Mehra et al., 2015). By targeting these facets of the bacilli, more effective and safer vaccines may be developed that may help to reduce the global TB burden. However, strategies must be established to evaluate pulmonary changes in response to vaccination to ensure that disease is not resulting from the use of these attenuated live vaccines.

Recent papers have emphasized a growing need for a multimodal approach to translational research that incorporates trained pathologists performing gross and microscopic pathology, particularly in the context of evaluating pulmonary inflammation (Meyerholz et al., 2018). Scoring systems are widely used in both human and veterinary pathology to allow for standardization and repeatability of assessment between pathologists; to be of most value, these systems must meet robust criteria (Cross, 1998; Gibson-Corley et al., 2013; Klopfleisch, 2013). There is a need for standardization in approaches to pulmonary pathology in the macaque model of TB, and for development of a repeatable, discriminating scoring system for pulmonary pathology that may help to elucidate subtle differences between ATBI and LTBI both in and in the absence of SIV coinfection with an aim to gain more comprehensive understanding of factors related to disease progression and retrovirus synergism to be used in conjunction with other approaches to TB and SIV research.

REFERENCES

Aaron, L., Saadoun, D., Calatroni, I., Launay, O., Mémain, N., Vincent, V., Marchal, G., Dupont, B., Bouchaud, O., Valeyre, D., et al. (2004). Tuberculosis in HIV-infected patients: a comprehensive review. Clin. Microbiol. Infect. *10*, 388–398.

Altet-Gómez, M.N., Alcaide, J., Godoy, P., Romero, M.A., and Hernández del Rey, I. (2005). Clinical and epidemiological aspects of smoking and tuberculosis: a study of 13038 cases.

Arthur M. Dannenberg, J. (1994). Rabbit Model of Tuberculosis. Tuberculosis 149–156.

Barberis, I., Bragazzi, N.L., Galluzzo, L., and Martini, M. (2017). The history of tuberculosis: from the first historical records to the isolation of Koch's bacillus. J. Prev. Med. Hyg. 58, E9–E12.

Basaraba, R.J. (2008). Experimental tuberculosis: the role of comparative pathology in the discovery of improved tuberculosis treatment strategies. Tuberculosis *88*, S35–S47.

Basaraba, R.J., Dailey, D.D., McFarland, C.T., Shanley, C.A., Smith, E.E., McMurray, D.N., and Orme, I.M. (2006). Lymphadenitis as a major element of disease in the guinea pig model of tuberculosis. Tuberculosis *86*, 386–394.

Boon, S. den, Lill, S.W.P. van, Borgdorff, M.W., Verver, S., Bateman, E.D., Lombard, C.J., Enarson, D.A., and Beyers, N. (2005). Association between smoking and tuberculosis infection: a population survey in a high tuberculosis incidence area. Thorax *60*, 555–557.

Brosch, R., Gordon, S.V., Marmiesse, M., Brodin, P., Buchrieser, C., Eiglmeier, K., Garnier, T., Gutierrez, C., Hewinson, G., Kremer, K., et al. (2002). A new evolutionary scenario for the *Mycobacterium tuberculosis* complex. Proc. Natl. Acad. Sci. *99*, 3684–3689.

Capuano, S.V., Croix, D.A., Pawar, S., Zinovik, A., Myers, A., Lin, P.L., Bissel, S., Fuhrman, C., Klein, E., and Flynn, J.L. (2003). Experimental Mycobacterium tuberculosis Infection of Cynomolgus Macaques Closely Resembles the Various Manifestations of Human M. tuberculosis Infection. Infect. Immun. *71*, 5831–5844.

Centers for Disease Control and Prevention (CDC) (2009). Plan to combat extensively drug-resistant tuberculosis: recommendations of the Federal Tuberculosis Task Force. MMWR Recomm. Rep. Morb. Mortal. Wkly. Rep. Recomm. Rep. 58, 1–43.

Chiavolini, D., Rangel-Moreno, J., Berg, G., Christian, K., Oliveira-Nascimento, L., Weir, S., Alroy, J., Randall, T.D., and Wetzler, L.M. (2010). Bronchus-associated lymphoid tissue (BALT) and survival in a vaccine mouse model of tularemia. PloS One 5, e11156.

Cieszanowski, A., Lisowska, A., Dabrowska, M., Korczynski, P., Zukowska, M., Grudzinski, I.P., Pacho, R., Rowinski, O., and Krenke, R. (2016). MR Imaging of Pulmonary Nodules: Detection Rate and Accuracy of Size Estimation in Comparison to Computed Tomography. PLoS ONE *11*.

Clark, M., and Cameron, D.W. (2006). The benefits and risks of bacille Calmette-Guérin vaccination among infants at high risk for both tuberculosis and severe combined immunodeficiency: assessment by Markov model. BMC Pediatr. *6*, 5.

Clark, S., Hall, Y., and Williams, A. (2015). Animal Models of Tuberculosis: Guinea Pigs. Cold Spring Harb. Perspect. Med. *5*.

van Crevel, R., and Dockrell, H.M. (2014). TANDEM: understanding diabetes and tuberculosis. Lancet Diabetes Endocrinol. *2*, 270–272.

Cronan, M.R., and Tobin, D.M. (2014). Fit for consumption: zebrafish as a model for tuberculosis. Dis. Model. Mech. *7*, 777–784.
Cross, S.S. (1998). Grading and scoring in histopathology. Histopathology *33*, 99–106.

Davies, P.D.O., Yew, W.W., Ganguly, D., Davidow, A.L., Reichman, L.B., Dheda, K., and Rook, G.A. (2006). Smoking and tuberculosis: the epidemiological association and immunopathogenesis. Trans. R. Soc. Trop. Med. Hyg. *100*, 291–298.

Davies, P.D.O., Yew, W.W., Ganguly, D., Davidow, A.L., Reichman, L.B., Dheda, K., and Rook, G.A. (2006). Smoking and tuberculosis: the epidemiological association and immunopathogenesis. Trans. R. Soc. Trop. Med. Hyg. *100*, 291–298.

Dheda, K., Gumbo, T., Gandhi, N.R., Murray, M., Theron, G., Udwadia, Z., Migliori, G.B., and Warren, R. (2014). Global control of tuberculosis: from extensively drug-resistant to untreatable tuberculosis. Lancet Respir. Med. *2*, 321–338.

Diedrich, C.R., and Flynn, J.L. (2011). HIV-1/Mycobacterium tuberculosis Coinfection Immunology: How Does HIV-1 Exacerbate Tuberculosis? Infect. Immun. *79*, 1407–1417.

Diedrich, C.R., Mattila, J.T., Klein, E., Janssen, C., Phuah, J., Sturgeon, T.J., Montelaro, R.C., Lin, P.L., and Flynn, J.L. (2010). Reactivation of Latent Tuberculosis in Cynomolgus Macaques Infected with SIV Is Associated with Early Peripheral T Cell Depletion and Not Virus Load. PLoS ONE *5*, e9611.

Driver, E.R., Ryan, G.J., Hoff, D.R., Irwin, S.M., Basaraba, R.J., Kramnik, I., and Lenaerts, A.J. (2012). Evaluation of mouse model forming necrotic granulomas using C3HeB/FeJ mice, for the testing of M. tuberculosis drugs. Antimicrob. Agents Chemother. AAC.00217-12.
Dutta, N.K., Mehra, S., Martinez, A.N., Alvarez, X., Renner, N.A., Morici, L.A., Pahar, B., Maclean, A.G., Lackner, A.A., and Kaushal, D. (2012). The stress-response factor SigH modulates the interaction between Mycobacterium tuberculosis and host phagocytes. PloS One *7*, e28958.

Foreman, T.W., Mehra, S., LoBato, D.N., Malek, A., Alvarez, X., Golden, N.A., Bucşan, A.N., Didier, P.J., Doyle-Meyers, L.A., Russell-Lodrigue, K.E., et al. (2016). CD4 $^{+}$ T-cell–independent mechanisms suppress reactivation of latent tuberculosis in a macaque model of HIV coinfection. Proc. Natl. Acad. Sci. *113*, E5636–E5644.

Foreman, T.W., Mehra, S., Lackner, A.A., and Kaushal, D. (2017). Translational Research in the Nonhuman Primate Model of Tuberculosis. ILAR J. *58*, 151–159.

Gardner, M.B., and Luciw, P.A. (2008). Macaque Models of Human Infectious Disease. ILAR J. *49*, 220–255.

Gautam, U.S., Foreman, T.W., Bucsan, A.N., Veatch, A.V., Alvarez, X., Adekambi, T.,

Golden, N.A., Gentry, K.M., Doyle-Meyers, L.A., Russell-Lodrigue, K.E., et al. (2018). In vivo inhibition of tryptophan catabolism reorganizes the tuberculoma and augments immune-mediated control of Mycobacterium tuberculosis. Proc. Natl. Acad. Sci. *115*, E62–E71.

Gibson-Corley, K.N., Olivier, A.K., and Meyerholz, D.K. (2013). Principles for Valid Histopathologic Scoring in Research. Vet. Pathol. *50*, 1007–1015.

Gormus, B.J., Blanchard, J.L., Alvarez, X.H., and Didier, P.J. (2004). Evidence for a rhesus monkey model of asymptomatic tuberculosis. J. Med. Primatol. *33*, 134–145.

Guo, M., Xian, Q.-Y., Rao, Y., Zhang, J., Wang, Y., Huang, Z.-X., Wang, X., Bao, R., Zhou, L., Liu, J.-B., et al. (2017). SIV Infection Facilitates Mycobacterium tuberculosis Infection of Rhesus Macaques. Front. Microbiol. *7*.

Hudock, T.A., Foreman, T.W., Bandyopadhyay, N., Gautam, U.S., Veatch, A.V., LoBato, D.N., Gentry, K.M., Golden, N.A., Cavigli, A., Mueller, M., et al. (2017). Hypoxia Sensing and Persistence Genes Are Expressed during the Intragranulomatous Survival of Mycobacterium tuberculosis. Am. J. Respir. Cell Mol. Biol. *56*, 637–647.

Kaushal, D., Mehra, S., Didier, P.J., and Lackner, A.A. (2012). The non-human primate model of tuberculosis. J. Med. Primatol. *41*, 191–201.

Klopfleisch, R. (2013). Multiparametric and semiquantitative scoring systems for the evaluation of mouse model histopathology - a systematic review. BMC Vet. Res. *9*, 123.

Kramnik, I., and Beamer, G. (2016). Mouse models of human TB pathology: roles in the analysis of necrosis and the development of host-directed therapies. Semin. Immunopathol. *38*, 221–237.

Larsen, M.H., Biermann, K., Chen, B., Hsu, T., Sambandamurthy, V.K., Lackner, A.A., Aye, P.P., Didier, P., Huang, D., Shao, L., et al. (2009). Efficacy and safety of live attenuated persistent and rapidly cleared Mycobacterium tuberculosis vaccine candidates in non-human primates. Vaccine *27*, 4709–4717.

van Leeuwen, L.M., van der Sar, A.M., and Bitter, W. (2015). Animal Models of Tuberculosis: Zebrafish. Cold Spring Harb. Perspect. Med. *5*.

Leistikow, R.L., Morton, R.A., Bartek, I.L., Frimpong, I., Wagner, K., and Voskuil, M.I. (2010). The Mycobacterium tuberculosis DosR Regulon Assists in Metabolic Homeostasis and Enables Rapid Recovery from Nonrespiring Dormancy. J. Bacteriol. *192*, 1662–1670.

Lin, P.L., Rodgers, M., Smith, L., Bigbee, M., Myers, A., Bigbee, C., Chiosea, I., Capuano, S.V., Fuhrman, C., Klein, E., et al. (2009). Quantitative Comparison of Active and Latent Tuberculosis in the Cynomolgus Macaque Model. Infect. Immun. *77*, 4631–4642.

LoBue, P.A., and Mermin, J.H. (2017). Latent tuberculosis infection: the final frontier of tuberculosis elimination in the USA. Lancet Infect. Dis. *17*, e327–e333.

LUCA, S., and MIHAESCU, T. (2013). History of BCG Vaccine. Mædica *8*, 53–58.

Manabe, Y.C., Kesavan, A.K., Lopez-Molina, J., Hatem, C.L., Brooks, M., Fujiwara, R., Hochstein, K., Pitt, M.L.M., Tufariello, J., Chan, J., et al. (2008). The aerosol rabbit model of TB latency, reactivation and immune reconstitution inflammatory syndrome. Tuberculosis *88*, 187–196.

Martinot, A.J. (2018). Microbial Offense vs Host Defense: Who Controls the TB Granuloma? Vet. Pathol. *55*, 14–26.

Mehra, S., Golden, N.A., Dutta, N.K., Midkiff, C.C., Alvarez, X., Doyle, L.A., Asher, M., Russell-Lodrigue, K., Monjure, C., Roy, C.J., et al. (2011). Reactivation of latent tuberculosis in rhesus macaques by coinfection with simian immunodeficiency virus. J. Med. Primatol. *40*, 233–243.

Mehra, S., Golden, N.A., Stuckey, K., Didier, P.J., Doyle, L.A., Russell-Lodrigue, K.E., Sugimoto, C., Hasegawa, A., Sivasubramani, S.K., Roy, C.J., et al. (2012). The Mycobacterium tuberculosis stress response factor SigH is required for bacterial burden as well as immunopathology in primate lungs. J. Infect. Dis. *205*, 1203–1213.

Mehra, S., Alvarez, X., Didier, P.J., Doyle, L.A., Blanchard, J.L., Lackner, A.A., and Kaushal, D. (2013). Granuloma Correlates of Protection Against Tuberculosis and Mechanisms of Immune Modulation by Mycobacterium tuberculosis. J. Infect. Dis. *207*, 1115–1127.

Mehra, S., Foreman, T.W., Didier, P.J., Ahsan, M.H., Hudock, T.A., Kissee, R., Golden, N.A., Gautam, U.S., Johnson, A.-M., Alvarez, X., et al. (2015). The DosR Regulon Modulates Adaptive Immunity and Is Essential for Mycobacterium tuberculosis Persistence. Am. J. Respir. Crit. Care Med. *191*, 1185–1196.

Meyerholz, D.K., Sieren, J.C., Beck, A.P., and Flaherty, H.A. (2018). Approaches to Evaluate Lung Inflammation in Translational Research. Vet. Pathol. *55*, 42–52.

O'Toole, R. (2010). Chapter 3 - Experimental Models Used to Study Human Tuberculosis. In Advances in Applied Microbiology, (Academic Press), pp. 75–89.

Palanisamy, G.S., Smith, E.E., Shanley, C.A., Ordway, D.J., Orme, I.M., and Basaraba, R.J. (2008). Disseminated disease severity as a measure of virulence of Mycobacterium tuberculosis in the guinea pig model. Tuberculosis *88*, 295–306.

Palmer, M.V. (2018). Emerging Understanding of Tuberculosis and the Granuloma by Comparative Analysis in Humans, Cattle, Zebrafish, and Nonhuman Primates. Vet. Pathol. *55*, 8–10.

Pawlowski, A., Jansson, M., Sköld, M., Rottenberg, M.E., and Källenius, G. (2012). Tuberculosis and HIV Co-Infection. PLoS Pathog. *8*.
Sakamoto, K. (2012). The Pathology of Mycobacterium tuberculosis Infection. Vet. Pathol. *49*, 423–439.

Scanga, C.A., and Flynn, J.L. (2014). Modeling Tuberculosis in Nonhuman Primates. Cold Spring Harb. Perspect. Med. *4*.

Sharpe, S., White, A., Gleeson, F., McIntyre, A., Smyth, D., Clark, S., Sarfas, C., Laddy, D., Rayner, E., Hall, G., et al. (2016). Ultra low dose aerosol challenge with Mycobacterium tuberculosis leads to divergent outcomes in rhesus and cynomolgus macaques. Tuberculosis *96*, 1–12.

Sharpe, S.A., Eschelbach, E., Basaraba, R.J., Gleeson, F., Hall, G.A., McIntyre, A., Williams, A., Kraft, S.L., Clark, S., Gooch, K., et al. (2009). Determination of lesion volume by MRI and stereology in a macaque model of tuberculosis. Tuberculosis *89*, 405–416.

Sharpe, S.A., White, A.D., Sibley, L., Gleeson, F., Hall, G.A., Basaraba, R.J., McIntyre, A., Clark, S.O., Gooch, K., Marsh, P.D., et al. (2017). An aerosol challenge model of tuberculosis in Mauritian cynomolgus macaques. PloS One *12*, e0171906.

Smith, D.W., and Harding, G.E. (1977). Animal model of human disease. Pulmonary tuberculosis. Animal model: Experimental airborne tuberculosis in the guinea pig. Am. J. Pathol. *89*, 273–276.

Tschernig, T., and Pabst, R. (2000). Bronchus-associated lymphoid tissue (BALT) is not present in the normal adult lung but in different diseases. Pathobiol. J. Immunopathol. Mol. Cell. Biol. *68*, 1–8.

Turner, O.C., Basaraba, R.J., and Orme, I.M. (2003). Immunopathogenesis of Pulmonary Granulomas in the Guinea Pig after Infection with Mycobacterium tuberculosis. Infect. Immun. *71*, 864–871.

Kumar, et al. (2015). Robbins and Cotran pathologic basis of disease (Philadelphia, PA: Elsevier/Saunders).

Tuberculosis - Diagnosis and treatment - Mayo Clinic.

WHO | Global tuberculosis report 2017.

CHAPTER 2: METHODOLOGY

All work was conducted in accordance with both the Tulane National Primate Research Center (TNPRC) Institutional Animal Care and Use Committee (IACUC) guidelines and in accordance with guidelines for humane animal care from the NIH.

Mtb infection

For all studies, captive-bred, male, Indian Rhesus macaques between 3 and 9 years of age were used. Animals were from a specific pathogen free colony known to be free of retrovirus and to be mycobacteria-naïve, and all animals had been bred and housed exclusively at the TNPRC. These macaques were experimentally aerosol-infected with a target dose of 25 CFU of *Mtb* CDC1551 in accordance with previous studies (Kaushal et al., 2015; Mehra et al., 2011, 2015). Briefly, animals were anesthetized under the guidance of laboratory animal veterinarians with intramuscular Ketamine at a dose of 5-7 mg/kg. Prior to placing the animal in the chamber, respiratory function was assessed to allow minute volume to be derived and a target dosage to be more accurately administered. Following anesthesia, animals were placed in dorsal recumbency, and with their head and neck extended, were positioned in a specialized, sealed, 16L class 3 biosafety cabinet that utilizes a dynamically run inhalation system to deliver aerosolized *MTb* bacilli. Animals respired normally for an appropriate length of time (typically about 10 minutes, based on their calculated minute and tidal volumes), after which they were removed from the chamber. During aerosolization, samples from the chamber air were collected, processed, and

cultured, to confirm suspected dosage range. This dosage is within the "low dose" range previously shown by this lab to result in LTBI ((Mehra et al., 2010, 2011). *Mtb* infection was confirmed with 3 consecutive positive Tuberculin skin tests (TST). Animals were stratified into LTBI and ATBI categories based on clinical parameters. Euthanasia was elected when animals met at least 4 of the pre-established criteria for euthanasia including: 1. Elevated body temperature 2°F beyond baseline for greater than or equal to 3 consecutive weeks, 2. Greater than or equal to a 15% loss in body weight, 3. Sustained elevations in serum C-reactive protein (CRP) values above 10 ug/mL for 3 or more consecutive weeks, 4. Thoracic radiograph scores higher than a 2 (on a scale of 0-4), 5. Respiratory discomfort resulting in vocalization, 6. Anorexia or near anorexia, or 7. Presence of bacilli in bronchioalveolar lavage (BAL) samples. These endpoints have been previously used as markers for time to euthanasia in previous studies from our lab (Kaushal et al. 2015).

SIV infection

Infection with SIV was carried out by inoculating naïve animals with 300 TCID50 (50% tissue culture infectious dose) of a pathogenic strain of SIV intravenously. The majority of animals were infected with SIVmac239. Few animals in the SIV only control group were inoculated with SIVmac251. In co-infected animals, SIV infection was carried out 9 weeks following *Mtb* infection at which time animals demonstrated positive TST but were classified as LTBI. Previous studies had demonstrated that a proportion of these animals would be likely to maintain latency, while some would be likely to progress to active TB(Foreman et al., 2016; Kaushal et al., 2015; Mehra et al., 2011). Humane endpoints for euthanasia for co-infected animals were the same as those described for the *Mtb* infected

animals, above. Humane endpoints for euthanasia for SIV only animals were established by the Kuroda lab from which these animals derived.

Control animals

Tissues from uninfected or naïve animals were selected for animals who had been euthanized for reasons unlikely to result in pulmonary lesions. These animals had not been exposed to either SIV or *Mtb*.

Euthanasia and necropsy procedures

Prior to euthanasia, the animals were anesthetized with xylazine and ketamine, and blood is collected via an intracardiac puncture. The animal was euthanized with 2mL of sodium pentobarbital euthanasia solution.

For *Mtb* infected animals, all procedures were carried out in a class 3 biosafety facility by veterinary pathologists or trained prosectors. For SIV only infected animals, necropsies were carried out in class 2 biosafety facilities by veterinary pathologists or trained prosectors. All necropsies were carried out according to well-established standard operating procedures by either trained prosectors or veterinary pathologists. For *Mtb*-infected animals, necropsies were carried out in class 3 biosafety facilities. Additional considerations for these necropsies included photographing the right and left side of the pluck, exposure and photography of the bronchial and hilar lymph nodes, weighing of the left and right side of the lungs, weighing and measuring the bronchial lymph nodes and collecting both fresh and fixed samples, and systematic but random (stereological) collection of lung samples from all lobes following collection of a bronchioalveolar lavage sample acquired by infusing PBS into and subsequently aspirating it from the right lower lung lobe. To do this collection, the left anterior, middle, and caudal lung lobes were sliced into 5 mm thick transverse sections, and

arranged nest to each other with the lateral margins of each section apposing the medial margin of the adjacent section. This was repeated for each section so that each row was composed of all sections from one lobe in the same orientation. A random sampling grid was then placed over the sections, and indelible ink was used to mark sampling locations on the grid. These sections were then dissected along with an adjacent piece of tissue; one was then collected for fixation and histologic processing, and one was submitted for culture. The same process was then repeated for the right lobes. Number of samples and a photograph of those collected was recorded. Samples were collected into 10% zinc-buffered formalin (Z-fix), and representative sections were collected and retained in Z-fix for 48 hours prior to proceeding with routine paraffin embedding, sectioning at approximately 5 um thick, and processed for standard automated hematoxylin and eosin staining for light microscopy (necropsy methods courtesy of R. Blair).

REFERENCES:

Kaushal, D., Foreman, T.W., Gautam, U.S., Alvarez, X., Adekambi, T., Rangel-Moreno, J., Golden, N.A., Johnson, A.-M.F., Phillips, B.L., Ahsan, M.H., et al. (2015). Mucosal vaccination with attenuated Mycobacterium tuberculosis induces strong central memory responses and protects against tuberculosis. Nat. Commun. *6*.

Mehra, S., Pahar, B., Dutta, N.K., Conerly, C.N., Philippi-Falkenstein, K., Alvarez, X., and Kaushal, D. (2010). Transcriptional reprogramming in nonhuman primate (rhesus macaque) tuberculosis granulomas. PloS One *5*, e12266.

Mehra, S., Golden, N.A., Dutta, N.K., Midkiff, C.C., Alvarez, X., Doyle, L.A., Asher, M., Russell-Lodrigue, K., Monjure, C., Roy, C.J., et al. (2011). Reactivation of latent tuberculosis in rhesus macaques by coinfection with simian immunodeficiency virus. J. Med. Primatol. *40*, 233–243.

Mehra, S., Foreman, T.W., Didier, P.J., Ahsan, M.H., Hudock, T.A., Kissee, R., Golden, N.A., Gautam, U.S., Johnson, A.-M., Alvarez, X., et al. (2015). The DosR Regulon Modulates Adaptive Immunity and Is Essential for Mycobacterium tuberculosis Persistence. Am. J. Respir. Crit. Care Med. *191*, 1185–1196.

CHAPTER 3: DEVELOPMENT AND VALIDATION OF A SEMI-QUANTITATIVE APPROACH FOR ASSESSMENT OF HISTOPATHOLOGIC DIFFERENCES IN RHESUS MACAQUES EXPERIMENTALLY INFECTED WITH M*YCOBACTERIUM TUBERCULOSIS* ALONE OR IN THE SETTING OF SIV COINFECTION

INTRODUCTION:

Despite advances in antibiotic therapy and epidemiological control since Robert Koch first identified Mycobacterium tuberculosis (*Mtb*) as the causative agent of tuberculosis (TB) in the 1800's, *Mtb* continues to be responsible for the largest number of human deaths from a single infectious agent worldwide(Brosch et al., 2002; WHO, 2017) . TB is typically classified into 1 of 2 clinical states: 1. Latent tuberculosis (LTBI), during which the bacilli are not actively replicating, the host immune system maintains the disease in a quiescent state, and the disease is not considered transmissible, or 2. Active tuberculosis (ATBI) when bacilli are actively replicating and disseminating, have evaded host immune control, and can be transmitted to others. While individuals latently infected with TB generally have a low risk of progression from LTBI to ATBI, several factors can increase risk of progression. Notably, infection with the lentivirus Human Immunodeficiency Virus, increases the risk for progression from LTBI to ATBI from 5-10% over the course of an infected individual's lifetime to 5-15% over the course of a year (Aaron et al., 2004; Pawlowski et al., 2012). The macaque provides a superior model of human TB as they fully recapitulate the spectrum of gross and histopathologic lesions seen in human disease, can be co-infected with Simian

Immunodeficiency Virus as an analogue for HIV co-infection, develop LTBI and will spontaneously reactivate to ATBI (Capuano et al., 2003; Gardner and Luciw, 2008; Scanga and Flynn, 2014).

However, despite significant advancements in the understanding of TB from numerous scientific approaches—including advanced imaging, the use of ever-sophisticated immunologic assays, and the advent of molecular techniques that have elucidated activities at the genetic level of both the host and the microbe—much of our understanding of the pathologic differences between disease states in tuberculosis remains unknown. ATBI and LTBI are still distinguished on the basis of clinical parameters, generally including the presence of acid fast bacilli within sputum or gastric aspirates, sustained elevated serum C-reactive protein levels above values shown to be correlated with ATBI, hyperthermia, weight loss and inappetance, positive *Mtb* specific IFN-gamma in peripheral blood mononuclear cells, and positive agar gel immundiffusion testing, and the presence of pulmonary granulomas on thoracic radiographs (Kaushal et al., 2012; Lin et al., 2009; Scanga and Flynn, 2014). Previous studies have shown the ability to detect overall differences in gross pathology as a total score at necropsy in ATBI and LTBI infected Cynomolgous macaques (Lin et al., 2009). However, no reports have been able to definitively distinguish between ATBI and LTBI histolologically in either humans or non-human primates. Historically, much of the focus in TB-related pathology has been on the granuloma itself; however, both LTBI and ATBI animals will show a spectrum of granulomas that do not allow distinction between disease states based on these changes alone (Foreman et al., 2017; Lin et al., 2009; Sharpe et al., 2009). While recent work has described the structure and function of the granuloma in TB, little is known about additional changes and progression of disease both within the lung itself and throughout the body (Cronan et al., 2016; Martinot, 2018; Palmer,

2018). Little attention has been paid to changes outside of the granuloma in lungs from non-human primates infected with TB.

Additionally, while synergism between both HIV and *Mtb* and SIV and *Mtb* has been well described (Aaron et al., 2004; Foreman et al., 2016; Mehra et al., 2011; Pawlowski et al., 2012) many of the mechanisms of that synergism remain largely unknown, and histopathological differences that may be associated with and contribute to that synergism have not been well-characterized.

Recent work has demonstrated a growing need for a multimodal approach to translational research that incorporates trained pathologists to perform gross and microscopic pathology, particularly in the context of evaluating pulmonary inflammation (Meyerholz et al., 2018). Both the Bill and Melinda Gates Foundation (BMGF) and the National Institutes of Health (NIH), the two premier sponsors of TB research worldwide, have adopted the NHP model as the premier system for evaluating the next generation of vaccine and drug candidates. Yet, because, 1. there are many different permutations of the NHP model (as described earlier), including the use of different NHP species [comprising most commonly old world macaques (e.g., Indian rhesus or Chinese, Philippine or Mauritian cynomolgus macaques) as well as new world monkeys like marmosets], and 2.because there are various methodologies of *Mtb* infection—with the use of both different *Mtb* strains (e.g, H37Rv, CDC1551, Erdman etc.) and routes of infection (i.e. via aerosol or bronchoscope)—a single universal approach cannot be applied to all situations. Thus, incorporating pathologists who have been comprehensively trained to evaluate pulmonary pathology in multiple species and scenarios becomes even more important to allow for consistency in interpretation of pulmonary pathology. To increase repeatability in these various scenarios

and between different pathologists, however, a standard method for interpretation of these pulmonary changes is needed. Scoring systems are widely used in both human and veterinary pathology to allow for standardization and repeatability of assessment between pathologists, and to be of most information, must satisfy robust criteria (Cross, 1998; Gibson-Corley et al., 2013; Klopfleisch, 2013). There is a need for standardization in approaches to pulmonary pathology in the macaque model of TB, and for development of a repeatable, discriminating scoring system for pulmonary pathology that may help to elucidate subtle differences between ATBI and LTBI both in and in the absence of SIV coinfection with an aim to gain more comprehensive understanding of factors related to disease progression and retrovirus synergism.

The aims of this study were thus:

1. To develop a repeatable histopathologic scoring system to evaluate aspects of pulmonary pathology between rhesus macaques (*Macaca mulatta*) infected with *Mtb* with either ATBI or LTBI and in animals coinfected with both *Mtb* and SIV with either ATBI or LTBI;
2. To determine whether there are differences in pathological parameters based on category of infection, and 3. To determine whether this histopathologic scoring system could be used to predict disease category status in experimentally infected animals. We hypothesized that ATBI animals would have greater degrees of pulmonary pathology for each of the given categories than LTBI animals, and that SIV co-infection would worsen pulmonary pathology scores for traditionally "virus-associated" parameters including type II pneumocyte hyperplasia, alveolar macrophages, perivasculitis, and vasculitis/lymphangitis.

MATERIALS AND METHODS:

Animal information

All work was conducted in accordance with both the Tulane National Primate Research Center (TNPRC) institutional animal care and use committee guidelines and in accordance with guidelines for humane animal care from the NIH. Archival lung samples were acquired from locally captive bred, co-housed male Indian Rhesus macaques (*Macaca mulatta*), ranging from 2-9 years old. Animals were divided into 6 groups based on disease status: uninfected, SIV only, *Mtb* infected-LTBI (LTBI), *Mtb* infected-ATBI (ATBI), SIV + *Mtb* infected-LTBI (LTBI+SIV), and SIV + *Mtb* infected-ATBI (ATBI+SIV). For all *Mtb*-infected groups, 3 animals per group were examined, with a total of 5-7 sections of lung per animal evaluated per animal by each pathologist. Eight uninfected animals were evaluated, with an average of 1 section of lung per animal available for review by the pathologists, with one animal (JN31) having 2 sections available for review. Eight SIV-only animals were reviewed by the pathologists, with each animal having between 1 and 3 sections of lung available for review, and the majority of animals having only 1 section available for review. Uninfected animals were colony animals that were euthanized for reasons unrelated to pulmonary disease or systemic inflammation. Following intravenous administration of 300 TCID50 (50% tissue culture infectious dose) of pathogenic strains of SIV—either SIVmac239 or SIVmac251 (see table 1 for animal information)—samples from SIV only animals were collected at necropsy between 10 and 225 days once animals had either met clinical criteria established by that study for euthanasia or had reached study end. All *Mtb* infected animals included in this analysis derived from a previously published study (Foreman et al., 2016). Briefly, ~25 CFU target dose of *Mycboacterium tuberculosis* CDC1551

were administered at a particle size deemed to be highly respirable within a sealed 16L class 3 biosafety cabinet to the head of ketamine-anesthetized animals who were allowed to respire normally while in dorsal recumbency for approximately 10 minutes (based on calculated tidal volume). Full methodology for our unique approach for *Mtb* aerosol administration has been previously reported (Dutta et al., 2010; Kaushal et al., 2015; Mehra et al., 2010). This dose has been shown to result in good rates of infection, with a proportion of animals naturally developing LTBI, and others naturally developing ATBI (Mehra et al., 2011). Prior to infection, animals were confirmed negative for *Mtb* infection with negative chest x-rays and three negative tuberculin skin tests (TST) in 3 consecutive 24 hour periods. Three positive TST within consecutive 24 hour periods post-inoculation were used to confirm *Mtb* infection. Of the LTBI animals, a subset were challenged 9 weeks post-*Mtb* infection with 300 TCID50 SIVmac251 administered IV. Following SIV coinfection, animals were stratified into LTBI and ATBI categories based on clinical parameters. Animals were euthanized when they met previously established clinical criteria, as previously described (Foreman et al., 2016; Kaushal et al., 2015).

CFU data and terminal viral load

Terminal average log CFU/gram of lung were determined for all *Mtb* infected animals by plating homogenized lung and tracheobronchial lymph nodes as described previously(Mehra et al., 2011). Terminal SIV viral load was determined on a sample of peripheral blood collected from each SIV infected animal following anesthesia immediately prior to euthanasia, and was reported as viral copies #/mL of plasma.

Necropsy, tissue collection, and slide processing

For uninfected and SIV only animals, necropsies were carried out by trained pathologists or prosectors in class 2 biosafety conditions. Lungs were infused with 10% zinc-buffered formalin (Z-fix), and representative sections were collected and retained in Z-fix for 48 hours prior to proceeding with routine paraffin embedding and processing for standard automated hematoxylin and eosin staining.

All necropsies for *Mtb*-infected animals were carried out in class 3 animal biosafety level 3 facilities. The right lower lung lobe was infused with 100 mL of PBS and aspirated as a bronchioalveolar lavage. Afterwards, the left and right lung lobes were processed separately, using a well-established, standardized, systematic approach that allowed for the use of a random sampling grid to stereologically select random, but representative sections of all lung lobes for histological assessment (full standard operating procedures provided courtesy of Dr. Robert Blair). Fresh samples for histopathologic processing were infused with Z-fix, and then placed in Z-fix for a minimum of 48 hours prior to proceeding with routine paraffin embedding and processing for standard automated hematoxylin and eosin staining.

Slide selection

Hematoxylin and eosin stained slides were routinely processed from zinc-formalin fixed and paraffin embedded lung sections stereologically collected at the time of necropsy were retrospectively examined by each of 3 board certified veterinary anatomic pathologists, 2 of whom had NHP experience. Pathologists were comprehensively blinded to disease category. For each of the *Mtb* infected animals, a minimum of 3 randomly selected, representative slides per animal were examined, for a total of 5-7 sections of lung per animal.

For the uninfected control and SIV only animals, all available lung slides were reviewed, ranging from 1-2 sections per animal.

Scoring system criteria

All lung sections were evaluated for changes in the following categories (Table 1): septal thickness (both average and maximum, in comparison to expected normal septal thickness of one cell (approximately 10-15 um) thick), septal cellularity (both average and maximum septal cellularity (counted cell thickness), degree of consolidation (based on both 10 point and 5 point scale, corresponding to estimated % affected), degree of type II pneumocyte hyperplasia, increase in alveolar macrophages, degree of perivasculitis, degree of vasculitis and/or lymphangitis, degree of inducible bronchus-associated lymphoid tissue (iBALT), presence or absence of granulomas, and total pathology. Type II pneumocyte hyperplasia, increase in alveolar macrophages, perivasculitis, vasculitis/lymphangitis, and degree of iBALT were given ordinal scores from 0-5 corresponding with degrees of severity ranging from none-severe. Thus, in this scoring system, septal thickness and cellularity (both average and maximum) and total score are classified as continuous variables, while remaining variables are considered ordinal variables. Representative histologic images for scoring criteria severities were provided to improve repeatability for some categories (Figure 1a-1e).

Avg. and max septal thickness	Avg. and max septal cellularity	Type II pneumocyte hyperplasia (0-5)	↑ Alveolar macrophages (0-5)	Consolidation (0-5)
Consolidation (0-10)	Perivasculitis (0-5)	Lymphangitis/ Vasculitis (0-5)	iBALT (0-5)	Granulomas? (yes or no)

Table 1: Scoring system criteria

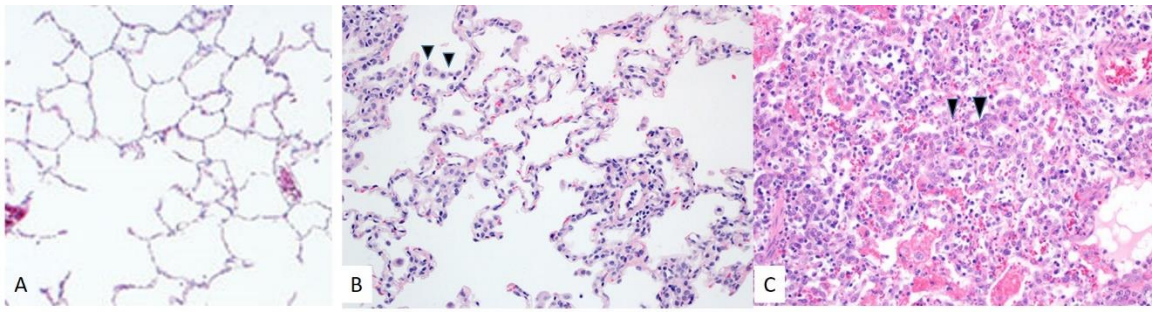

Figure 1a: Histologic scoring images: Type 2 pneumocyte hyperplasia. From left to right **(A)** = score of 0 (normal), **(B)** = score 2 out of 5 (arrowheads denote hypertrophied type II pneumocytes), **(C)** = score 4 out of 5 (note diffuse hypertrophy in this section).

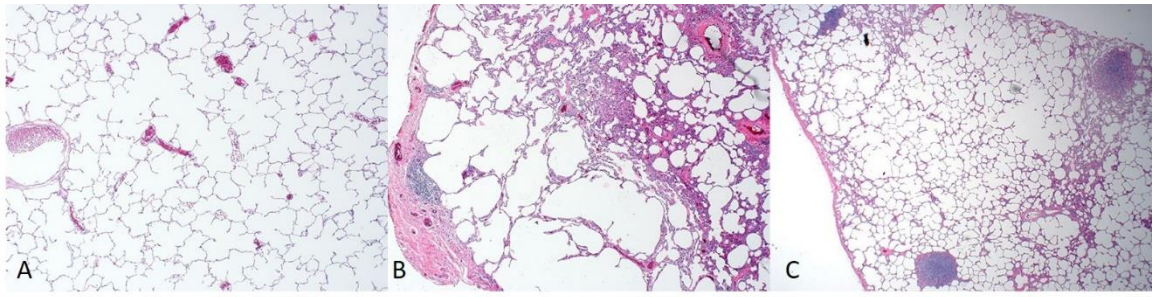

Figure 1b: Histologic scoring images: iBALT. From left to right **(A)** = 0 (normal, no lymphoid follicles), **(B)** = score 1 out of 5 (few small nodular lymphoid aggregates throughout the interstitium, no distinct architecture), **(C)** = score 5 out of 5 (numerous large, well-organized lymphoid follicles visible from low magnification, many with discrete germinal centers or tangible body macrophages).

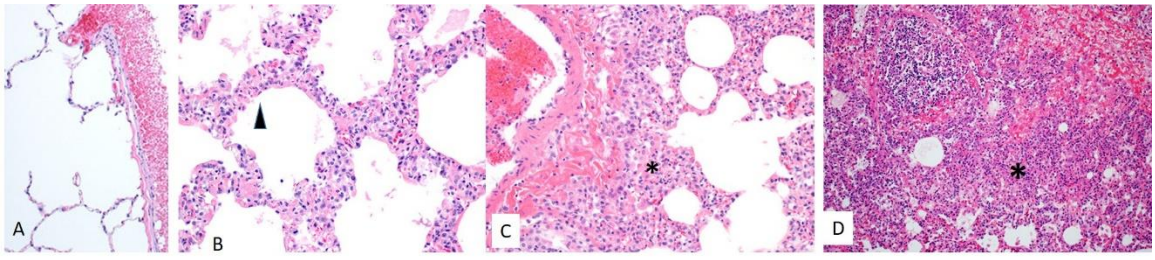

Figure 1c: Histologic scoring images: miscellaneous. From left to right **(A)** = normal (note thin septa and thin perivascular space), **(B)** = septal thickness 3x normal and 3x septal cellularity (arrowhead), **(C)** = increase in alveolar macrophages score 3 out of 5 (note partial filling of alveolar lumens by foamy macrophages (asterisk), **(D)** = increase in alveolar macrophages score 5 out of 5 (note nearly complete filling of alveolar lumens by macrophages in areas not directly associated with a granuloma).

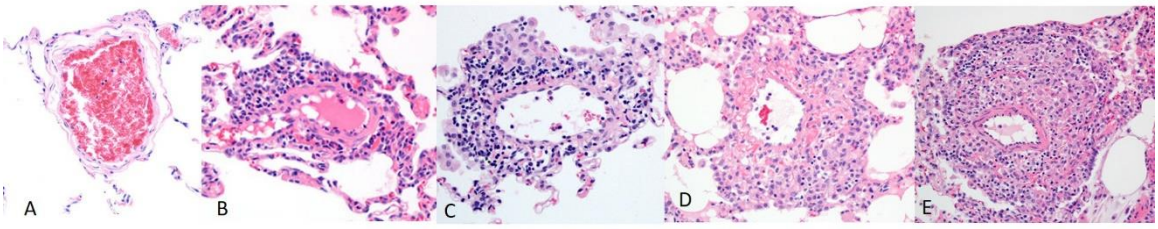

Figure 1d: Histopathologic scoring images: Perivasculitis. From left to right **(A)** = score of 0 out of 5 (normal), **(B)** = score 2 out of 5 (note mild expansion of perivascular space by mixed inflammatory cells), **(C)** = score 3 out of 5, **(D)** = score 4 out of 5, **(E)** = score 5 out of 5 (note marked expansion of perivascular space by lymphocytes and macrophages, and occasional nodular aggregates of macrophages within perivascular space suggestive of nascent granuloma formation).

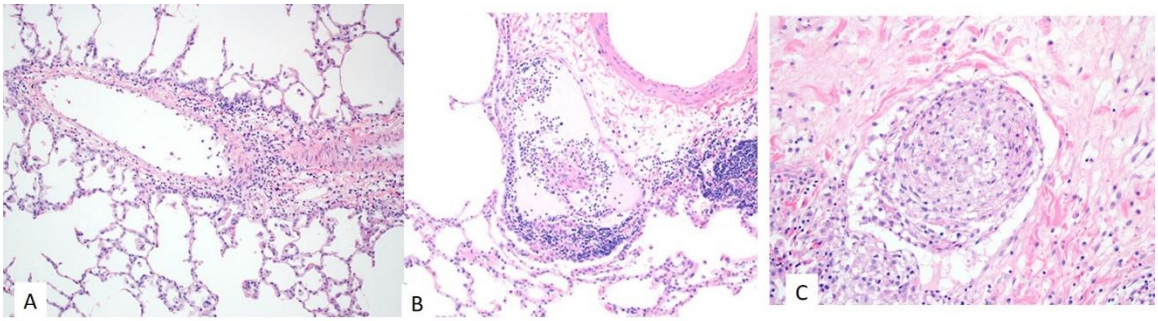

Figure 1e: Histopathologic scoring criteria: Vasculitis/lymphangitis. From left to right **(A)** = vasculitis score 2 out of 5 (note segmental infiltration of vessel wall by mixed

inflammatory cells), **(B)** = lymphangitis/vasculitis score 2 out of 5 (note filling of lumen by necrotic debris and mixed inflammation and extension of mixed inflammation into vessel wall), **(C)** = lymphangitis/vasculitis score 4 out of 5 (note near complete obstruction of lumen by necrotic and inflammatory debris and segmental infiltration of similar inflammation along bottom portion of vessel wall.

Statistical analysis

Of utmost importance in development of histologic scoring systems is strong and repeatable interobserver agreement (Gibson-Corley et al., 2013). Thus, interobserver variability was determined by calculating the intraclass correlation (ICC) across scores for each category with each slide read by all pathologists. All categories in which the ICC was less than 0.4 were considered irreproducible and not included in further analysis. The ICC values were calculated using the ICC function of the irr package (Gamer et al., 2012) in R. Univariable analysis was conducted by fitting ordinal logistic regression models for each of the categories by disease status, with animal held as a random effect, using the clmm function of the ordinal package (Christensen, 2018) in R. For total score, a linear regression model was fit with animal held as a random effect, using the lmer function of the lmerTest package (Kuznetsova et al., 2017; Venables and Ripley, 2002) in R. For presence of granulomas, a logistic regression model was fit using the glm function of the MASS package(Venables and Ripley, 2002) in R; as presence of granulomas was not a scored value, random effects were not required. The ability of the scoring system to predict disease status types was assessed through multivariate analysis. For this, a logistic regression model was fit for each of the following disease status types: TB infection, LTBI, ATBI, SIV, and SIV-ATBI. All covariates that were significantly related in the ordinal logistic regression were

included as linear variables. Backwards stepwise model selection was used to select the best model for each outcome. All models were fit using the glm function of the MASS package in R. Univariate analysis was performed for effects of single versus coinfection on pathologic findings for both *Mtb* and SIV infections. Univariate analysis was also performed to analyze pairwise comparisons between individual pathologic parameters for the following disease category comparisons to determine the ability of the scoring system both to detect differences between ATBI and LTBI and to detect differences with SIV coinfection: 1. All ATBI vs. all LTBI, 2. ATBI only vs. LTBI only, and 3. ATBI + SIV vs. LTBI + SIV.

Descriptive statistics were performed for all parameters and all disease categories, specifically assessing median, minimum and maximum values, 10% and 90% percentiles, and 95% confidence intervals for each category, using Graphpad prism statistical software. Terminal lung *Mtb* CFU were compared between ATBI, LTBI, ATBI-SIV, and LTBI-SIV animals using one-way ANOVA with Tukey's test for multiple comparisons in Graphpad Prism. Terminal SIV plasma viral loads were compared between SIV infected groups by one-way ANOVA with Tukey's multiple comparisons test using Graphpad prism statistical software. Dr. Rebecca Smith at the University of Illinois College of Veterinary Medicine performed statistical analysis for all statistics done in R. D. LoBato performed all remaining statistical analyses in Graphpad Prism.

Immunofluorescence

Selected formalin-fixed and paraffin-embedded sections of lung were sectioned at 5 um and stained in accordance with previously established standard protocols by the confocal microscopy core facility at the Tulane National Primate Research Center with fluorescent

antibodies against *Mtb*, caveolin (for pulmonary vessels), and topro (for nuclei). Additional sections were stained with antibodies for SIV and nuclei. Images were then captured.

RESULTS:

This scoring system showed good interobserver agreement and repeatability, with the ICC for the categories ranging from 0.38 to 0.72; all were significantly greater than 0 (Table 2). Only one category, iBALT, had an ICC below 0.4; it was therefore excluded from further analysis.

	ICC	Lower Bound	Upper Bound	p-value
Avg. septal thickness x normal	0.62	0.46	0.75	4.20E-13
Max septal thickness x normal	0.72	0.59	0.82	2.90E-18
Avg septal cellularity	0.46	0.28	0.62	1.50E-07
Max septal cellularity	0.61	0.45	0.74	1.00E-12
Consolidation out of 10	0.7	0.57	0.81	2.20E-17
Consolidation out of 5	0.69	0.55	0.8	9.80E-17
Type II pneumocyte hyperplasia	0.62	0.47	0.75	3.00E-13
Alveolar macrophage increase	0.47	0.29	0.63	7.70E-08
Perivasculitis	0.72	0.59	0.82	2.30E-18
Lymphangitis	0.58	0.42	0.72	1.40E-11
iBALT	0.38	0.2	0.56	1.20E-05
Granulomas	0.55	0.39	0.7	1.50E-10

Table 2: Intraclass correlation (ICC) for each scored category across 3 pathologists.

Distribution of scores for each of the remaining measured factors by disease group are shown in Figure 2. For the categories of alveolar macrophages, consolidation (out of both 10 and 5), lymphangitis, perivasculitis, type II pneumocyte hyperplasia, and total pathology, ATBI animals have higher pathology scores and an increased likelihood of pathology as determined by the odds ratios (see Table 3) vs. LTBI animals. SIV co-infection increases pathology scores for alveolar macrophages in SIV-LTBI vs. LTBI animals, for type II pneumocyte hyperplasia in both SIV-LTBI vs. LTBI and in SIV-ATBI vs. ATBI animals,

and for both perivasculitis and vasculitis/lymphangitis in both co-infected groups vs. either singly-infected group. Type II pneumocyte hyperplasia and both perivasculitis and lymphangitis/vasculitis in particular, but also maximum septal cellularity to a lesser degree were also features of SIV single infection. Granulomas were present in all TB groups, and were more common than in the non-TB control groups, as expected.

Descriptive statistics were used to compare medians, maximum and minimum values, 90% and 10% percentiles, and 95% confidence intervals for all disease categories for all pathology parameters. These results are displayed in Table 4.

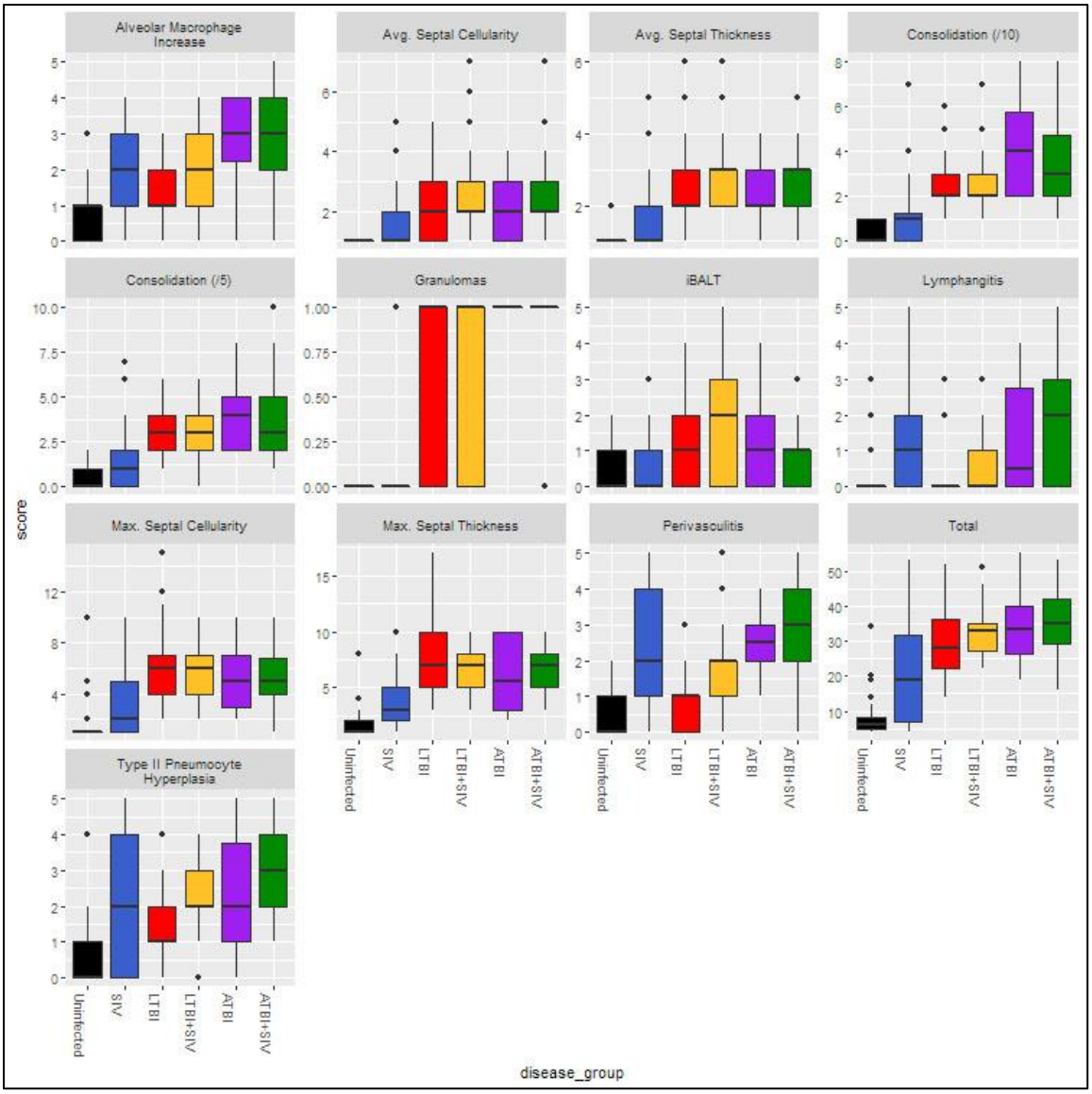

Figure 2: Distribution of scores by disease group.

	All		ATBI only vs. LTBI only		ATBI-SIV vs. LTBI-SIV	
	OR	p-value	OR	p-value	OR	p-value
Avg septal thickness x normal	0.655	0.123	0.485	0.0859	0.806	0.559
Max septal thickness x normal	**0.760**	**0.283**	**0.326**	**0.00647**	**1.181**	**0.627**
Avg septal cellularity	0.851	0.542	0.632	0.261	1.004	0.992
Max septal cellularity	**0.602**	***0.0482***	**0.444**	***0.0432***	**0.698**	***0.291***
Consolidation out of 10	1.919	0.0125	2.801	0.0125	1.578	0.183
Consolidation out of 5	**3.287**	**1.52E-05**	**5.989**	**5.53E-05**	**2.380**	**0.0142**
Type II pneumocyte hyperplasia	2.915	7.50E-05	3.561	0.00397	2.140	0.0321
Alveolar macrophage increase	**8.846**	**1.29E-12**	**20.287**	**3.21E-08**	**4.953**	**2.49E-05**
Perivasculitis	**6.890**	**5.00E-11**	**26.050**	**4.67E-09**	**3.597**	**0.000513**
Lymphangitis	**6.890**	**2.36E-09**	**21.542**	**0.000115**	**5.104**	**2.68E-05**
Granulomas	0.900	0.938	1.6E8	0.998	2.51E-8	0.996
Total	-5.21	0.018	-5.21	0.018	0.000	0.018

Table 3: Results of univariate analysis for effects of active TB on pathological findings. Estimates and p-values are in comparison to latent TB. Blue categories = where SIV makes a difference.

	Uninfected	SIV	LTBI	LTBI-SIV	ATBI	ATBI-SIV
	Median (minimum,maximum)					
avg septal thickness x normal	1(1,2)	1(1,5)	2(1,6)	3(2,6)	2(1,4)	3(1,5)
max septal thickness x normal	1(1,8)	3(1,10)	7(3,17)	7(3,10)	5.5(2,10)	7(3,10)
avg septal cellularity	1(1,1)	1(1,5)	2(1,5)	2(1,7)	2(1,4)	2(1,7)
max septal cellularity	1(1,10)	2(1,10)	6(2,15)	6(2,10)	5(2,10)	5(1,10)
consolidation/10	0(0,2)	1(0,7)	3(1,6)	3(0,6)	4(2,8)	3(1,10)
consolidation/5	0(0,1)	1(0,7)	2(1,6)	2(1,7)	4(2,8)	3(1,8)
type II pneumocyte hyperplasia	0(0,4)	2(0,5)	1(0,4)	2(0,4)	2(0,5)	3(1,5)
alveolar macrophage increase	1(0,3)	2(0,4)	1(0,3)	2(0,4)	3(0,4)	3(0,5)
perivasculitis	0(0,2)	2(0,5)	1(0,3)	2(0,5)	2.5(1,4)	3(0,5)
lymphangitis	0(0,3)	1(0,5)	0(0,3)	0(0,3)	0.5(0,4)	2(0,5)
iBALT	0(0,2)	0(0,3)	1(0,4)	2(0,5)	1(0,4)	1(0,3)
granulomas	0(0,0)	0(0,1)	1(0,1)	1(0,1)	1(1,1)	1(0,1)

Table 4: Descriptive statistics for pathology parameters by disease category.

The univariable analysis found that disease status was not significantly associated with average septal cellularity or presence of granulomas ($p > 0.05$), but was significantly associated with all other scores. Granulomas were more common in any TB disease status than in SIV only or uninfected animals, as expected, though there was no difference in presence of granulomas between TB disease groups. There were significant differences between uninfected animals and disease groups for all remaining pathologic parameters included within the scoring system ($p < 0.05$, Table 5).

	Septal Thickness				Septal Cellularity				Consolidation			
	Average		Maximum		Average		Maximum		out of 10		out of 5	
	Est.	p-value	Est.	p-value	Est.	p-value	Est.	p-value	Est.	p-value	Est.	p-value
SIV only	2.5	0.044	2.3	3.30E-05	29	0.5	2.9	3.20E-07	7	1.90E-14	11	1.10E-18
LTBI	6.5	2.00E-06	2.9	2.30E-07	22	0.61	3.4	9.50E-09	7.7	1.50E-16	11	4.20E-20
LTBI-SIV	6.7	8.10E-07	3.4	2.00E-09	24	0.57	4.1	9.70E-12	8.4	9.40E-19	12	6.00E-21
ATBI	5.7	3.20E-05	4	4.50E-12	24	0.57	4.8	7.00E-15	9.3	9.40E-21	2.1	0.08
ATBI-SIV	6.7	5.20E-07	4.4	4.60E-14	24	0.58	5.5	1.40E-18	1.8	0.066	7.4	2.60E-06

	Type II Pneumocyte Hyperplasia		Alveolar Macrophage Increase		Perivasculitis		Lymphangitis		Granulomas		Total Score	
	Est.	p-value	Est.	p-value	Est.	p-value	Est.	p-value	Est.	p-value	Est.	p-value
SIV only	2.4	0.069	1.5	0.048	3.5	0.00015	2.2	0.0042	18	1	8.5	0.048
LTBI	3	0.065	1	0.24	1.8	0.11	-1.4	0.2	20	1	20	0.00088
LTBI-SIV	5.1	0.0021	2.3	0.0087	3.9	0.00039	1.1	0.17	39	1	23	0.00019
ATBI	4.7	0.0045	4.3	4.10E-06	4.8	2.00E-05	2	0.017	39	1	26	6.10E-05
ATBI-SIV	6	1.60E-05	4.4	1.70E-07	5.1	2.70E-07	2.8	0.00036	21	1	28	3.50E-07

Table 5: Results of univariable analysis for effect of disease status on pathological findings. Uninfected animals are the comparator for all analyses.

The multivariable analysis (Table 6) found that the factors that were predictive of tuberculosis infection differed from those predictive of SIV infection. In this analysis, the factors most strongly associated with TB were degree of consolidation out of 5 (OR = 2.445), maximum septal thickness (OR = 2.433), and increase in alveolar macrophages (OR = 1.493); these associations were more pronounced in ATBI. The categories most strongly associated with SIV infection included type II pneumocyte hyperplasia (OR = 2.020), degree

of perivasculitis (OR = 2.206), and average septal thickness (OR = 1.772). Perivasculitis was less likely in LTBI than in ATBI (OR for in LTBI = 0.709 vs. 1.512 in ATBI). Acting as a model of disease, this scoring system predicted disease status well, particularly in regards to ATBI, as demonstrated by the area under the curve in Figure 3. This model has an overall accuracy for detection of *Mtb* infection of 94%, with an overall accuracy for detection of ATBI status of 89%. Overall accuracy for detection of LTBI status was lower, but still considered strong at 69%. The combined relevant scoring parameters were used to create a model to assess how well the scoring system could predict disease states using a receiver operating characteristic (ROC) curve analysis (Figure 3). According to the ROC curve, the histopathologic scoring system is able to predict appropriate disease categories—particularly in regards to TB and ATBI—with high probability, with area under the curve values (corresponding to predicted probability) of 94% for any TB, 89% for ATBI, 68% for LTBI, 82% for any SIV, 80% for SIV-TB, and 84% for SIV-ATBI.

	TB		LTBI		ATBI		SIV		SIV+TB		SIV+ATBI	
	OR	p value	OR	p value	OR	p value	OR	p value	OR	p value	OR	p value
Avg. septal thickness x normal			2.323	0.000	0.480	0.007	1.772	0.008	1.693	0.014		
Max septal thickness x normal	2.433	0.000			1.722	0.000			1.272	0.026	1.563	0.000
Max septal cellularity	0.706	0.062	1.614	0.000	0.554	0.000	0.774	0.004	0.771	0.024	0.596	0.001
Consolidation out of 10												
Consolidation out of 5	2.445	0.000	0.688	0.010	1.794	0.000	0.596	0.000	0.750	0.013		
Type II pneumocyte hyperplasia							2.020	0.000	1.523	0.006		
Alveolar macrophage increase	1.493	0.086	0.722	0.039	2.578	0.000			1.371	0.042	2.002	0.000
Perivasculitis			0.709	0.051	1.512	0.005	2.206	0.000	1.570	0.003	1.356	0.074
Lymphangitis	0.415	0.000	0.431	0.000					0.816	0.146	1.315	0.071

Table 6A:

	max septal thickness x normal CI	avg septal cellularity CI	consolidation out of 5 CI	consolidation out of 10 CI	alveolar macrophage increase CI	perivasculitis CI	iBALT CI	granulomas CI	avg septal thickness x normal CI	max septal thickness x normal CI	max septal cellularity CI	Type II pneumocyte hyperplasia CI
	2.5%, 97.5% Confidence intervals											
SIV	0.069,5	1.2,3.4	-250,300	1.8,4.1	5.2,8.8	8.3,13	-0.19,5	0.012,3	1.7,5.3	0.69,3.7	-0.62,1.5	1.2,16
LTBI	3.8,9.2	1.8,4	-250,300	2.2,4.5	5.8,9.5	8.9,14	-0.19,6.2	-0.68,2.8	-0.37,3.9	-3.5,0.72	0.51,2.5	11,29
LTBI-SIV	4.1,9.4	2.3,4.5	-250,300	2.9,5.3	6.5,10	9.9,15	1.8,8.3	0.58,4	1.7,6.1	-0.48,2.8	1.3,3.4	14,33
ATBI	3,8.4	2.9,5.1	-250,300	3.6,6	7.3,11	-0.24,4.4	1.5,8	2.5,6.1	2.6,7	0.37,3.7	-0.015,2.1	17,35
ATBI-SIV	4.1,9.3	3.3,5.5	-250,300	4.3,6.7	-0.12,3.8	4.3,10	3.3,8.7	2.7,6	3.1,7	1.3,4.4	-0.1,1.9	20,36

Table 6B:

Table 4: (A) Odds ratios (OR) and p-values for disease states as predicted by the stated pathology parameters and (B) 2.5% and 97.5% confidence intervals for the pathology parameters by disease categories.

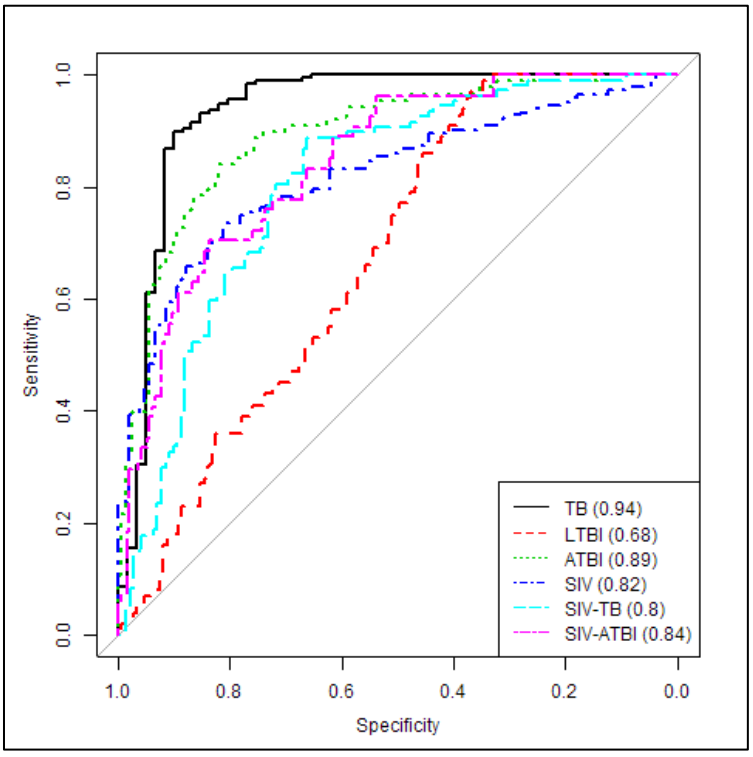

Figure 3: ROC curves for prediction of disease states (AUC).

The combined relevant scoring parameters were used to create a model to assess how well the scoring system could predict disease states (Figure 4). Figure 4 shows that the scoring system is able to predict appropriate disease categories with high probability, although ATBI cases may be misidentified as having SIV infection if the SIV model results are not compared to the ATBI scoring system results. With SIV coinfection, the ability to detect differences between LTBI-SIV and ATBI disease states becomes more difficult.

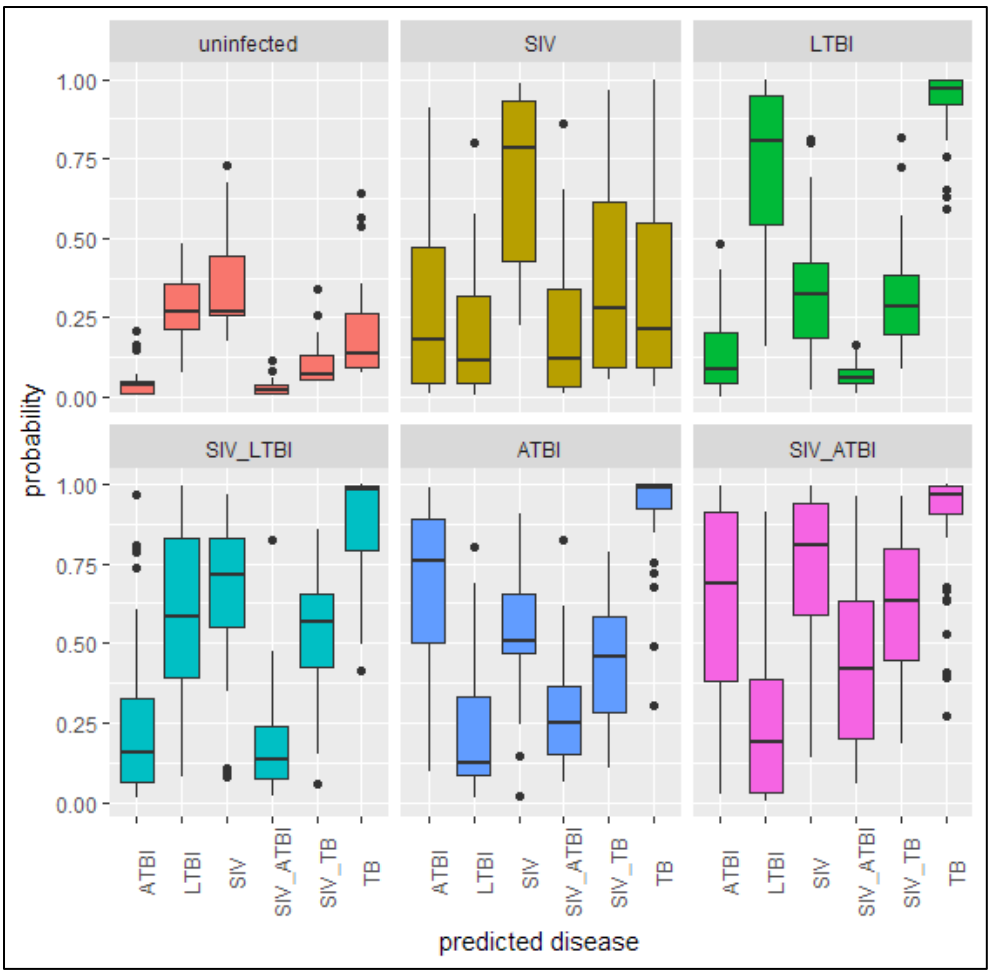

Figure 4: Boxplots of predicted probability of being in a particular disease category, by actual disease category. TB = any animal infected with *Mtb*, regardless of clinical TB state; SIV_TB = any animal co-infected with SIV and *Mtb*, regardless of clinical TB state.

Pairwise comparisons were then performed using univariate analysis comparing groups to LTBI for individual score categories (Figure 2, Table 3). In the absence of SIV coinfection, there were strong differences between ATBI and LTBI animals based on pathologic scoring criteria, with ATBI animals having consistently significantly higher scores in the categories of maximum septal thickness, maximum septal cellularity, degree of consolidation (both out of 10 and out of 5, with greater sensitivity when measured out of 5), degree of type II pneumocyte hyperplasia, increase in alveolar macrophages, and degree of perivasculitis and vasculitis/lymphangitis (all $p < 0.05$, see Table 3 for specific values). Granulomas were significantly more likely to be present in animals with TB than in those without (Figure 2, Table 7), but there was no difference in presence of granulomas between TB disease categories. It is important to clarify that for this study, granulomas were only recorded as present or absent. In the absence of SIV infection, LTBI animals were more likely to have expanded septal thickness and cellularity in comparison to ATBI animals, with odds ratios less than 1 (Table 3).

In co-infected animals, similar effects were observed, but with less strength, as indicated by lower odds ratios (Table 3). Significant differences remained, with ATBI + SIV animals displaying higher scores in the areas of consolidation (out of 5), type II pneumocyte hyperplasia, increase in alveolar macrophages, perivasculitis, and vasculitis/lymphangitis (all $p< 0.05$, Table 3). Interestingly, the odds ratio for maximum septal thickness in the setting of SIV co-infection shifted from a value of <1 in the absence of SIV infection to a value of 1.181 in the presence of SIV infection, suggesting that SIV may have a slight onfounding switching effect for this particular parameter in ATBI.

One-way ANOVA with Tukey's multiple comparisons demonstrated significant differences in the log CFU/g of lung of *Mtb* recovered from LTBI animals vs. ATBI animals ($p = 0.0094$, Figure 5) and between LTBI and ATBI + SIV animals ($p = 0.0026$). There were no additional significant differences between groups ($p > 0.05$). Similarly, one-way ANOVA with multiple comparisons was used to compare differences in viral loads between all SIV infected groups. No differences in terminal viral loads were detected between any groups ($p > 0.05$, Figure 6).

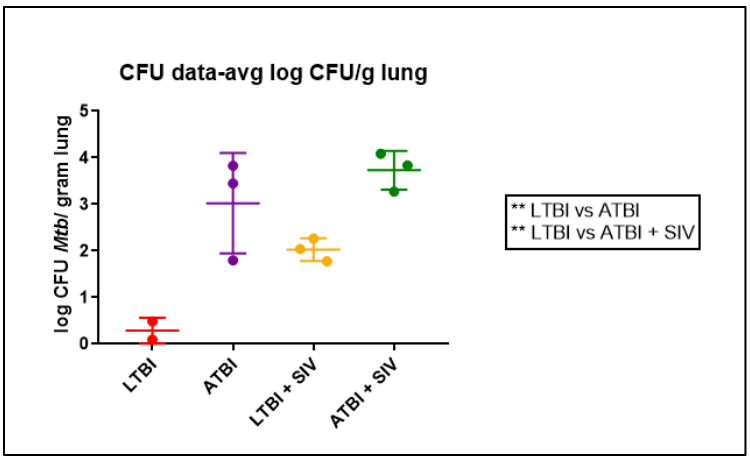

Figure 5: Comparison of log CFU/g of lung of *Mtb* recovered at necropsy. log CFU/g *Mtb* were significantly higher in ATBI animals vs. LTBI animals ($p = 0.0094$) and in ATBI-SIV animals vs. LTBI animals ($p = 0.0026$). There were no additional significant differences between groups ($p = 0.3906$).

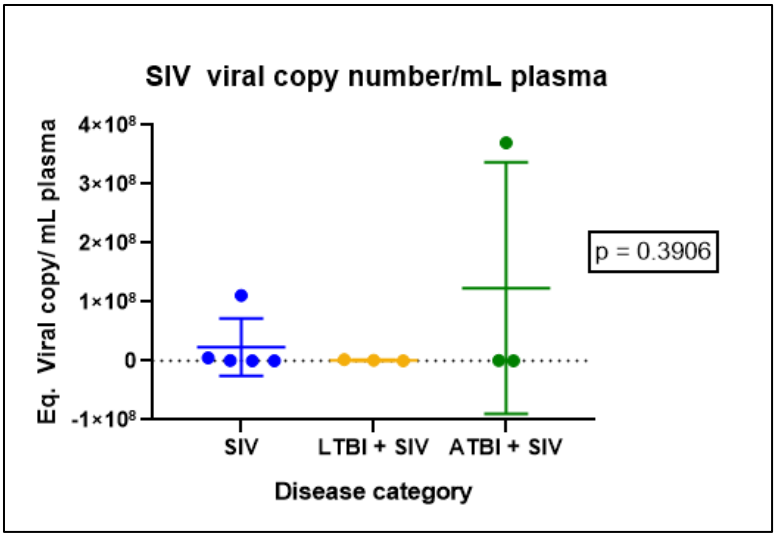

Figure 6: Comparison of terminal plasma viral loads of SIV infected animals. There is no significant difference in viral loads between any disease category (p = 0.3906).

	MTB		SIV	
	OR	p-value	OR	p-value
Avg septal thickness x normal	1.096	0.757	0.464	0.013
Max septal thickness x normal	0.862	0.595	0.399	0.00342
Avg septal cellularity	1.047	0.877	0.445	0.0101
Max septal cellularity	1.047	0.871	0.532	0.0391
Consolidation out of 10	0.748	0.301	0.273	5.80E-05
Consolidation out of 5	0.744	0.292	0.196	8.39E-07
Type II pneumocyte hyperplasia	1.354	0.289	0.247	1.32E-05
Alveolar macrophage increase	1.200	0.519	0.125	2.72E-09
Perivasculitis	1.188	0.544	0.177	1.60E-07
Lymphangitis	0.810	0.536	0.169	4.96E-07
Granulomas	1.000	1	0.125	0.0499
Total	4.53	0.354	21.1	0.00054

Table 7: Results of univariate analysis for effects of single vs. coinfection on pathological findings. Estimates and p-values are in comparison to co-infected animals

Immunofluorescence

Immunofluorescence demonstrated numerous intact and degraded *Mtb* within perivascular inflammation of selected animals with marked pervasculitis (Figure 7).

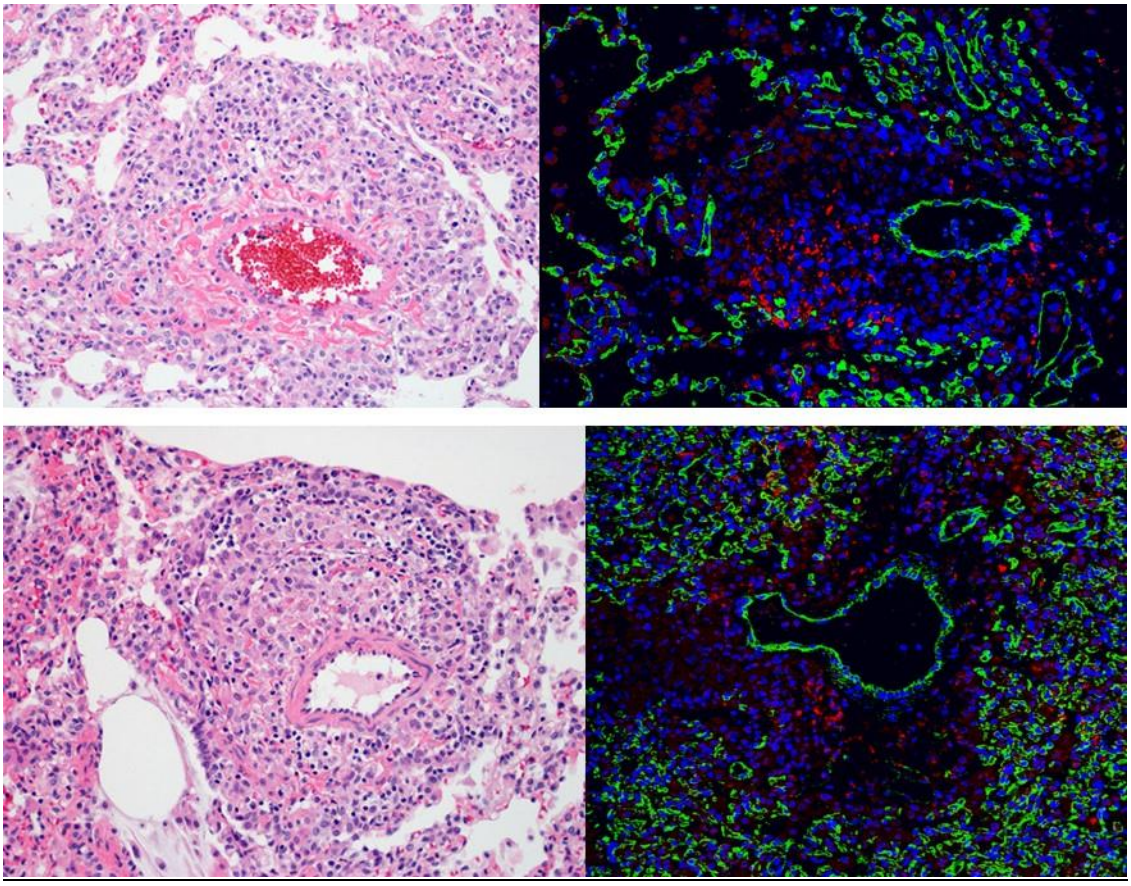

Figure 7: Hematoxylin and eosin staining (left) and immunofluorescence (right) of pulmonary vessels from an ATBI-SIV animal (animal HP22) demonstrating marked perivasculitis. With H&E staining, the perivascular space is markedly expanded by lymphocytes, macrophages, and plasma cells. Immunofluorsescence staining is as follows: green = caveolin-1 (a maker expressed on pulmonary endothelial cell membranes), blue = topro3 (a marker of nuclei), and red = *Mtb* (bacteria and debris). Note *Mtb* (red staining) within perivascular inflammation (blue nuclei surrounding green vessel lumen).

DISCUSSION:

This scoring system shows overall good reproducibility and strong significance, with ability to detect differences between categories of infection for most parameters examined. An exception to this is inducible bronchus-associated lymphoid tissue (iBALT), which was not included in the scoring system analysis because of relatively low intraclass correlation. This is likely due to the high degree of species variability in degree of iBALT accumulation (Tschernig and Pabst, 2000). Indeed, some species, such as rabbits, naturally have a high degree of pulmonary BALT, while in other species, such as monkeys and man, healthy lungs should have little to no BALT, though its formation can be induced in response to inflammation or infection (Chiavolini et al., 2010; Tschernig and Pabst, 2000). Without previous experience in assessing normal macaque lung, it would be difficult to appropriately score this species specific change, even for an experienced veterinary pathologist, and even when scoring reference images are provided in an attempt to assist as this change is really best scored from low magnification. Two of the collaborating pathologists (DNL and RB) did have NHP experience; however, the remaining collaborator did not, which may explain the discrepancy in this category.

Remaining parameters, however, showed relatively strong agreement between pathologists. The most significant findings were the ability to distinguish histologic differences between ATBI and LTBI animals. Of the parameters examined, the most striking differences between these disease categories were noted in degree of consolidation, increase in alveolar macrophages, degree of type II pneumocyte hyperplasia, degree of perivasculitis, and degree of vasculitis/lymphangitis. For all of these categories, ATBI animals were more likely to be affected than LTBI animals, with strongly significant p values for all parameters. LTBI animals showed more likelihood of average and maximum septal thickness and cellularity in the absence of SIV infection in comparison to ATBI infection. While this seems

counterintuitive, we have reported similar findings in an earlier study (Foreman et al., 2016). It may be that LTBI animals septa are expanded by increased protein in comparison to ATBI animals, though the true reason for this change remains unknown. The use of special stains to better characterize this thickening (i.e. Masson's Trichrome for collagen) or potential electron microscopy may be of some benefit in future. In co-infected animals, pathology parameters changed in the same direction, though associations were generally less strong.

In addition to determining differences between pathology parameters based on disease category, the parameters were combined to create models used to attempt to predict disease category based on scoring criteria. The model showed very strong ability to distinguish between factors consistent with TB infection vs. those consistent with SIV infection. In this model, the factors most associated with TB were degree of consolidation out of 5 and degree of alveolar macrophages, both of which were most significantly increased in ATBI. The categories most strongly associated with SIV infection were type II pneumocyte hyperplasia, degree of perivasculitis, and average septal thickness. The fact that type II pneumocyte hyperplasia is strongly associated with SIV infection is logical, as this feature is often strongly associated with viral associated pneumonias (Kumar et al., 2015). The model showed good ability to accurately predict disease status, with particularly strong ability to detect ATBI status. While with this model there is some possibility for misclassifying ATBI infection as SIV infection based purely off of the model if the SIV model results are not compared to the ATBI scoring system results, in reality this is unlikely to occur as the infection status of the animal is likely to be known, and—even if not—other supporting evidence of viral infection, such as the presence of syncytial cells, would likely help the trained pathologist to suspect SIV co-infection. Furthermore, pathologist

interpretation is required for model generation in the first place. With SIV coinfection, the ability to detect differences between LTBI-SIV and ATBI disease states becomes more difficult, which likely points to the effect that SIV co-infection has on increasing pathology parameters, as outlined elsewhere in the manuscript and as shown by decreasing strength of odds ratios in Table 3.

Granulomas were more common in *Mtb* infected monkeys than in those that were not infected with *Mtb*, as expected. However, no additional interpretation on granulomas' significance and their potential role in a pathologic scoring system can be made at this time, as their presence was only assessed as present or absent. This was done in part to focus on the non-granulomatous changes in the remainder of the lung, as numerous studies have emphasized granulomatous pathology with no significant differences detected between active and latent states (Capuano et al., 2003; Lin et al., 2009; Mehra et al., 2013; Sharpe et al., 2009). However, in future studies, including granuloma assessment would be valuable to determine if there are differences between ATBI and LTBI, particularly if specific granuloma parameters including size, organization and structure, percentage of necrosis, and percent of section affected were assessed. However, to be most complete, serial sections of lung would likely need to be compared for each selected section to allow for evaluation of the 3 dimensional structure of the granuloma if evaluating certain of those parameters (such as degree of necrosis or granuloma subtype), as plane of section can artificially skew appearances of these structures. Participation in a recent study evaluating Indoleamine 2,3-dioxygenase (IDO) expression and tryptophan inhibition suggested that percentage of granuloma necrosis may be correlated with degree of IDO expression and cellular infiltration (not yet published), and it would be interesting to see how those findings may correlate with disease status if at all.

Much of the initial interest in this work was aimed at the hopes to better understand dissemination of *Mtb* bacilli within the lungs as well as to better elucidate pathophysiologic mechanisms behind disease synergism between *Mtb* and HIV/SIV co-infection. Immunofluorescence staining demonstrated numerous intact and degraded *Mtb* bacilli within perivascular inflammation. With perivasculitis being more prevalent in ATBI and SIV-ATBI animals, it is possible that this lesion may contribute to or facilitate dissemination of bacilli throughout the tissue. While the mechanisms of synergism remain poorly understood, better characterization of the morphologic changes in these disease states may provide a framework in which to ask additional research questions in the future, particularly in regards to vascular-associated pathology and its relation to disease progression.

This study, as with many NHP studies faces several limitations. The largest of these is sample size. This was a retrospective study by nature, and thus reliant on being able to access materials within the archives. While larger numbers of animals and slides were initially scored by the primary pathologist (DNL), it was not feasible to have all of those sections scored by all pathologists for this project. Thus, a smaller subset of representative sections from 3 animals per TB treatment group were examined, with 5-6 sections scored in replicate to increase confidence. Only 3 pathologists scored each of the sections as well, only 2 of whom had NHP experience. In future, it would be ideal to include more animals in each group and potentially more blinded pathologists, both with and without NHP experience, to increased the robustness of the dataset, and to likely increase the strength of some of the associations and the generated models. However, even with these constraining factors, the strength of the odds ratios and significance of the p-values were very strong for most of the examined categories, indicating a strong foundation for the scoring system that would likely only be solidified by an increased sample size.

In our study, this scoring system is applied only to Indian origin Rhesus macaques. Cynomolgus macaques are the other most commonly used NHP for the study of TB, both alone and in the setting of SIV co-infection. It would be valuable to apply this scoring system to that species to determine if the changes observed in Rhesus macaques are applicable to Cynomolgus macaques, and from there, potentially, to humans. There is an established scoring system for evaluating overall changes in gross pathology between Cynomolgus macaques with ATBI and LTBI (Lin et al., 2009) and there is one for using imaging criteria to detect differences, in combination with that gross scoring system, in Rhesus macaques (Sharpe et al., 2009). Combining those systems with the microscopic criteria established here could provide the most complete assessment for differences in disease categories in experimentally infected animals, and could help to elucidate mechanisms heretofore poorly understood that may be involved in disease progression.

Ultimately, this study adds support to the notion that thorough morphologic evaluation by trained pathologists can provide valuable information in translational research settings, particularly in studies involving pulmonary inflammation (Meyerholz et al., 2018). The methodology used in this study is strong and repeatable, and was able to demonstrate both key differences between ATBI and LTBI in this animal model, as well as to illustrate changes with SIV coinfection in each of these groups. Importantly, ATBI animals had higher scores and a greater likelihood of pathology in the areas of consolidation, increase in alveolar macrophages, degree of type II pneumocyte hyperplasia, degree of perivasculitis, and degree of vasculitis/lymphangitis; SIV-coinfection worsened each of these categories in both ATBI and LTBI infected animals. Importantly, this work also demonstrates that may features typically attributed to SIV-related pathology in early work (Foreman et al., 2016; Foreman et al. 2017) may indeed be features of *Mtb* infection itself; this further highlights the importance

of a systematic approach for evaluation of these parameters. Finally, epidemiological approaches to modeling that emerged from this work demonstrate a strong capability of this scoring system to both accurately categorize and predict disease states based on this scoring system, which has applications to future research in this area. Many of the included parameters in this study are subtle, and would be likely to be missed by those without specific, advanced training in comparative histopathology. However, by working collaboratively with immunologists, microbiologists, and aerobiologists, together we may be able to advance the study of tuberculosis beyond what any of us could do in isolation. And that, perhaps, is how we can move forward.

REFERENCES

Aaron, L., Saadoun, D., Calatroni, I., Launay, O., Mémain, N., Vincent, V., Marchal, G., Dupont, B., Bouchaud, O., Valeyre, D., et al. (2004). Tuberculosis in HIV-infected patients: a comprehensive review. Clin. Microbiol. Infect. *10*, 388–398.

Brosch, R., Gordon, S.V., Marmiesse, M., Brodin, P., Buchrieser, C., Eiglmeier, K., Garnier, T., Gutierrez, C., Hewinson, G., Kremer, K., et al. (2002). A new evolutionary scenario for the *Mycobacterium tuberculosis* complex. Proc. Natl. Acad. Sci. *99*, 3684–3689.

Capuano, S.V., Croix, D.A., Pawar, S., Zinovik, A., Myers, A., Lin, P.L., Bissel, S., Fuhrman, C., Klein, E., and Flynn, J.L. (2003). Experimental Mycobacterium tuberculosis Infection of Cynomolgus Macaques Closely Resembles the Various Manifestations of Human M. tuberculosis Infection. Infect. Immun. *71*, 5831–5844.

Chiavolini, D., Rangel-Moreno, J., Berg, G., Christian, K., Oliveira-Nascimento, L., Weir, S., Alroy, J., Randall, T.D., and Wetzler, L.M. (2010). Bronchus-associated lymphoid tissue (BALT) and survival in a vaccine mouse model of tularemia. PloS One *5*, e11156.

Christensen, R. H. B. (2018). ordinal - Regression Models for Ordinal Data. R package version 2018.8-25. http://www.cran.r-project.org/package=ordinal/.

Cronan, M.R., Beerman, R.W., Rosenberg, A.F., Saelens, J.W., Johnson, M.G., Oehlers, S.H., Sisk, D.M., Jurcic Smith, K.L., Medvitz, N.A., Miller, S.E., et al. (2016). Macrophage Epithelial Reprogramming Underlies Mycobacterial Granuloma Formation and Promotes Infection. Immunity *45*, 861–876.

Cross, S.S. (1998). Grading and scoring in histopathology. Histopathology *33*, 99–106.

Dutta, N.K., Mehra, S., Didier, P.J., Roy, C.J., Doyle, L.A., Alvarez, X., Ratterree, M., Be, N.A., Lamichhane, G., Jain, S.K., et al. (2010). Genetic Requirements for the Survival of Tubercle Bacilli in Primates. J. Infect. Dis. *201*, 1743–1752.

Foreman, T.W., Mehra, S., LoBato, D.N., Malek, A., Alvarez, X., Golden, N.A., Bucşan, A.N., Didier, P.J., Doyle-Meyers, L.A., Russell-Lodrigue, K.E., et al. (2016). CD4 $^{+}$ T-cell–independent mechanisms suppress reactivation of latent tuberculosis in a macaque model of HIV coinfection. Proc. Natl. Acad. Sci. *113*, E5636–E5644.

Foreman, T.W., Veatch, A.V., LoBato, D.N., Didier, P.J., Doyle-Meyers, L.A., Russell-Lodrigue, K.E., Lackner, A.A., Kousoulas, K.G., Khader, S.A., Kaushal, D., et al. (2017). Nonpathologic Infection of Macaques by an Attenuated Mycobacterial Vaccine Is Not Reactivated in the Setting of HIV Co-Infection. Am. J. Pathol. *187*, 2811–2820.

Gamer, Matthias, Jim Lemon and Ian Fellows Puspendra Singh <puspendra.pusp22@gmail.com> (2012). irr: Various Coefficients of Interrater. Reliability and Agreement. R package version 0.84. https://CRAN.R-project.org/package=irr

Gardner, M.B., and Luciw, P.A. (2008). Macaque Models of Human Infectious Disease. ILAR J. *49*, 220–255.

Gibson-Corley, K.N., Olivier, A.K., and Meyerholz, D.K. (2013). Principles for Valid Histopathologic Scoring in Research. Vet. Pathol. *50*, 1007–1015.

Kaushal, D., Mehra, S., Didier, P.J., and Lackner, A.A. (2012). The non-human primate model of tuberculosis. J. Med. Primatol. *41*, 191–201.

Klopfleisch, R. (2013). Multiparametric and semiquantitative scoring systems for the evaluation of mouse model histopathology - a systematic review. BMC Vet. Res. *9*, 123.

Kumar, Vinay, AK Abbas, and JC Aster. (2015). Robbins and Cotran pathologic basis of disease (Philadelphia, PA: Elsevier/Saunders).

Kuznetsova A, Brockhoff PB and Christensen RHB (2017). "lmerTest Package: Tests in Linear Mixed Effects Models." _Journal of Statistical Software_, *82*(13), pp. 1-26. doi: 10.18637/jss.v082.i13 (URL: http://doi.org/10.18637/jss.v082.i13).

Lin, P.L., Rodgers, M., Smith, L., Bigbee, M., Myers, A., Bigbee, C., Chiosea, I., Capuano, S.V., Fuhrman, C., Klein, E., et al. (2009). Quantitative Comparison of Active and Latent Tuberculosis in the Cynomolgus Macaque Model. Infect. Immun. *77*, 4631–4642.

Martinot, A.J. (2018). Microbial Offense vs Host Defense: Who Controls the TB Granuloma? Vet. Pathol. *55*, 14–26.

Mehra, S., Golden, N.A., Dutta, N.K., Midkiff, C.C., Alvarez, X., Doyle, L.A., Asher, M., Russell-Lodrigue, K., Monjure, C., Roy, C.J., et al. (2011). Reactivation of latent tuberculosis in rhesus macaques by coinfection with simian immunodeficiency virus. J. Med. Primatol. *40*, 233–243.

Mehra, S., Alvarez, X., Didier, P.J., Doyle, L.A., Blanchard, J.L., Lackner, A.A., and Kaushal, D. (2013). Granuloma Correlates of Protection Against Tuberculosis and Mechanisms of Immune Modulation by Mycobacterium tuberculosis. J. Infect. Dis. *207*, 1115–1127.

Meyerholz, D.K., Sieren, J.C., Beck, A.P., and Flaherty, H.A. (2018). Approaches to Evaluate Lung Inflammation in Translational Research. Vet. Pathol. *55*, 42–52.

Palmer, M.V. (2018). Emerging Understanding of Tuberculosis and the Granuloma by Comparative Analysis in Humans, Cattle, Zebrafish, and Nonhuman Primates. Vet. Pathol. *55*, 8–10.

Pawlowski, A., Jansson, M., Sköld, M., Rottenberg, M.E., and Källenius, G. (2012). Tuberculosis and HIV Co-Infection. PLoS Pathog. *8*.

Scanga, C.A., and Flynn, J.L. (2014). Modeling Tuberculosis in Nonhuman Primates. Cold Spring Harb. Perspect. Med. *4*.

Sharpe, S.A., Eschelbach, E., Basaraba, R.J., Gleeson, F., Hall, G.A., McIntyre, A., Williams, A., Kraft, S.L., Clark, S., Gooch, K., et al. (2009). Determination of lesion volume by MRI and stereology in a macaque model of tuberculosis. Tuberculosis *89*, 405–416.

Tschernig, T., and Pabst, R. (2000). Bronchus-associated lymphoid tissue (BALT) is not present in the normal adult lung but in different diseases. Pathobiol. J. Immunopathol. Mol. Cell. Biol. *68*, 1–8.

Venables, W.N., and Ripley, B.D. (2002). Modern Applied Statistics with S (New York: Springer-Verlag).

WHO | Global tuberculosis report 2017.

CHAPTER 4: CD4$^+$ T CELL-INDEPENDENT MECHANISMS SUPPRESS REACTIVATION OF LATENT TUBERCULOSIS IN A MACAQUE MODEL OF HIV CO-INFECTION

Summary of my contribution to the work:

Developed and applied a novel scoring system in a blinded fashion to assess pulmonary pathology for sections of all lung lobes for 5 animals per treatment group. Performed some of the statistical analyses to assess differences between groups. Performed chromagen immunohistochemical staining for lymphoid follicle identification. Wrote pathology portion of the manuscript, and took and edited pathology photomicrographs. Collaborated on preparing figures for publication. Edited manuscript prior to publication. The manuscript is provided below as it was published in the 2016 *Proceedings of the National Academy of Sciences of the United States of America* 113(38): E5636-E5644.

Short title:

Novel immune control of reactivation of latent TB

Taylor W. Foreman[a,b,1], Smriti Mehra[a,c,d,1], Denae N. LoBato[a], Adel Malek[e], Xavier Alvarez[a], Nadia A. Golden[a], Allison N. Bucşan[a,b], Peter J. Didier[a], Lara A. Doyle[a], Kasi E. Russell-Lodrigue[a], Chad J. Roy[a], James L. Blanchard[a], Marcelo J. Kuroda[a], Andrew A. Lackner[a,b], John Chan[e], Shabaana A. Khader[f], William R. Jacobs, Jr.[e,2], and Deepak Kaushal[a,b,2]

[a]Tulane National Primate Research Center, Covington, LA, 70471, USA; [b]Department of Microbiology and Immunology, Tulane University School of Medicine, New Orleans, LA, 70112, USA; [c]Center for Biomedical Research Excellence, Louisiana State University School of Veterinary Medicine, Baton Rouge, LA, 70803, USA; [d]Department of Pathobiological Sciences, Louisiana State University School of Veterinary Medicine, Baton Rouge, LA, 70803, USA; [e]Department of Microbiology and Immunology, Howard Hughes Medical Institute, Albert Einstein College of Medicine, Bronx, New York, USA; [f]Department of Molecular Microbiology, Washington University School of Medicine, St. Louis, Missouri, 63110, USA

[1]Contributed equally

[2]To whom correspondence may be addressed:

Deepak Kaushal, Ph.D., Professor of Microbiology and Immunology, Tulane University School of Medicine and Tulane National Primate Research Center, 18703 Three Rivers Road, Covington, Louisiana, 70433, USA; Tel. 1-985-871-6254; dkaushal@tulane.edu

or William R. Jacobs, Jr., Ph.D., Howard Hughes Investigator and Professor of Microbiology and Immunology, Albert Einstein College of Medicine, 1301 Morris Park Avenue, Bronx, New York, 10461, USA; Tel. 1-718-678-1075; jacobsw@hhmi.org

Abbreviations: ATB, active TB; BAL, bronchoalveolar lavage; BCG, bacille Calmette-Guérin; CFU, colony-forming unit; CRP, C-reactive protein; CXR, thoracic radiograph, chest X-ray; iBALT, inducible bronchus-associated lymphoid tissue; LTBI, latent tuberculosis infection; *Mtb, Mycobacterium tuberculosis*; NHPs, non-human primates; NK, natural killer (cells); NKT, natural killer T (cells); PBMC, peripheral blood mononuclear cell; TB, tuberculosis; TNPRC, Tulane National Primate Research Center; TST, tuberculin skin test.

ABSTRACT

The synergy between *Mycobacterium tuberculosis* (*Mtb*) and HIV in co-infected patients has profoundly impacted global mortality due to tuberculosis (TB) and AIDS. HIV significantly increases rates of reactivation of latent TB infection (LTBI) to active disease, with the decline in $CD4^+$ T cells believed to be the major causality. In this study, non-human

primates (NHPs) were co-infected with *Mtb* and simian immunodeficiency virus (SIV), recapitulating human co-infection. A majority of animals exhibited rapid reactivation of *Mtb* replication, progressing to disseminated tuberculosis and increased SIV-associated pathology. Although a severe loss of pulmonary $CD4^+$ T cells was observed in all co-infected macaques, a subpopulation of the animals was still able to prevent reactivation and maintain LTBI. Investigation of pulmonary immune responses and pathology in this cohort demonstrated that increased $CD8^+$ memory T cell proliferation, higher granzyme B production, and expanded B cell follicles correlated with protection from reactivation. Our findings reveal novel mechanisms that control SIV- and TB-associated pathology. These CD4-independent protective immune responses warrant further studies in HIV co-infected humans able to control their TB infection. Moreover, these findings will provide insight into natural immunity to *Mtb* and will guide development of novel vaccine strategies and immunotherapies.

Keywords: Non-human Primate, Macaque, Tuberculosis, CD4 T cells, CD8 T cells, B cells, SIV, Co-infection

SIGNIFICANCE STATEMENT

According to the World Health Organization, one in three humans is latently infected with *Mtb* and 10% of these individuals risk developing active, clinical tuberculosis over their lifetimes. Co-infection with HIV increases this risk substantially, with depletion of $CD4^+$ T cells believed to drive disease progression. Although a minority of co-infected individuals can control the infection, the mechanisms underlying this phenomenon remain unknown. Modeling co-infection using macaques, we discovered that one-third of the animals

maintained latency despite complete ablation of lung $CD4^+$ T cells. We report that protective immune responses mediated by $CD8^+$ T cells and B cells correlate with TB control. These novel findings have important implications in development of both prophylactic and therapeutic measures against TB and AIDS.

INTRODUCTION

The emergence of AIDS in the 1980s resulted in the syndemic relationship with TB whereby progression of each infection exacerbates the other disease (1). Early studies in the murine model highlighted the role for $CD4^+$ T cells in the control of *Mtb* (2), and the initial observations that HIV-induced $CD4^+$ T cell depletion correlated with increased risk of TB disease cemented this paradigm (3, 4). $CD4^+$ T cells respond to infected pulmonary macrophages and limit bacterial growth through synergistic IFN-γ/TNF-α signaling (5); these responses to foci of infected macrophages initiate the formation of the tuberculoid granuloma, which is composed of lymphocytes, macrophages, dendritic cells, and neutrophils (6). The granuloma acts to contain bacteria; however, the events that ensue upon interaction of *Mtb* with the host can result in microenvironmental changes leading to an enduring subclinical infection defined as LTBI (7, 8). Despite the critical role of $CD4^+$ T cells, their influx into granulomas does not necessarily correlate with protection (9). Furthermore, some co-infected patients retain increased risk of reactivation despite maintaining $CD4^+$ T cell counts, and the complete causality of reactivation remains unknown. Nonetheless, $CD4^+$ T cell depletion due to HIV infection remains the prominent justification for increased rates of LTBI reactivation.

Although the innate immune response to TB infection initializes protective responses (10), the granuloma is neither structurally nor functionally complete without T cells that recognize specific *Mtb* antigens (11). $CD8^+$ T cells have an essential, but underappreciated,

role in the control of TB (12) and are critical for both natural and vaccine-induced immunity in NHPs (13, 14). In contrast, the role of B cells in immunity to TB is less well understood, although it appears they are required for the development of optimal immune responses to *Mtb* via various regulatory mechanisms (15-17).

HIV dysregulates many aspects of TB immunity by causing chronic immune activation (18), skewing the T_{reg}/T_H17 balance (19), and perturbing B cell signaling and memory formation (20). HIV further blocks TNF-α-mediated macrophage activation and apoptosis, thus favoring the persistence of *Mtb* (21). While these studies have been informative, the detailed immunological regulation of LTBI reactivation due to HIV co-infection remains to be completely defined.

Macaques serve as excellent models of human *Mtb*-HIV co-infection since they can establish LTBI and are susceptible to SIV, providing a valuable surrogate model for pathogenic HIV infection (22-26). Co-infected macaques recapitulate key aspects of the human disease, including $CD4^+$ T cell depletion, reactivation of LTBI, and dissemination of the bacilli (22, 25). As part of the current investigation, we sought to understand the dynamics of TB disease progression following high-dose SIV co-infection in rhesus macaques and to establish the correlates associated with reactivation of LTBI. Our results indicate that a significant minority of macaques with LTBI did not exhibit reactivation immediately after SIV co-infection, despite productive viremia and substantial depletion of pulmonary $CD4^+$ T cells during the acute phase of SIV infection. Instead, protective immune responses were characterized by memory $CD8^+$ T cell proliferation and the expanded presence of bronchus-associated lymphoid tissue (BALT), correlating with increased control of LTBI after SIV co-infection.

RESULTS

Clinical correlates of infection during *Mtb*/SIV co-infection. Thirty-seven macaques were exposed to low-dose aerosols of *Mtb* CDC1551 delivering approximately 25 colony-forming units (CFUs) into the lungs (Fig. 1A). Delivery in a low dose, as opposed to a high dose (e.g., 1000 CFUs) (14) or intermediate dose (e.g., 100 CFUs) (26), was used to establish a state of LTBI devoid of clinical signs of active TB. All animals were infected by *Mtb* as evidenced by conversion of tuberculin skin test (TST) and PRIMAGAM (Table S1). Macaques remaining TST/PRIMAGAM positive at 7 weeks post infection but not exhibiting symptoms of disease, such as elevated serum C-reactive protein (CRP), high thoracic radiograph (CXR) scores, or the presence of culturable *Mtb* in bronchoalveolar lavage (BAL), were deemed asymptomatic and the infection was classified as latent TB (LTB). The quantifiable measures described above were paired with inputs from our veterinarians about respiratory rates, anorexia, pyrexia, and progressive weight loss.

Table S1. Features and infection status of animals used in this study

Animals	Status	Time to humane killing (days from challenge)	TST* (prechallenge)	TST* (postchallenge)	Infection 1 Mtb CDC1551	Infection 2 SIVmac239
EB23	ATB	61	NNN	PPP	25 CFU	
EE25	ATB	104	NNN	PPP	25 CFU	
HA46	ATB	77	NNN	PPP	25 CFU	
HA77	ATB	84	NNN	PPP	25 CFU	
HJ93	ATB	63	NNN	PPP	25 CFU	
DJ57	ATB	75	NNN	PPP	25 CFU	
CG58	ATB	75	NNN	PPP	25 CFU	
HB43	ATB	56	NNN	PPP	25 CFU	
HB38	ATB	71	NNN	PPP	25 CFU	
GN05	ATB	57	NNN	PPP	25 CFU	
GM97	ATB	79	NNN	PPP	25 CFU	
HC20	ATB	144	NNN	PPP	25 CFU	
HC38	ATB	63	NNN	PPP	25 CFU	
HG80	ATB	34	NNN	PPP	25 CFU	
HH06	ATB	34	NNN	PPP	25 CFU	
FE10	LTBI	166	NNN	PPP	25 CFU	
FJ05	LTBI	181	NNN	PPP	25 CFU	
HA90	LTBI	166	NNN	PPP	25 CFU	
HB74	LTBI	181	NNN	PPP	25 CFU	
HC90	LTBI	173	NNN	PPP	25 CFU	
HJ01	LTBI	145	NNN	PPP	25 CFU	
FH68	LTBI	188	NNN	PPP	25 CFU	
CA75	LTBI	106	NNN	PPP	25 CFU	
FR67	LTBI	113	NNN	PPP	25 CFU	
DN97	LTBI	188	NNN	PPP	25 CFU	
IT07	LTBI	135	NNN	PPP	25 CFU	
HC92	LTBI	128	NNN	PPP	25 CFU	
HC60	LTBI	173	NNN	PPP	25 CFU	
HJ91	LTBI	117	NNN	PPP	25 CFU	
ID91	R	127	NNN	PPP	25 CFU	300 TCID50
HT09	R	104	NNN	PPP	25 CFU	300 TCID50
HP22	R	113	NNN	PPP	25 CFU	300 TCID50
HP41	R	111	NNN	PPP	25 CFU	300 TCID50
ID18	R	102	NNN	PPP	25 CFU	300 TCID50
DH56	R	111	NNN	PPP	25 CFU	300 TCID50
DT35	R	114	NNN	PPP	25 CFU	300 TCID50
HT81	R	112	NNN	PPP	25 CFU	300 TCID50
GI94	R	117	NNN	PPP	25 CFU	300 TCID50
ID01	NR	153	NNN	PPP	25 CFU	300 TCID50
HB12	NR	167	NNN	PPP	25 CFU	300 TC1D50
ER44	NR	167	NNN	PPP	25 CFU	300 TCID50
HV08	NR	167	NNN	PPP	25 CFU	300 TCID50
HI36	NR	113	NNN	PPP	25 CFU	300 TCID50

*TST: N and P indicate if the test was negative or positive. Macaques were assessed for positivity to tuberculin at 24, 48, and 72 h after administration. Hence, NNN indicates that the animal was negative for TST at all three time points, whereas PPP indicates a positive response at each of the three time points.

Of the 37 animals exposed to *Mtb*, ten animals developed active TB (ATB) and were excluded from the subsequent LTB/reactivation protocol. This subset and six historical controls (n=16) were used to obtain clinical, microbiological, and lung pathology data for comparison and were defined as the Active TB control group (Fig. 1A, B). Twenty-seven animals did not show signs of active TB by week 9 post *Mtb* infection, such as progressive weight loss (Fig. 1C), pyrexia (Fig. 1D), CRP elevation (Fig. 1E), or radiological presence of pulmonary granulomatous disease (Fig. 1F). This group was classified as the LTB group and animals were randomly divided into two subgroups either to receive SIV intravenously (defined as the LTB test group, n=14), or remain SIV naive (defined as the LTB control group, n=13).

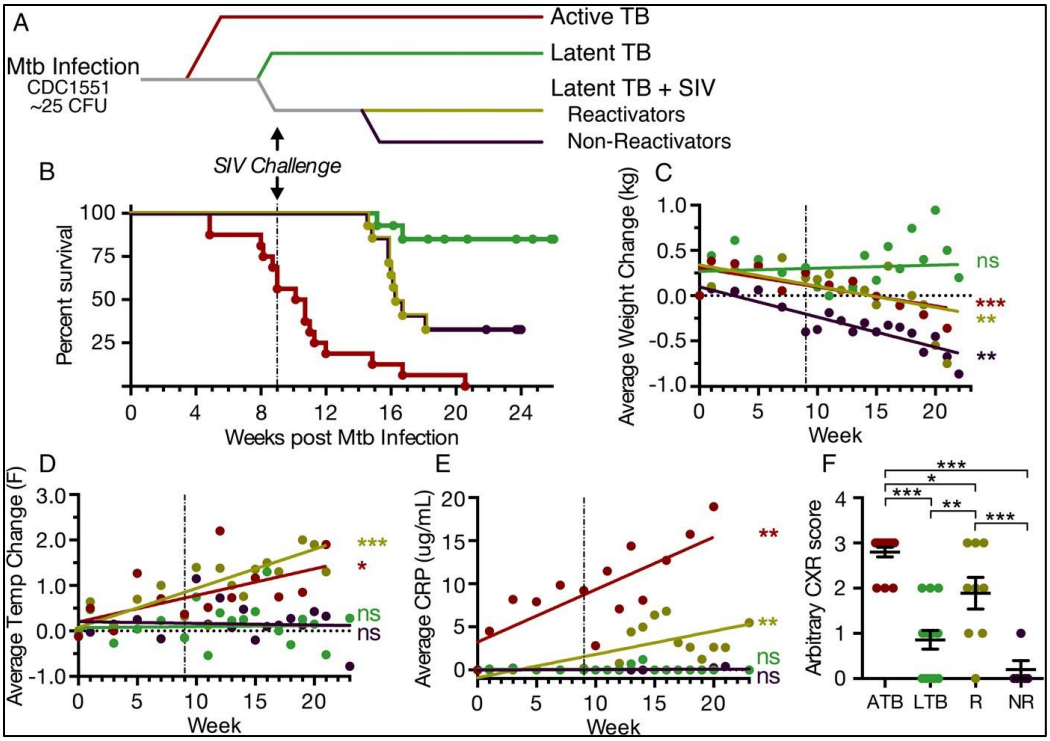

Fig. 1. Clinical correlates of *Mtb*/SIV coinfection. (*A*) Schematic indicating the different animal groups under study and marking key time points shown in *B*. Thirty-seven Indian rhesus macaques were infected with a low dose of *Mtb* CDC1551 (~25 CFU). Coinfected animals were injected with SIVmac239, and LTB control animals were injected with saline only. (*B*) Survival curves, displayed as days after *Mtb* infection. Dashed vertical line indicates day of SIV infection. (*C*) Linear regressions over time of average weight change (in kilograms); (*D*) average temperature change (in °F); (*E*) average serum CRP values (μg/mL); and (*F*) CXR scores, in the four groups: ATB, active TB (red); LTB, latent TB (green); R, coinfected reactivators (gold); NR, coinfected nonreactivators (purple). $*P < 0.05$, $**P < 0.01$, $***P < 0.001$ using (*B*) Wilcoxon test, (*C–E*) Linear regression analysis, and (*F*) one-way ANOVA. Data are means ± SD.

Survival was used as a key reporter of reactivation. Animals developing extensive TB after SIV co-infection were termed reactivators, and these animals were humanely euthanized at prescribed time points after evaluation by our veterinarian, as described in detail in the

methods section. Nine *Mtb*/SIV co-infected animals out of 14 (~64%) in the LTB test group showed reactivated TB and were euthanized within 13-19 weeks post *Mtb* infection. Five co-infected animals (~36%) survived, did not meet the clinical criteria for reactivated TB, and were termed non-reactivators (Fig. 1A, B). This cohort was euthanized 19-21 weeks post *Mtb* infection for collection of tissues for analysis following necropsy. Although these animals maintained LTBI throughout acute SIV infection, they did not develop AIDS within the 10-12 weeks post SIV challenge. A majority of the animals in the LTB control group (11/13, 84%) and none of the animals in the active control group (0/16, 0%) survived to the termination of the study (Fig. 1B). Two animals in the LTB control group spontaneously reactivated despite remaining SIV uninfected throughout the study. The survival difference between the co-infected animals in the LTB test group and the animals in the LTB control group was significant, using both a Wilcoxon ($P = 0.0002$) and a log-rank ($P = 0.0005$) test.

As expected, the ATB control group displayed significant weight loss, recapitulating the wasting seen in human TB (Fig. 1C). Subsequent to SIV co-infection, both reactivators and non-reactivators exhibited significant weight loss compared to the LTB control group, likely due to progressive SIV infection (Fig. 1C). Unlike with weight loss, for pyrexia, results for reactivators were significantly different from those of both non-reactivators and the LTB control group, with temperature increases similar to those of the ATB control group (Fig. 1D). The reactivators and ATB group also displayed higher CRP levels in the peripheral blood, an indication of severe inflammation (Fig. 1E), and they exhibited identical patterns when chest X-rays (CXRs) were analyzed for the severity of granulomatous disease (Fig. 1F). Together, these clinical manifestations highlight the robustness of the NHP model of co-infection for emulating human active, latent, and reactivated TB.

Microbiological aspects of ATB, LTB, and co-infection. We investigated the bacterial burden in BAL and various organs of the infected macaques following euthanasia. Following SIV infection, reactivators exhibited mean BAL CFU values significantly higher (10^4) than those of non-reactivators (~10^2) or animals in the LTB control group, with results indistinguishable from those of animals with ATB (Fig. 2A). Interestingly, two out of five non-reactivating animals showed detectable, culturable *Mtb* in BAL at the endpoint of the study indicating potential late reactivation (Fig. 2A). An approximate mean of 100 bacilli/gram could be cultured from the lung of animals with LTB, indistinguishable from the non-reactivators ($P = 0.988$), whereas a highly significant, ~100-fold increase in bacilli could be cultured from the lungs of reactivators (Fig. 2B); these reactivators had as much culturable *Mtb* in their lungs as animals with ATB (10^4 CFU/gram). We also measured *Mtb* burdens in extrathoracic tissues, including bronchial lymph node (Fig. 2C), spleen (Fig. 2D), liver (Fig. S1) and kidney (Fig. S1). In bronchial lymph node, the CFU burden in both the ATB group and reactivators was significantly higher than in the LTB control group and non-reactivators (Fig. 2C). In general, reactivators not only harbored greater bacterial burden in their spleen, liver, and kidney relative to LTB and non-reactivators but also relative to animals with ATB. These microbiological results display similar qualities to human TB/HIV co-infection where high bacterial burden and increased dissemination have been well documented (27, 28).

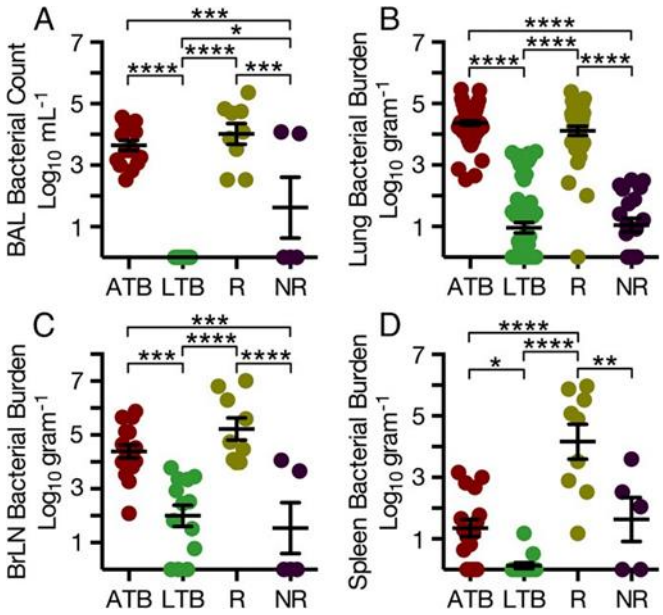

Fig. 2. Bacterial burden in lungs and extrathoracic organs. (*A*) *Mtb* CFUs in total BAL samples and (*B*) per gram of lung tissue at killing shown for each animal, with multiple sections of lung sampled per animal; active TB (ATB), latent TB (LTB), reactivator (R) and nonreactivator (NR) groups. (*C* and *D*) Bacterial burdens per gram of tissue for (*C*) bronchial lymph node and (*D*) spleen. $*P < 0.05$, $**P < 0.01$, $***P < 0.001$, $****P < 0.0001$, one-way ANOVA with Tukey's multiple testing correction.

Peripheral viral loads. Since differential viral replication and titers could possibly explain the differences in the reactivator versus non-reactivator subgroups with respect to reactivation, we measured plasma viral loads after SIV infection in four randomly selected animals from both groups, using previously described methods (22) (Fig. S1). The mean $\log_{10}$ plasma viral load at 2 weeks post-SIV was 7.02 and 6.70 for reactivators and non-reactivators, respectively, and these differences were not significant. Plasma viral loads were not significantly different between the two groups at any time point, clearly suggesting that disparate peripheral viral loads were not the reason for differential reactivation of LTB in the two subsets of the LTB test group.

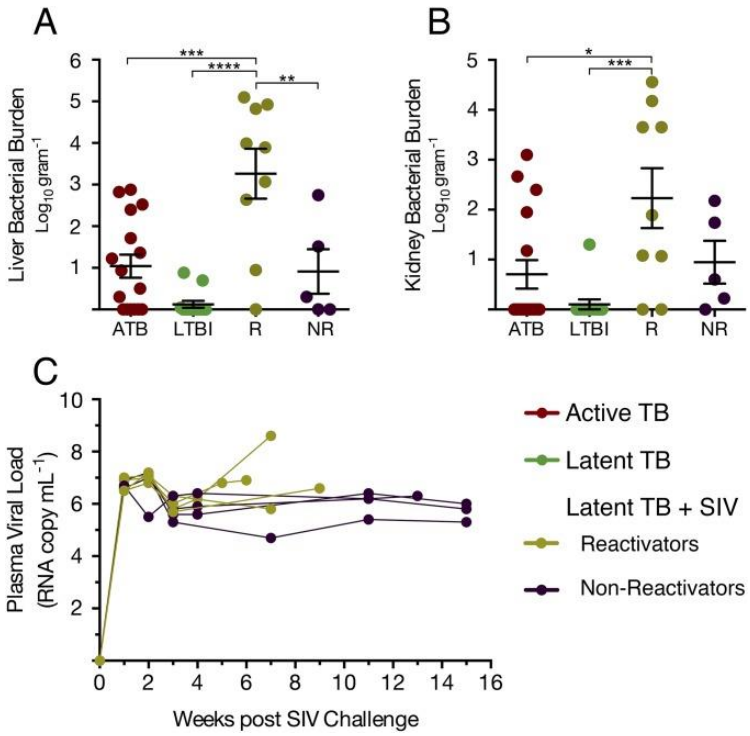

Figure S1: Pathogen burden in the periphery. Bacterial burdens per gram of tissue for (*A*) liver and (*B*) kidney. (*C*) Plasma viral load in reactivators and nonreactivators, shown as weeks after SIV challenge. **P* < 0.05, ***P* < 0.01, ****P* < 0.001, *****P* < 0.0001, using one-way ANOVA with Tukey's multiple testing correction

TB- and SIV-associated pathology. The pulmonary pathology analyses correlated well with clinical and microbiological findings. Co-infected animals that reactivated exhibited significantly more pulmonary lesions relative to non-reactivators and animals from the LTB control group, as determined by gross (Fig. S2) and histopathological examination (Fig. 3A-D), and by morphometric quantitation (Fig. 3E). Thus, the LTB control group animals (Fig. 3B) and non-reactivators (Fig. 3D) had significantly fewer granulomas, with an average of 4-5% of the total lung area affected by TB lesions. These animals also displayed reduced TB-related pathology, inclusive of edema, pneumonia, and generalized foci of inflammation. In contrast, reactivators (Fig. 3C) displayed ~30% lung involvement on average, comparable to

an average involvement of ~40% of the lung of animals with ATB (Fig. 3E). Importantly, the differences in the extent of lung pathology between reactivators and non-reactivators were highly significant ($P = 0.004$), despite a smaller group size for the latter (Fig. 3E).

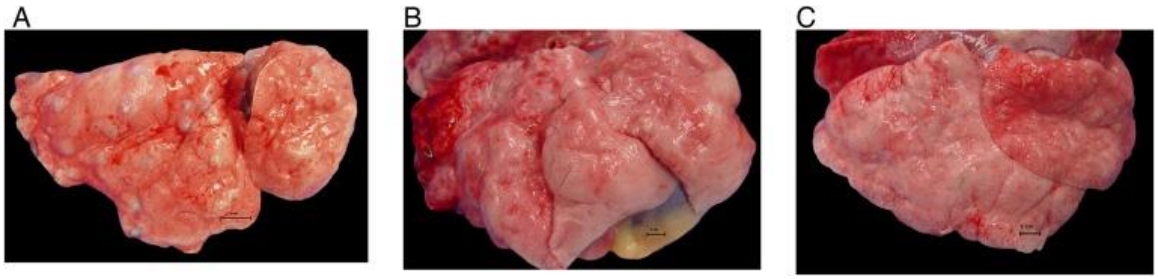

Figure S2: Gross pathology of lung. Gross pathology of lungs at necropsy of (*A*) ATB, (*B*) LTBI, and (*C*) reactivated animals. (Scale bar, 1 cm.)

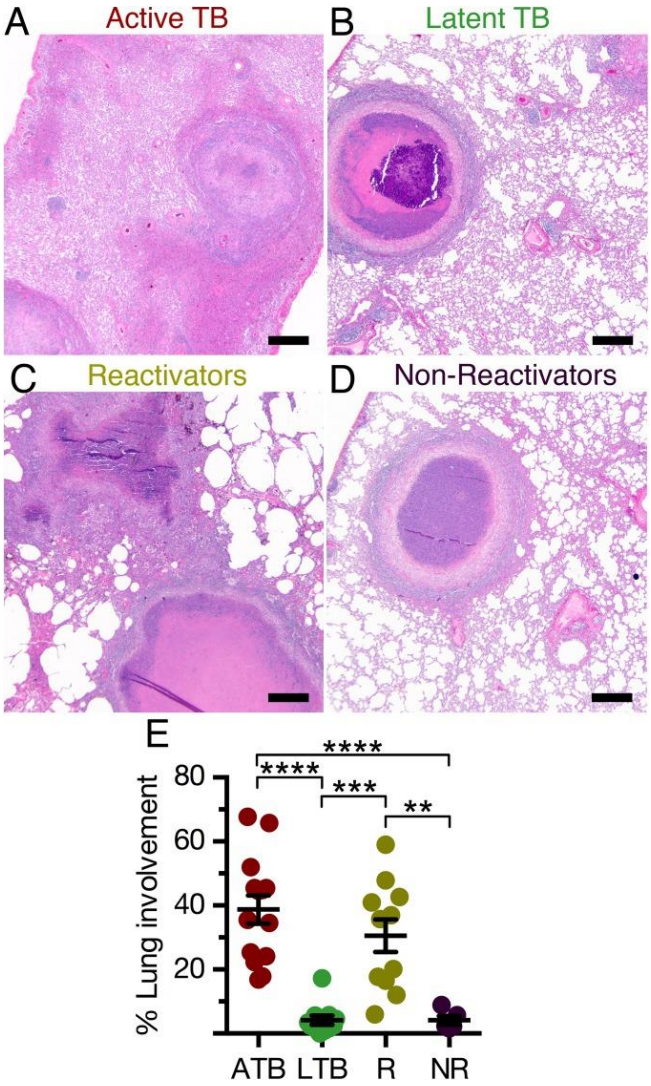

Figure 3: Comparative TB pathology. H&E staining of lung sections from animals with (*A*) ATB, (*B*) LTB, (*C*) *Mtb*/SIV coinfected reactivators, and (*D*) *Mtb*/SIV coinfected nonreactivators. (*E*) Quantification of overall pathology as percentage of lung involvement. (Scale bars, *A*–*D*, 250 μ.) $^{**}P < 0.01$, $^{***}P < 0.001$, $^{****}P < 0.0001$, using a one-way ANOVA with Tukey's multiple testing correction.

All co-infected animals demonstrated lesions consistent with SIV-induced pulmonary pathology, including lymphohistiocytic interstitial pneumonia and septal thickening (Fig. 4A, E), type II pneumocyte hyperplasia (Fig. 4A, F), increased accumulation of foamy alveolar macrophages (Fig. 4G), lymphocytic perivasculitis (Fig. 4B, H), and lymphangitis (Fig. 4C, I).

Whereas all co-infected animals displayed signs of SIV-induced pathology, reactivators showed significantly increased total pathology (Fig. 4D). Moreover, reactivators scored higher than non-reactivators on each measure of pathology (Fig. 4F-I), with the exception of septal thickening (Fig. 4E). Finally, Ziehl-Neelsen staining revealed a high bacterial burden in the lymphocytic perivasculitis lesions, suggesting a possible causality of dissemination to extrathoracic organs (Fig. 4J).

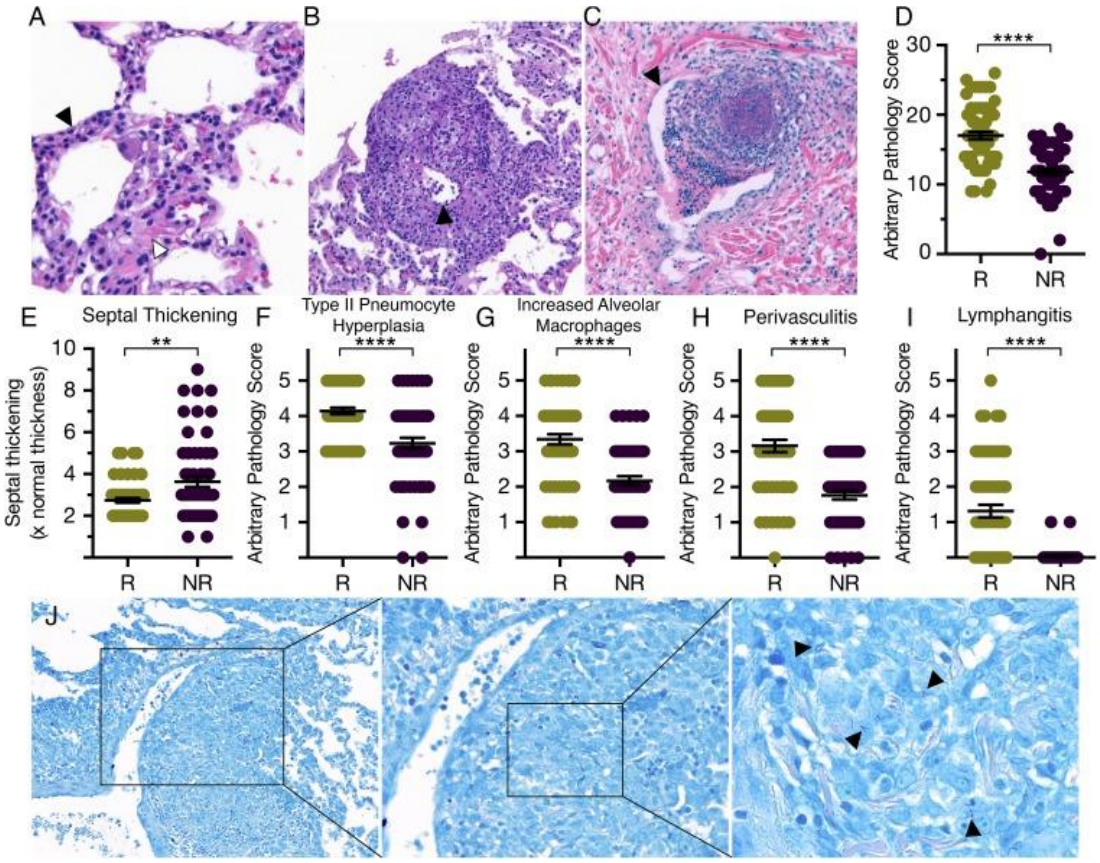

Figure 4: SIV-induced pathology and the presence of bacilli perivascular lesions. H&E staining of lung sections from *Mtb*/SIV coinfected reactivators and nonreactivators displayed exacerbated pathology, including (*A*) interstitial pneumonia with septal thickening (white arrowhead), type II pneumocyte hyperplasia (black arrowhead), and lymphohistiocytic infiltration; (*B*) perivasculitis (black arrowhead showing blood vessel wall); and (*C*) lymphangitis (black arrowhead showing lymphatic vessel membrane). (*D–I*) Multiple lung sections from reactivators and nonreactivators were scored in a single-blinded fashion by a board-certified veterinary

pathologist and quantitatively compared as (*D*) total SIV-induced pathology, (*E*) septal thickening, (*F*) type II pneumocyte hyperplasia, (*G*) increased alveolar macrophages, (*H*) perivasculitis, and (*I*) lymphangitis. Samples from three animals in each group were analyzed, with 12 lung sections analyzed per animal. Each dot corresponds to a section analyzed. $^{**}P < 0.01$; $^{****}P < 0.0001$ using Student's *t* test. (*J*) Ziehl–Neelsen staining revealed the presence of numerous intact, rod-like tubercle bacilli, indicated by black arrowheads in a perivascular lesion in a reactivator. *Right* panel is a magnified image of the boxed region from *Left* and *Center* panels. (Magnification, *A*, 50×; *B*, *C*, and *J*, 40×.)

Although the peripheral viral loads were comparable, the increased SIV-associated pathology may suggest increased viral replication in the lung of reactivators. We therefore further assessed pulmonary viral replication by analyzing lung sections for the presence of SIV mRNA by *in situ* hybridization. Viral titers in serum were similar among all SIV co-infected animals, whereas reactivators harbored significantly more SIV-infected cells (Fig. 5A-D). Whereas the majority of cells infected by SIV were $CD3^+$ T cells (Fig. 5C), a few macrophages ($CD68^+CD163^+$) were also SIV-positive (29). These data, together with the increased TB-associated pathology, demonstrate that both pathogens appear to synergize to overcome the immune control at the microenvironmental level of the granuloma.

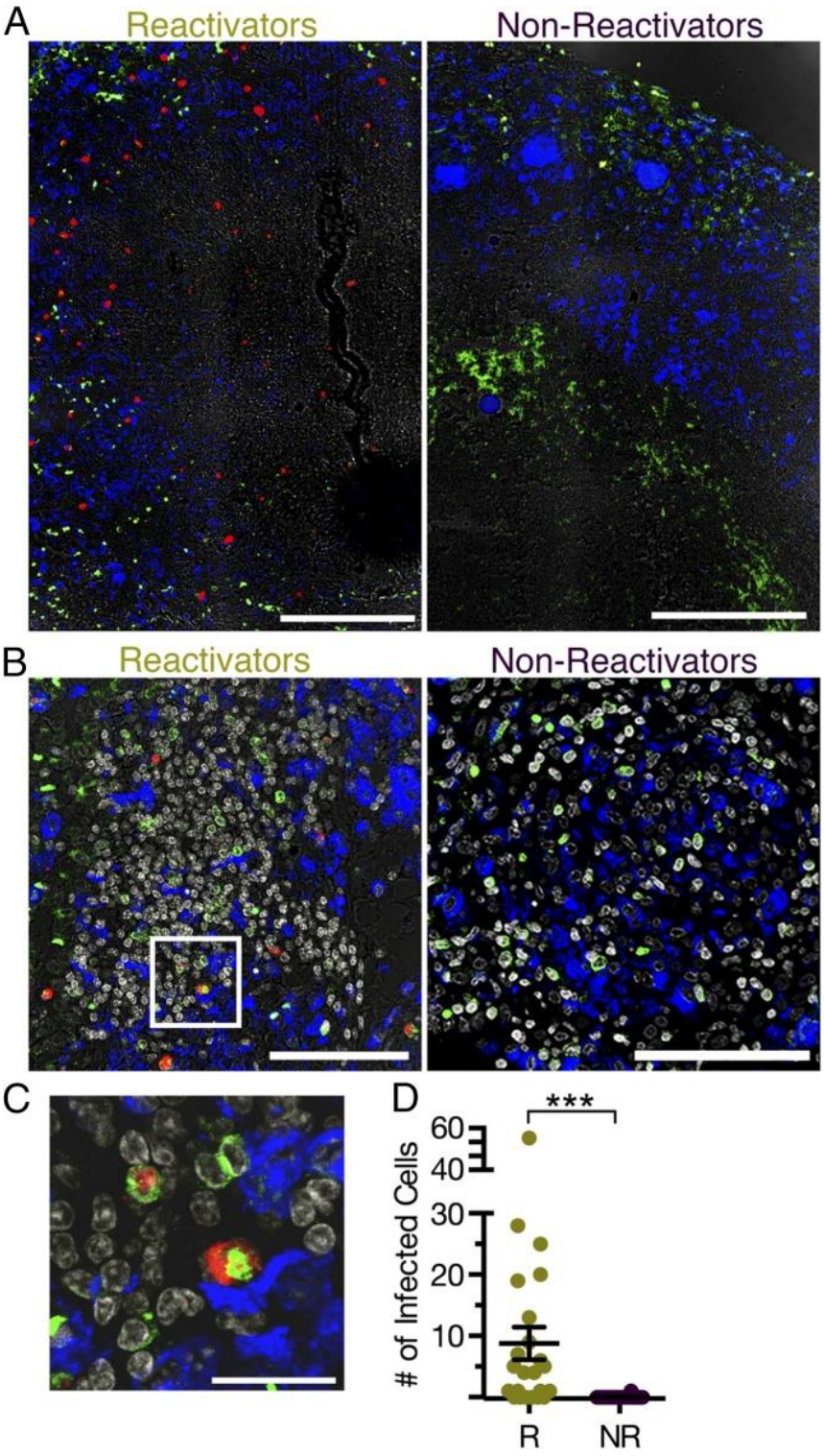

Figure 5: SIV-infected cells in the granulomas of coinfected animals. (*A* and *B*) In situ hybridization of lung tissue demonstrating SIV mRNA in cells (red); macrophages, as marked by both CD68 and CD163, (blue); T cells, as marked by CD3 (green); and differential interference contrast (white). (*A*) Centrally caseating lesions

and (*B*) nonnecrotizing granulomas in reactivators versus nonreactivators show the presence of numerous virus-infected cells in reactivators, with additional nuclei staining in the bottom images (white). (*C*) Close-up image of white box from *B*. (*D*) Quantification of number of infected cells per field of image in reactivators (R) and nonreactivators (NR). ***$P < 0.001$ using Student's *t* test. (Scale bars, *A*, 250 μ; *B*, 100 μ; and *C*, 25 μ.)

Immune correlates of *Mtb*/SIV co-infection. We studied the accumulation of various immune cell types in both whole blood and BAL in a subset of animals from each co-infected group to investigate the kinetics and mechanisms of SIV-mediated reactivation of LTBI in macaques. SIV co-infection led to a massive depletion of $CD4^+$ T cells in the lungs of all co-infected animals. The percentages of $CD4^+$ T cells in BAL of reactivators and non-reactivators dropped to 2.6% and 2.8%, respectively, of $CD3^+$ T cells three weeks after SIV infection (Fig. 6A), in contrast to ~31% in the LTB control group. Notably, the depletion of $CD4^+$ T cells in peripheral blood was actually significantly greater in non-reactivators, comprising 26% of $CD3^+$ lymphocytes compared to 40% in reactivators (Fig. 6B). Greater depletion of $CD4^+$ T cells in tissues relative to the peripheral blood following SIV infection is well documented in both humans and macaques (30), and this was consistent with our findings that the fold change in the CD4:CD8 ratio in the BAL of reactivators and non-reactivators was approximately 12- and 13-fold, respectively (Fig. 6C). On the contrary, the comparative change in whole blood was only ~2-fold in both reactivators and non-reactivators (Fig. 6C). These findings demonstrate the comparable extent of $CD4^+$ T cell depletion from the lungs of animals with two distinct clinical outcomes after SIV co-infection. Moreover, the absolute numbers of $CD4^+$ T cells in BAL of reactivators and non-reactivators were not significantly different (Fig. S3). Consistent with our findings in BAL, $CD4^+$ T cells taken from the lung at euthanasia displayed similar frequencies, comprising ~4% of total $CD3^+$ T cells (Fig. S3).

Furthermore, characterization of lung sections by staining showed comparable spatial distributions of $CD4^+$ cells in pulmonary lesions from both reactivators and non-reactivators (Fig. S3). Taken together, these data demonstrate that comparable depletion of $CD4^+$ T cells occurred in both reactivators and non-reactivators and therefore that this depletion is not responsible for the varying clinical outcomes among the co-infected macaques.

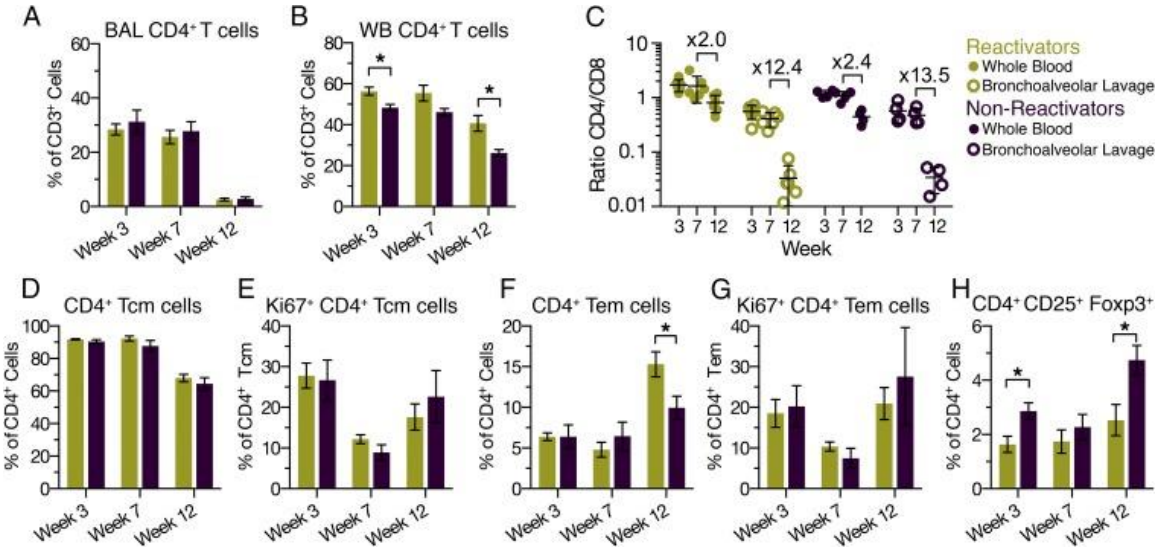

Figure 6: Comparative $CD4^+$ T-cell responses in reactivators and nonreactivators. Comparison of BAL cells from reactivators and nonreactivators in weeks 3 and 7 after *Mtb* infection and week 3 after SIV infection. Quantification of $CD4^+$ T cells in (*A*) BAL and (*B*) whole blood (WB), as a percentage of all $CD3^+$ T cells. (*C*) Ratio of $CD4^+$:$CD8^+$ T cells in whole blood (closed circles) and in BAL (open circles) with indicated fold-change between week 7 after *Mtb* infection and week 3 after SIV infection. (*D*) Analysis of central memory ($CD28^+CD95^+$) $CD4^+$ T cells and (*E*) their proliferation. (*F*) Analysis of effector memory ($CD28^-CD95^+$) $CD4^+$ T cells and (*G*) their proliferation. (*H*) Percentage of T_{reg} cells responding as a percentage of $CD4^+$ T cells. $^*P < 0.05$ using two-way ANOVA. Data are means ± SD.

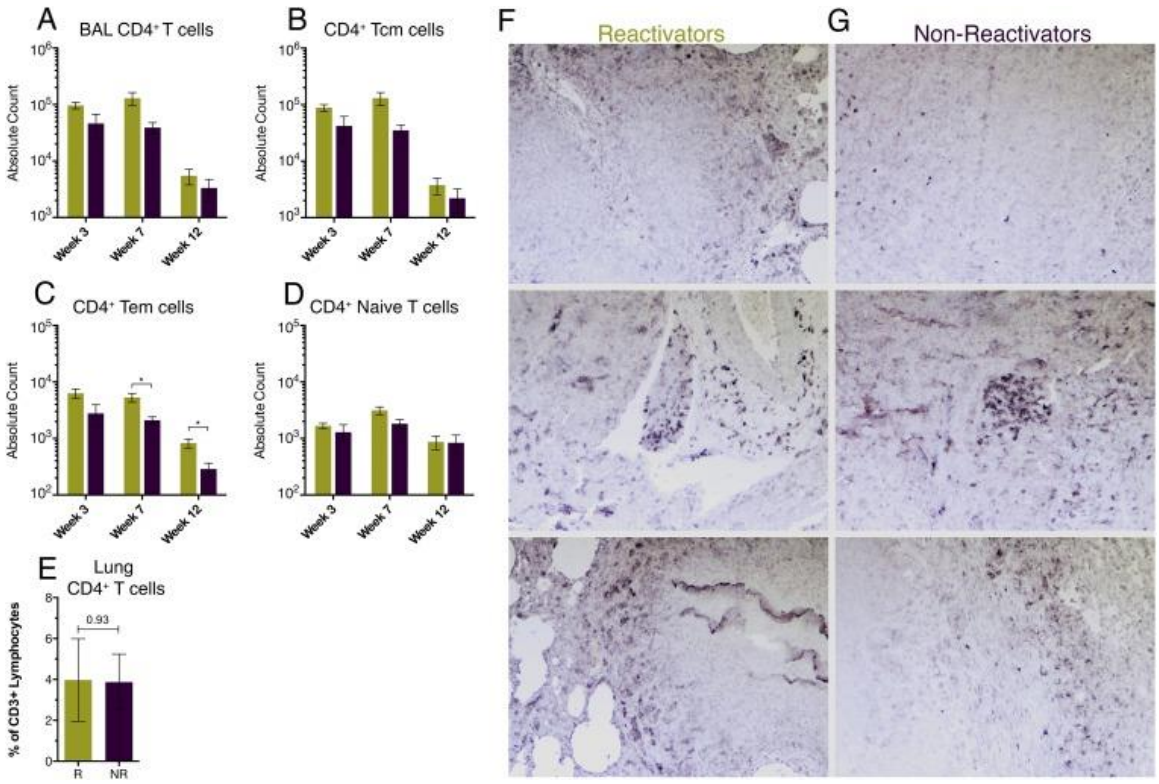

Figure S3: Analysis of CD4+ T cells and CD4 expression in the lung. Flow cytometric analysis of the (*A*) absolute number of CD4+ T cells, (*B*) CD4+T_{CM} cells, (*C*) CD4+ T_{EM} cells, and (*D*) CD4+ naïve T cells in BAL, and (*E*) percentage of CD4+ T cells out of total CD3+ lymphocytes in the lung. *$P < 0.05$ using two-way ANOVA. Data are means ± SD. Chromogenic staining for CD4 in the lungs of (*F*) reactivators and (*G*) nonreactivators in cellular granulomas (*Top*), lymphoid follicles (*Middle*), and necrotizing granulomas (*Bottom*) showing equal depletion and distribution of the remaining CD4+ T cells. (Magnification, *F* and *G*, 40×.)

When comparing different subgroups of the relatively few $CD4^+$ T cells in BAL, there was no significant difference in the percentage of central memory ($CD28^+CD95^+$) cells (Fig. 6D) or their rate of proliferation, as marked by $Ki67^+$ (Fig. 6E). When comparing effector memory cells ($CD28^-CD95^+$), reactivators had a significantly higher percentage of cells in BAL (Fig. 6F), albeit the rate of turnover was not significantly different (Fig. 6G). As expected, the absolute number of central (T_{CM}) and effector (T_{EM}) memory cells sharply declined after SIV

infection, such that both reactivators and non-reactivators retained approximately 4% and 5% T_{CM}, and 15% and 13% T_{EM}, respectively (Fig. S3). When comparing the absolute numbers of memory cells responding, the difference in T_{CM} was not significant between the two groups (Fig. S3), whereas reactivators had significantly more T_{EM} in BAL seven weeks post *Mtb* infection and three weeks post SIV infection (Fig. S3). Comparison of the number of naive ($CD28^+CD95^-$) cells revealed that reactivators and non-reactivators retained approximately 52% and 65%, respectively, indicating that truly naive cells are spared from SIV-induced depletion (Fig. S3). Furthermore, the percentage of $CD4^+$ T regulatory (T_{reg}) cells ($CD25^+Foxp3^+$) found in BAL three weeks after SIV infection was significantly higher in non-reactivators (Fig. 6H). This increase in $CD4^+$ T_{regs} in non-reactivators, coincident with decreased $CD4^+$ T_{em}, suggests a role for these regulatory cells in limiting disease-causing pathology, which was increased in reactivators (Fig. 3, 4). Although there were significantly more T_{CM} in the periphery of non-reactivators (Fig. S4), this finding was not observed at the site of infection (Fig. 6D). Additionally, there was no marked difference in the percentage of $CD4^+$ T cells in peripheral blood expressing the lymph node homing marker CCR7 or the tissue homing marker CCR5 (Fig. S4).

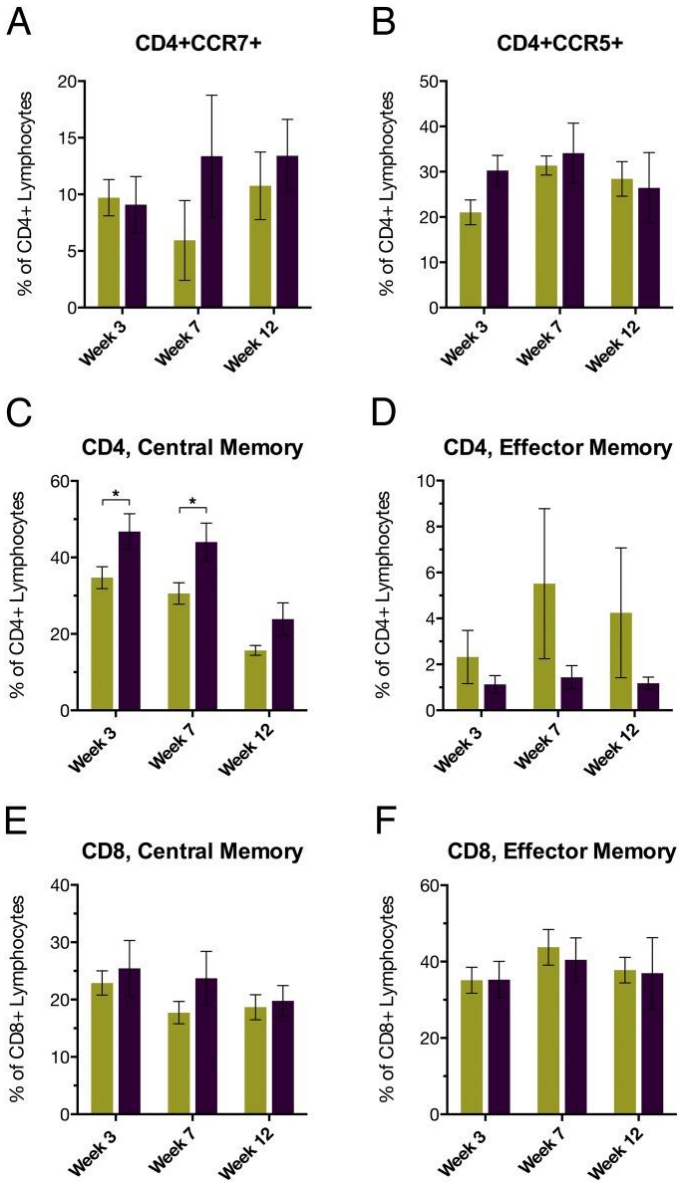

Figure S4: Comparative T-cell responses in peripheral blood. Analysis of whole blood from reactivators and nonreactivators at weeks 3 and 7 after *Mtb*infection and week 3 after SIV infection. Quantification of (*A*) $CD4^+$ $CCR7^+$ cells and (*B*) $CD4^+$ $CCR5^+$ as a percentage of all $CD4^+$ T cells. Analysis of (*C* and *E*) central memory ($CD28^+CD95^+$) and (*D* and *F*) effector memory ($CD28^-CD95^+$), (*C* and *D*) $CD4^+$ and (*E* and *F*) $CD8^+$ T cells. $*P < 0.05$ using two-way ANOVA. Data are means ± SD.

The percentage of $CD8^+$ T cells recruited to BAL expectedly increased due to SIV co-infection, thus contributing to a sharp decrease in the CD4:CD8 ratio in all co-infected animals, irrespective of their reactivation status (Fig. 6C, 7A-B). Whereas there was no statistically significant difference in the percentage or the number of central and effector memory $CD8^+$ T cells present in the BAL after co-infection (Fig. 7C, E), non-reactivators however had a significantly higher rate of turnover, as marked by $Ki67^+$, indicating these cells were active and proliferating (Fig. 7D, F). To further study the role of $CD8^+$ T cells at the site of infection, we assessed the extent of granzyme B production, by immunohistochemistry. Reactivators displayed significantly reduced production of granzyme B in the lungs as compared to the non-reactivators (Fig. 7G-I), indicating a correlation between increased granzyme B production, which occurs at least partly within $CD8^+$ T cells (31, 32), and increased control of both SIV- and TB-associated pathology. Although the majority of cells expressing granzyme B were $CD3^+$ lymphocytes (Fig. 7H), natural killer (NK) cells likely represent the CD3-negative cells producing granzyme B. We used flow cytometry to further assess whether the disparate responses in the two subgroups following SIV co-infection could result from changes in the profiles of natural killer T (NKT) cells or NK cells. Changes in the percentage and absolute numbers of NKT ($CD3^+CD8^+CD56^+$) and NK ($CD3^-CD8^+CD56^+$) cells, including subsets expressing perforin, were not significantly different based on the reactivation phenotype (Fig. S5). However, there was a general trend towards slightly greater accumulation of both NKT and NK cells in the lungs of non-reactivators relative to reactivators. Together, these data showing increased proliferation in both the central and effector memory populations lend credence to the roles of $CD8^+$ T cells and granzyme B in the control of *Mtb* infection.

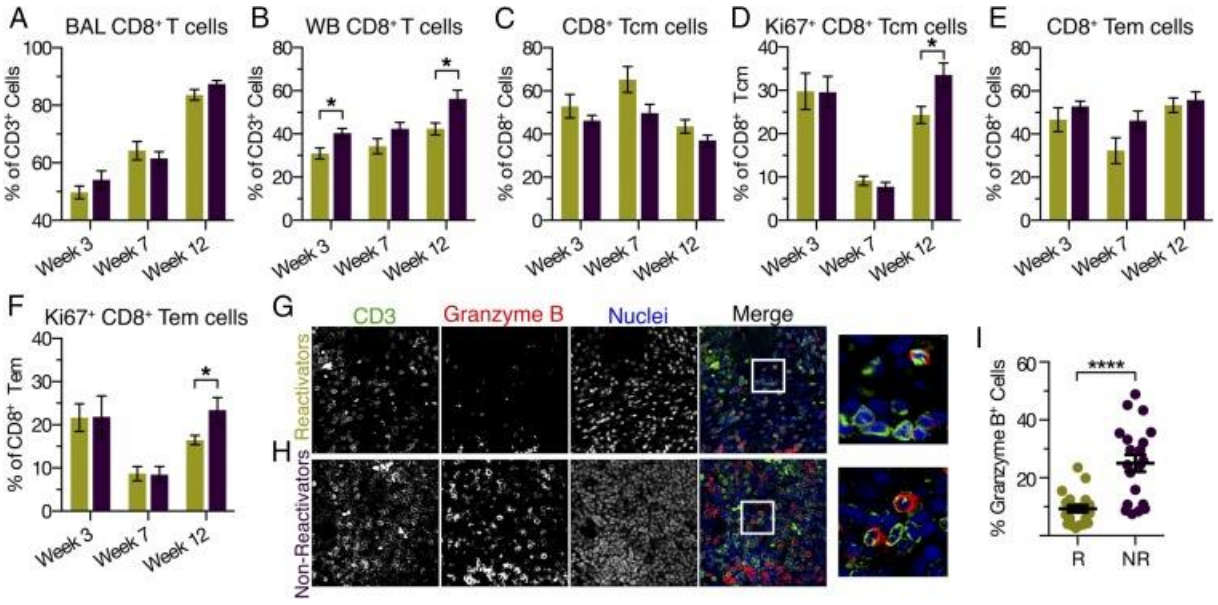

Figure 7: Proliferative and functional CD8+ T-cell responses. Analysis of CD8+ T cells in (*A*) BAL and (*B*) whole blood, as a percentage of all CD3+T cells. (*C*) Analysis of central memory CD8+ T cells and (*D*) their proliferation. (*E*) Analysis of effector memory CD8+ T cells and (*F*) their proliferation. Immunohistochemical staining for (*G*) reactivators and (*H*) nonreactivators; in greyscale for (*Left*) CD3, (*Center Left*) granzyme B, and (*Center Right*) nuclei, and in color for (*Right*) merged images of lung sections. Far *Right* panel is a magnified image of the boxed region from the proximal panels. (Magnification, *G* and *H*, 40×.) (*I*) Quantification of the percentage of cells producing granzyme B. *$P < 0.05$; ****$P < 0.0001$ (*A*–*F*) using two-way ANOVA or (*I*) using Student's *t* test. Data are means ± SD (*A*–*F, I*) reactivators (R), gold; nonreactivators (NR), purple.

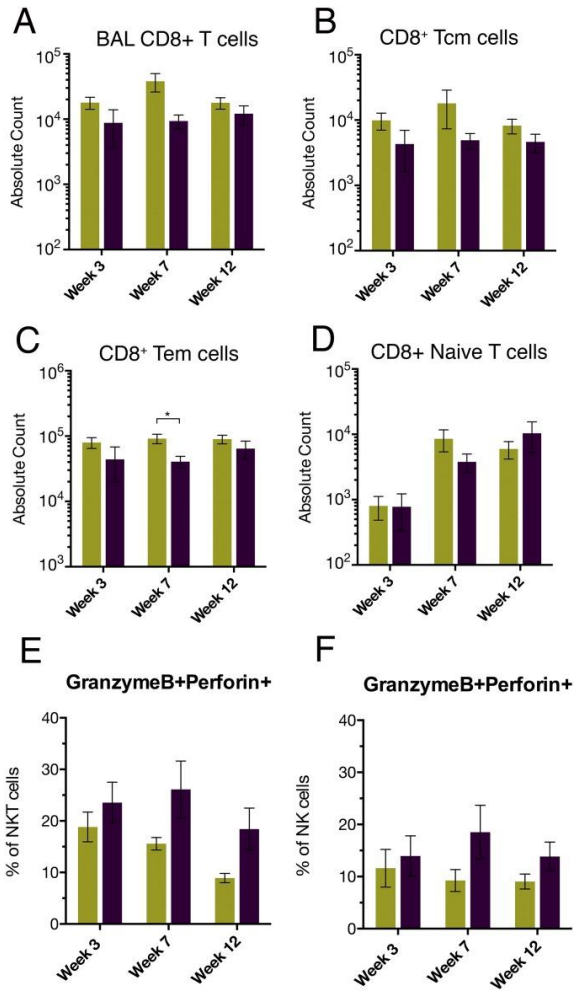

Figure S5: Analysis of CD8$^+$ T cells in the lung. Flow cytometric analysis of the (*A*) absolute number of CD8$^+$ T cells, (*B*) CD8$^+$ T_{CM} cells, (*C*) CD8$^+$$T_{EM}$ cells, and (*D*) CD8$^+$ naïve T cells in BAL. Analysis of granzyme B and perforin production in (*E*) NKT cells (CD56$^+$CD8$^+$CD3$^+$) and (*F*) NK cells (CD56$^+$CD8$^+$CD3$^-$) in BAL. *$P < 0.05$ using two-way ANOVA. Data are means ± SD.

Bronchus-associated lymphoid tissue proximal to granulomas. We have previously demonstrated that the presence of inducible lymphoid follicles, also termed inducible bronchus-associated lymphoid tissue (iBALT), correlates with protection from TB (33). Animals with LTBI harbor greater areas of iBALT within lung lesions relative to animals with ATB, in which BALT was replaced by neutrophils (34). In our current study, non-

reactivators often formed multiple, well-organized areas of lymphoid follicles, as observed by hematoxylin and eosin staining, as well as by chromogenic staining against CD20 (Fig. 8A-D). Although there is complete ablation of $CD4^+$ T cells in the lungs, BALT still persisted in non-reactivators, occupying a greater average percentage area of the lungs than in reactivators (Fig. 8E-F). Protection strongly correlates with extensive BALT formation as we have observed that macaques mucosally vaccinated with a BALT-inducing isogenic mutant, *Mtb ΔsigH,* exhibited complete protection upon lethal challenge (14). Notably, iBALT in non-reactivators exclusively harbored tingible body macrophages (Fig. 8G), specialized macrophages that are involved in germinal center reactions (35) and that are especially critical for the phagocytosis of apoptotic B cells undergoing affinity maturation (36). Overall, our findings indicate that protection from reactivation of *Mtb* infection occurs independently of $CD4^+$ T cell depletion and correlates rather with increased levels of iBALT.

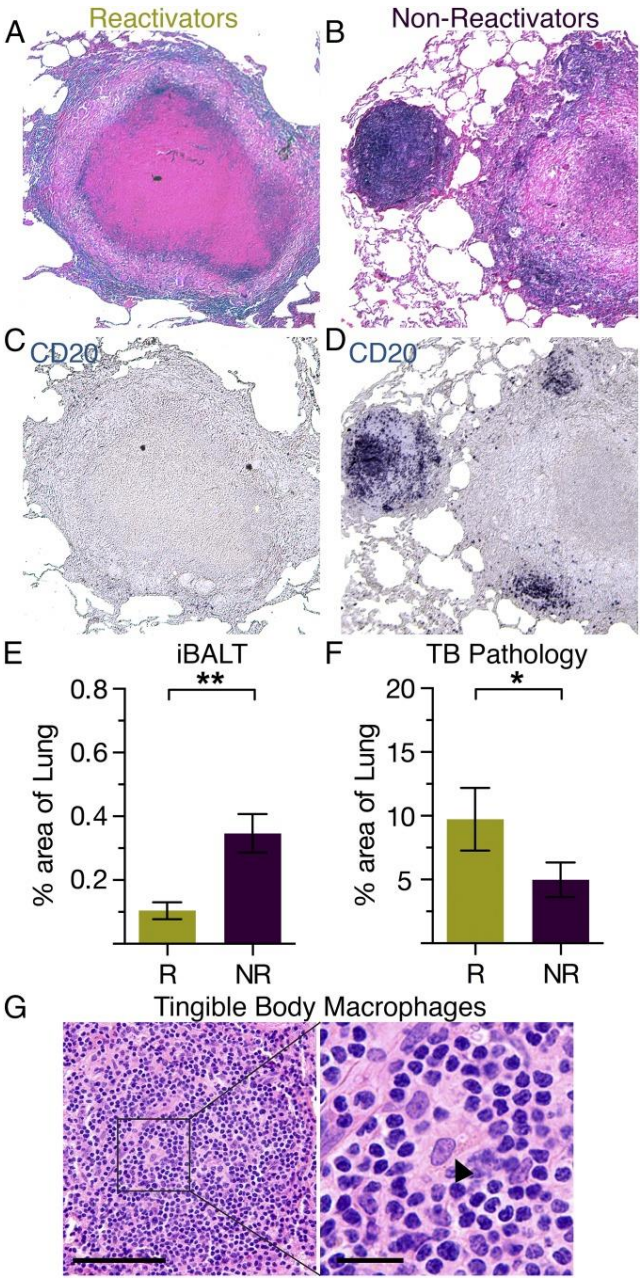

Figure 8: Persistence of iBALT correlates with protection from reactivation. H&E staining of lung sections from (*A*) reactivating animals and (*B*) nonreactivating animals, with the same sections of lung chromogenically stained in *C* and *D*, respectively, for $CD20^+$ B cells. Quantification of percentage area of (*E*) iBALT formation and (*F*) tuberculosis-associated pathology per lung section in reactivating (R) versus nonreactivating (NR) animals. $*P < 0.05$, $**P < 0.01$, using Student's *t* test. (*G*) H&E staining of tingible body macrophages found in BALT follicles, indicated by the black arrow in the magnified image. [Scale bar, 50 μ (*Left*) and 25 μ (*Right* magnified image).] (Magnification, *A*–*D*, 10×.)

DISCUSSION

One-third of the world's population has LTBI, and yet the mechanisms by which latent tuberculous infections are controlled have not been defined. The emergence of the HIV epidemic revealed the significance of $CD4^+$ T cells in controlling TB in humans (1). However, in our study, a subset of co-infected macaques retained control of LTBI despite complete ablation of pulmonary $CD4^+$ T cells. Protection from reactivation correlated with enhanced $CD8^+$ T cell function, increased iBALT persistence, and the resulting effects on local pathology. The precise roles of these CD4-independent components in HIV co-infected humans warrant further investigations.

Despite contrasting clinical outcomes, every co-infected macaque in our study exhibited indistinguishable pulmonary $CD4^+$ T cell depletion. Non-reactivating animals had an enhanced effector $CD8^+$ T cell population, conceivably leading to suppression of both viral replication and SIV-related pathology. In comparison, animals with reactivation TB had lower effector CD8+ T cell counts and showed increased SIV- as well as TB-associated pathology. To counter immune control, it is highly likely that the two pathogens synergize within the lungs of reactivated animals and exacerbate pathology. This hypothesis is supported by data that reactivators had significantly more SIV-infected cells within the granuloma. In addition, the perivascular lesions were significantly aggravated, had high bacterial burdens, and possibly led to increased bacterial dissemination. Although the co-localization of the virions and the bacilli within the same cells in granulomatous lesions has been described previously (22), their interactions in this local environment remain undercharacterized. We propose that, in reactivators, microenvironmental changes provide specific niches conducive to replication of

both pathogens. Based on our findings, we hypothesize that $CD8^+$ T cell-mediated responses can suppress SIV replication in tuberculous granulomas and limit SIV-induced pathology.

In non-reactivators, both $CD8^+$ T cell proliferation and function were found to be increased. Whereas the percentages of $CD8^+$ T cells recruited to the lung were similar, the proliferation of central and effector memory $CD8^+$ T cells was significantly enhanced in non-reactivators. Furthermore, granzyme B expression in $CD3^+$ T cells suggests a correlation between the presence of functional $CD8^+$ T cells and protection from SIV-mediated reactivation in primates (32). These results are consistent with previous observations that macaques not only lose BCG vaccination-induced protective immunity upon experimental depletion of $CD8^+$ T cells but also reactivate *Mtb* infections suppressed by chemotherapy at a higher rate (13). In addition, the presence of $CD3^-$ cells producing granzyme lends credibility to the role of NK cells in mediating control of both SIV and *Mtb* infection (37, 38). The effector role of $CD8^+$ T cells in the control of *Mtb* infection in humans has recently been described to inversely correlate with bacterial load in sputum (39), and HIV co-infection can impair *Mtb*-specific $CD8^+$ T degranulation and proliferation (40). Thus, the effector roles of $CD8^+$ T cells in curtailing reactivation need to be further investigated.

In addition to $CD8^+$ T cells and altered pathology, we also found that the presence of BALT proximal to the granuloma strongly correlates with control of TB reactivation. Previously, we have shown that increased BALT presence was associated with increased protection in mice, NHPs, and humans (33, 34). More importantly, protective immunity to TB, induced by a novel vaccine, also correlated strongly with the presence of BALT (14). In this study, we showed that the persistence of BALT increased protection from reactivation. Although the precise role of B cells in TB infection control remains to be determined, existing

evidence suggests that B cells are required for optimal development of immune responses against *Mtb* (15, 16, 41). Moreover, the presence of tingible body macrophages in BALT suggests that B cells are undergoing affinity maturation and/or that cross-priming of $CD8^+$ T cells occurs within these lymphoid follicles, allowing site-directed activation of macrophages (33, 35, 42, 43). We postulate that these protective lymphoid follicles proximal to the granuloma lead to localized T cell activation and enhanced B cell and humoral immunity.

Immune correlates of protective immunity and the mechanism of HIV-induced enhanced susceptibility to reactivation TB are largely unknown. Mechanistic studies into $CD4^+$ T cell-independent immune control of human TB, particularly the roles of $CD8^+$ T cells, B cells, and the resulting pathologies, are needed. This knowledge will facilitate design of novel interventions against TB, including vaccines and immunotherapeutics.

MATERIALS AND METHODS

Nonhuman primate infection, sampling, clinical procedures and euthanasia. All animal procedures were approved by the Institutional Animal Care and Use Committee of Tulane University, New Orleans, Louisiana, USA and were performed in strict accordance with NIH guidelines. Prior data suggested two different outcomes were possible when latently *Mtb*-infected macaques were exposed to SIV: reactivation in a majority of animals or continued latency in a small subset (22). Thirty-seven specific-pathogen-free, retrovirus-free, mycobacteria-naive, adult rhesus macaques that were bred and housed at the Tulane National Primate Research Center (TNPRC) and that ranged from 3–12 years of age were assigned to two groups, based on power calculations to detect, with sufficient power, statistically significant differences between the reactivating and non-reactivating groups following co-infection with SIV. All macaques were aerosol-exposed, as described earlier (14, 22, 26, 44),

to a low dose (~25 CFU implanted) of *Mtb* CDC1551. A subset of the macaques was also exposed approximately nine weeks later to 300 TCID50 (50% tissue culture infectious dose) of SIVmac239 administered intravenously in 1 mL saline, as described earlier (22). The control subset received an equal volume of saline intravenously.

Criteria for euthanasia included presentation of four or more of the following conditions: i) body temperatures consistently greater than 2^0F above pre-infection values for three or more weeks in a row; ii) 15% or more loss in body weight; iii) serum CRP values higher than 10 mg/mL for three or more consecutive weeks, CRP being a marker for systemic inflammation that exhibits a high degree of correlation with active TB in macaques (22, 23); iv) CXR values higher than 2 on a scale of 0-4; v) respiratory discomfort leading to vocalization; vi) significant or complete loss of appetite, and vii) detectable bacilli in BAL samples.

Samples were collected prior to and post *Mtb* infection, as well as post SIV infection. TSTs were performed one or two weeks before infection and at three weeks post *Mtb* infection, as previously described (22, 23). CXRs were acquired two weeks prior to *Mtb* infection and at 3, 7, 11, and 14 weeks post *Mtb* infection, as previously described (14, 22). The CXRs were scored by veterinary clinicians in a blinded fashion on a subjective scale of 0–4, with a score of 0 denoting normal lung and a score of 4 denoting severe tuberculous pneumonia, as previously described (14). Prior to vaccination/infection, all 37 animals received a normal score of 0. Blood was drawn one or two weeks prior to *Mtb* infection and then weekly thereafter for measuring complete blood count and serum chemistry (22, 26). Blood collected in EDTA tubes (Sarstedt AG & Co.) was used for whole blood flow cytometry using the panels described earlier (14, 26, 31). BAL samples were obtained, as previously

described, two weeks prior to *Mtb* infection, again at 3, 7, 11, and 14 weeks (22, 26), and then analyzed for CFUs and flow cytometry.

Humane endpoints were predefined in the animal use protocol and applied as a measure of reduction of discomfort (14). The TNPRC Institutional Animal Care and Use Committee approved all animal-related procedures and activities. At necropsy, lung, spleen, and liver tissues were collected and processed, as previously described, using two sections of pulmonary tissue that represented every lung lobe in at least one sample (14); CFU were determined per gram of tissue (22, 26). Lung pathology at necropsy was determined as described earlier (22, 26). TB pathology was determined for multiple sections in each lung and averaged for each animal in the study. SIV-induced pathology was reported per section from three reactivators and three non-reactivators, with multiple sections analyzed per animal.

Flow cytometry. Flow cytometry was performed on whole blood and BAL samples from all animals, as previously described (14, 26, 31).

Immunohistochemistry. Fluorescent immunohistochemistry, chromogenic staining, and *in situ* hybridization were performed on formalin-fixed, paraffin-embedded tissue as previously described (45).

Statistical analyses. Statistical comparisons were performed using one-way or two-way analysis of variance (ANOVA) in GraphPad Prism with Sidak's correction for multiple hypotheses, or Students t-test, as noted in figure legends and as described earlier (14).

ACKNOWLEDGMENTS. This research was supported by NIH awards to DK (AI089323, HL106790, RR026006), SM (P30110760), SAK/DK (AI111914) and the TNPRC (OD011104, AI058609).

Author Contributions. T.W.F. carried out the experiments, analyzed the results, and participated in manuscript preparation; S.M. and X.A. carried out the experiments and analyzed the results; D.N.L. performed pathology, analyzed results, and prepared that component for manuscript preparation; M.J.K. analyzed results; A.M, J.C., and W.R.J. analyzed the results and participated in manuscript preparation; N.A.G. and A.N.B. carried out experiments; L.A.D., K.E.R-L., and J.L.B. provided veterinary assistance**;** C.J.R. provided expertise on NHP aerobiology; P.J.D. performed veterinary pathology; S.A.K. provided funding and analyzed the results; A.A.L. performed veterinary pathology and participated in manuscript preparation; D.K. provided funding, advised on the experimental design**,** carried out the experiments, analyzed the results, and participated in manuscript preparation. All authors reviewed the manuscript before submission.

REFERENCES

1. Kwan CK, Ernst JD (2011) HIV and tuberculosis: a deadly human syndemic. *Clin Microbiol Rev* 24(2):351-376.
2. Orme IM, Collins FM (1983) Protection against *Mycobacterium tuberculosis* infection by adoptive immunotherapy. Requirement for T cell-deficient recipients. *J Exp Med* 158(1):74-83.
3. Selwyn PA*, et al.* (1989) A prospective study of the risk of tuberculosis among intravenous drug users with human immunodeficiency virus infection. *New Engl J Med* 320(9):545-550.
4. Barnes PF, Bloch AB, Davidson PT, & Snider DE, Jr. (1991) Tuberculosis in patients with human immunodeficiency virus infection. *New Engl J Med* 324(23):1644-1650.
5. Urdahl KB, Shafiani S, Ernst JD (2011) Initiation and regulation of T-cell responses in tuberculosis. *Mucosal Immunol* 4(3):288-293.
6. Flynn JL, Chan J (2001) Immunology of tuberculosis. *Annu Review Immunol* 19:93-129.
7. Lenaerts A, Barry CE, 3rd, Dartois V (2015) Heterogeneity in tuberculosis pathology, microenvironments and therapeutic responses. *Immunol Rev* 264(1):288-307.
8. Mehra S*, et al.* (2013) Granuloma correlates of protection against tuberculosis and mechanisms of immune modulation by *Mycobacterium tuberculosis*. *J Infect Dis* 207(7):1115-1127.
9. Dutta NK, McLachlan J, Mehra S, Kaushal D (2014) Humoral and lung immune responses to *Mycobacterium tuberculosis* infection in a primate model of protection. *Trials Vaccinol* 3:47-51.
10. Sia JK, Georgieva M, Rengarajan J (2015) Innate Immune Defenses in Human Tuberculosis: An Overview of the Interactions between *Mycobacterium tuberculosis* and Innate Immune Cells. *J Immunol Res* 2015:747543.
11. Orme IM, Robinson RT, Cooper AM (2015) The balance between protective and pathogenic immune responses in the TB-infected lung. *Nat Immunol* 16(1):57-63.
12. Kamath A, Woodworth JS, Behar SM (2006) Antigen-specific CD8+ T cells and the development of central memory during *Mycobacterium tuberculosis* infection. *J Immunol* 177(9):6361-6369.
13. Chen CY*, et al.* (2009) A critical role for CD8 T cells in a nonhuman primate model of tuberculosis. *PLoS Pathog* 5(4):e1000392.
14. Kaushal D*, et al.* (2015) Mucosal vaccination with attenuated *Mycobacterium tuberculosis* induces strong central memory responses and protects against tuberculosis. *Nat Commun* 6:8533.
15. Chan J*, et al.* (2014) The role of B cells and humoral immunity in *Mycobacterium tuberculosis* infection. *Sem Immunol* 26(6):588-600.
16. Kozakiewicz L*, et al.* (2013) B cells regulate neutrophilia during *Mycobacterium tuberculosis* infection and BCG vaccination by modulating the interleukin-17 response. *PLoS Pathog* 9(7):e1003472.

17. Zhu Q, *et al.* (2016) Human B cells have an active phagocytic capability and undergo immune activation upon phagocytosis of *Mycobacterium tuberculosis*. *Immunobiol* 221(4):558-567.
18. Moir S, Chun TW, Fauci AS (2011) Pathogenic mechanisms of HIV disease. *Annu Rev Pathol* 6:223-248.
19. Kanwar B, Favre D, McCune JM (2010) Th17 and regulatory T cells: implications for AIDS pathogenesis. *Curr Opin HIV AIDS* 5(2):151-157.
20. Hu Z, *et al.* (2015) HIV-associated memory B cell perturbations. *Vaccine* 33(22):2524-2529.
21. Patel NR, *et al.* (2007) HIV impairs TNF-alpha mediated macrophage apoptotic response to *Mycobacterium tuberculosis*. *J Immunol* 179(10):6973-6980.
22. Mehra S, *et al.* (2011) Reactivation of latent tuberculosis in rhesus macaques by coinfection with simian immunodeficiency virus. *J Med Primatol* 40(4):233-243.
23. Kaushal D, Mehra S, Didier PJ, Lackner AA (2012) The non-human primate model of tuberculosis. *J Med Primatol* 41(3):191-201.
24. Flynn JL, Gideon HP, Mattila JT, Lin PL (2015) Immunology studies in non-human primate models of tuberculosis. *Immunol Rev* 264(1):60-73.
25. Diedrich CR, *et al.* (2010) Reactivation of latent tuberculosis in cynomolgus macaques infected with SIV is associated with early peripheral T cell depletion and not virus load. *PLoS One* 5(3):e9611.
26. Mehra S, *et al.* (2015) The DosR Regulon Modulates Adaptive Immunity and Is Essential for *Mycobacterium tuberculosis* Persistence. *Am J Respir Crit Care Med* 191(10):1185-1196.
27. Sharma SK, Mohan A, Sharma A, Mitra DK (2005) Miliary tuberculosis: new insights into an old disease. *Lancet Infect Dis* 5(7):415-430.
28. Aaron L, *et al.* (2004) Tuberculosis in HIV-infected patients: a comprehensive review. *Clin Microbiol Infect* 10(5):388-398.
29. Li Y, *et al.* (2015) SIV Infection of Lung Macrophages. *PLoS One* 10(5):e0125500.
30. Mattapallil JJ, *et al.* (2005) Massive infection and loss of memory CD4+ T cells in multiple tissues during acute SIV infection. *Nature* 434(7037):1093-1097.
31. Phillips BL, *et al.* (2015) LAG3 expression in active *Mycobacterium tuberculosis* infections. *Am J Pathol* 185(3):820-833.
32. Mazzaccaro RJ, *et al.* (1998) Cytotoxic T lymphocytes in resistance to tuberculosis. *Adv Exp Med Biol* 452:85-101.
33. Slight SR, *et al.* (2013) CXCR5(+) T helper cells mediate protective immunity against tuberculosis. *J Clin Invest* 123(2):712-726.
34. Gopal R, *et al.* (2013) S100A8/A9 Proteins Mediate Neutrophilic Inflammation and Lung Pathology during Tuberculosis. *Am J Respir Crit Care Med* 188(9):1137-1146.
35. Smith JP, Burton GF, Tew JG, Szakal AK (1998) Tingible body macrophages in regulation of germinal center reactions. *Devel immunol* 6(3-4):285-294.
36. Kranich J, *et al.* (2008) Follicular dendritic cells control engulfment of apoptotic bodies by secreting Mfge8. *J Exp Med* 205(6):1293-1302.
37. Shang L, *et al.* (2014) NK cell responses to simian immunodeficiency virus vaginal exposure in naive and vaccinated rhesus macaques. *J Immunol* 193(1):277-284.

38. Portevin D, Via LE, Eum S, Young D (2012) Natural killer cells are recruited during pulmonary tuberculosis and their ex vivo responses to mycobacteria vary between healthy human donors in association with KIR haplotype. *Cell Microbiol* 14(11):1734-1744.
39. Silva BD, Trentini MM, da Costa AC, Kipnis A, Junqueira-Kipnis AP (2014) Different phenotypes of CD8+ T cells associated with bacterial load in active tuberculosis. *Immunol Lett* 160(1):23-32.
40. Kalokhe AS*, et al.* (2015) Impaired degranulation and proliferative capacity of *Mycobacterium tuberculosis*-specific CD8+ T cells in HIV-infected individuals with latent tuberculosis. *J Infect Dis* 211(4):635-640.
41. Achkar JM, Chan J, Casadevall A (2015) B cells and antibodies in the defense against *Mycobacterium tuberculosis* infection. *Immunol Rev* 264(1):167-181.
42. Hey YY, O'Neill HC (2012) Murine spleen contains a diversity of myeloid and dendritic cells distinct in antigen presenting function. *J Cell Mol Med* 16(11):2611-2619.
43. Schaible UE*, et al.* (2003) Apoptosis facilitates antigen presentation to T lymphocytes through MHC-I and CD1 in tuberculosis. *Nat Med* 9(8):1039-1046.
44. Mehra S*, et al.* (2010) Transcriptional reprogramming in nonhuman primate (rhesus macaque) tuberculosis granulomas. *PLoS One* 5(8):e12266.
45. Li Q, Skinner PJ, Duan L, Haase AT (2009) A technique to simultaneously visualize virus-specific CD8+ T cells and virus-infected cells in situ. *J Vis Exp* 30:e1561, doi:10.3791/1561

CHAPTER 5: HYPOXIA SENSING AND PERSISTENCE GENES ARE EXPRESSED DURING THE INTRA-GRANULOMATOUS SURVIVAL OF *M. TUBERCULOSIS*

Summary of my contribution to the work:

In accordance with the study, assessed pulmonary pathology changes and granuloma subtype. Classified changes as 1. Representative pathology, 2. Classical granulomas (with casea), and 3. Non-necrotizing granulomas to facilitate microdissection. Took and edited photomicrographs. Wrote pathology portion of the manuscript. Edited manuscript as a whole. Provided pathology consultation for microdissection. Collaborated on figure preparation for manuscript. The manuscript is provided below as it was published in the 2017 *American Journal of Respiratory Cell and Molecular Biology* 56(5): 637-647.

Running title: Intra-granulomatous transcriptome of *Mtb* in macaques

Authors: Teresa A. Hudock[1*], Taylor W. Foreman[1*], Nirmalya Bandyopadhyay[2], Uma S. Gautam[1], Ashley Veatch[1], Denae N. LoBato[1], Kaylee M. Gentry[1], Nadia A. Golden[1], Amy Cavigli[1], Michelle Mueller[1], Shen-An Hwang[3], Robert L. Hunter[3], Xavier Alvarez[1], Andrew A. Lackner[1], Joel S. Bader[2], Smriti Mehra[4#], Deepak Kaushal[1#]

Author affiliations: [1]Tulane National Primate Research Center (TNPRC), Covington, LA 70433; [2]Whitaker Biomedical Engineering Institute, Whiting School of Engineering, Johns Hopkins University, Baltimore, MD 21205; [3]Department of Pathology and Laboratory

Medicine, University of Texas Health Science Center, Houston, TX 77030; Tulane University Health Sciences, New Orleans, LA 70112; [4]Department of Pathobiological Sciences, Louisiana State University School of Veterinary Medicine, Baton Rouge, LA;

[#]**Correspondence**: Deepak Kaushal, PhD, Professor of Microbiology & Immunology, Tulane National Primate Research Center, dkaushal@tulane.edu (email); OR Smriti Mehra, PhD, Associate Professor of Pathobiological Sciences, Louisiana State University School of Veterinary Medicine, smehra@lsu.edu (email).

Abbreviations: *Mycobacterium tuberculosis*, *Mtb*; Tuberculosis, TB; Active TB, ATB; Latent Tuberculosis Infection, LTBI; Tuberculin Skin Test, TST; Primate interferon-gamma release assay, PRIMAGAM; nonhuman primate, NHP; C-Reactive Protein, CRP; Formalin fixed paraffin embedded, FFPE; Linear models for microarray analysis, Limma; Dormancy survival regulon, *dosR*; pimonidazole hydrochloride, PIMO; Toxin-antitoxin, TA; Designer Arrays for Defined Mutant Analysis, DeADMAn; Transposon site hybridization, TraSH; Proline-Glutamate, PE; Proline-Proline-Glutamate, PPE; HIF-1, hypoxia-inducible factor 1.

Author contributions: Research –TAH, AC, MM, TWF, USG, AVV, KMG, DNL; Analysis – TH, NB, JB, SAH, RLH, AAL, DK, DNL, AVV, USG TWF, SM; provided clinical TB samples - SAH, RLH; Writing – TH, AAL, DK, TWF and SM; Funding – DK, AAL, SM.

Keywords: *Mycobacterium tuberculosis*; macaque, granuloma, microarray, transcriptome, micro-dissection, hypoxia, *dos*R

ABSTRACT:

Background: While it is accepted that the environment within the granuloma profoundly affects *Mycobacterium tuberculosis (Mtb)* and infection outcome, our ability to understand *Mtb* gene expression in these niches has been limited. We determined intragranulomatous gene expression in human like lung lesions derived from nonhuman primates with both active (ATB) and latent (LTBI) tuberculosis.

Methods: We employed a non-laser based approach to micro-dissect individual lung lesions and interrogate the global transcriptome of *Mtb* within granulomas. *Mtb* genes expressed in classical granulomas with central, caseous necrosis as well as within the caseum itself were identified and compared to other *Mtb* lesions, in animals with ATB (n=7) or LTBI (n=7). Results were validated using both an oligonucleotide approach and RT-PCR on macaque samples and by using human TB samples.

Findings: We detected approximately 2900 and 1850 statistically significant genes in ATB and LTBI lesions, respectively (Limma analysis, Bonferroni corrected, $p<0.05$). Of these genes, the expression of approximately 1300 (ATB) and 900 (LTBI) was positively induced. We identified the induction of key regulons and compared our results to genes previously determined to be required for *Mtb* growth.

Interpretation: Our results indicate pathways *Mtb* utilizes to ensure its survival in a highly stressful environment *in-vivo*. A large number of genes are commonly expressed in

granulomas with ATB and LTBI. Additionally, the enhanced expression of the *dos*R regulon was a key feature of lesions in animals with LTBI, stressing its importance in the persistence of *Mtb* during the chronic phase of infection.

Funding: This work was funded supported by Public Health Service grants AI089323 and HL106790, AI091457, OD011104, OD011124, AI058609 and GM103424, the Louisiana Board of Regents, the TNPRC Office of the Director, the Tulane Research Enhancement Fund, the Tulane Office of Vice-President for Research and the Wetmore Foundation of Louisiana.

INTRODUCTION:

Mycobacterium tuberculosis (*Mtb)* is constantly subjected to stress *in-vivo* and must successfully adapt in order to survive its ever-changing extracellular milieu (1). The study of mycobacterial state *in-vivo* is further complicated by variability in granuloma pathology, physiology, and morphology. We currently do not fully understand the drivers of *Mtb* reactivation in the lung (2), and disease progression can be highly variable given the differences in host-genetics, environment, microbiota, and the presence of comorbidities. A comparative systems biology approach that incorporates the pathological complexities of *Mtb* infection would allow us to better understand the physiology of the pathogen.

Various approaches have been used to attempt to understand the importance of *Mtb* genes and therefore better elucidate TB pathogenesis. Initially the TB field focused on a gene-by-gene approach and with time and technological advancements began shifting to

whole-genome based approaches. Leveraging transposon site hybridization (TraSH), genes required for *Mtb* growth have been identified in mice, murine macrophages and computationally. Another mutant based technique, Designer Arrays for Defined Mutant Analysis (DeADMAn), have been used in mice, guinea pigs and nonhuman primates (NHPs). Additionally, several groups have attempted to model the granuloma environment; while others have detected the expression of a small number of specific *Mtb* genes in human macrophages. Some have conducted massively parallel RNA-PCR of *Mtb* transcriptome using the mouse model. Yet others have identified whole-genome *Mtb* gene expression in various mouse models and used *in-vitro* granuloma models. These studies have provided insight into genes required for *Mtb* growth in survival, but no studies to date, have profiled *in-vivo* gene profiles within its natural microenvironment and characteristic pulmonary lesion, the granuloma, while also utilizing a model that most closely recapitulates the human disease spectrum. As such, failure to effectively control *Mtb* infections and TB disease, via devising new vaccinations and therapeutic strategies, has been crippled by the lack of effective disease models and fundamental knowledge of the pathogen in its natural niches.

Here we change the way we identify *Mtb* treatment and vaccine strategies by switching from traditionally utilized peripheral responses to a localized approach via assessing *Mtb* gene induction within the pulmonary granulomatous environment. Due to many similarities between infected NHPs and humans, NHPs are the ideal model for addressing these questions (3). NHPs such as rhesus (*Macaca mulatta*) (2-18) and cynomolgus (*Macaca fascicularis*) (19, 20) macaques recapitulate the wide spectrum of human TB pathology and outcomes upon experimental infection with *Mtb*. We currently lack an understanding of the physiology and the metabolic state of *Mtb* in this granulomatous environment during different states of infection. Understanding the physiology and metabolism of the intra-

granulomatous environment is critical because effective vaccines and drugs must target this state to eradicate the bacteria and subsequently control the infection. We therefore propose to study and compare the intra-granulomatous gene expression of *Mtb* during ATB, LTBI and reactivation.

We hypothesize that the *Mtb* transcriptional profiles, with respect to metabolism and physiology, exhibit changes over time and upon interaction with both a variety of environmental cues and host immune responses. Consequently, we hypothesize that different infective stages as well as amongst different areas of the granuloma would lead to differential bacillary expression profiles. Further, and more importantly, we propose that these changes can be used to understand the physiology of the pathogen as well as its virulence.

The purpose of evaluating the entire granulomatous pathology, i.e. the combination of all lesion and granuloma types on the formalin fixed paraffin embedded (FFPE) lung slides, is to generate a bacterial transcriptome profile that is representative of the entire infective state. Additionally, the purpose of specifically evaluating the classical, caseating, type granuloma is to evaluate the bacterial transcripts specific to this lesion type. Overall, evaluation of the mycobacterial transcriptome in granulomatous tissue is likely to further our understanding of the mechanisms involved in their formation and maintenance as well as those genes that are expressed in each state of the infection. Analysis of *Mtb* gene-expression within this environment *in-vivo* will further our understanding of the environmental stressors *Mtb* encounters within this specific niche, allow us to identify genetic programs that are critical for the transition between ATB and LTBI. This information can be used to facilitate development of *Mtb* vaccines, diagnostics, and

therapeutics and consequently generate a more targeted approach to prevent, identify, and treat TB infection.

METHODS:

Study Design and Statistical Analysis

The goal of this study was to assess the *in-vivo Mtb* transcriptome in defined micro-anatomic compartments typical of ATB (Fig. 1a-b, Supplementary Fig. 1) and LTBI (Fig. 1c-d, Supplementary Fig. 2). We observed that LTBI correlated with solitary lesions with well-defined central necrosis (caseum) and defined cellular layers including fibrosis. There were referred to as "classical granulomata" or "classical granulomas". On the contrary, pulmonary pathology in ATB was characterized by the presence of a wide variety of granulomata, including coalescing of classical granulomas with caseum as well as other less organized TB-related lesions, which include but are not limited to: 1) Granulomatous inflammation characterized by poorly organized cellular infiltration predominately consisting of macrophages, but also consisting of other inflammatory cells; 2) Non-necrotizing granulomas with a thin layer of lymphocytes surrounding a central core of predominantly epithelioid macrophages. Also, due to the increased diversity of lesions in ATB, *Mtb* transcriptome were examined in the amalgamation of ATB induced lesions by dissecting an area referred to as "representative pathology" consisting of all of the aforementioned lesion types evident on the section. Sections of FFPE lung tissue obtained from two groups of previously infected *Mtb* infected NHPs (ATB (n=7) or LTBI (n=7)) (Supplementary Table 1) (4, 18) were micro-dissected, tissue digested, and RNA extracted as described (21). Animals with ATB had higher serum C-reactive protein (CRP) levels (Fig 2a) ($P<0.01$), significantly more percent weight-loss (Fig 2b) ($P<0.05$), significantly higher lung bacterial burden (Fig 2c) ($P<0.005$), and lung pathology (Fig 2d) ($P<0.005$), as compared to animals

with LTBI. These results are further supported by the *Mtb*-specific staining of lung sections, using multilabel confocal microscopy (Fig 2e-g) and chromogen staining (Fig 2h-i). In each of these instances, significantly higher *Mtb* burden was detected by staining fixed random lung tissue sections with *Mtb*-specific antibodies in the animals with ATB relative to LTBI. In the case of confocal, we were able to quantify these signals and found that the quantity of *Mtb* present per square mm was significantly higher in the lungs of animals with ATB, relative to LTBI ($P<0.005$). Since the extracted heterogeneous RNA samples contain predominately host specific transcripts, RNA was amplified (Ovation® FFPE WTA System) and purified (QIAGEN QIAquick PCR Purification Kit). For microarray analysis, 3µg cDNA samples (Alexa Fluor® 5) and 3µg CDC1551 gDNA (Alexa Fluor® 3, BEI Resources) were labeled. *Mtb* microarrays were used to compare samples to control (4). Statistically significant genes were determined using, LIMMA (22). Multiple hypothesis error was corrected using a Bonferroni correction ($P< 0.05$) that has been previously described (14, 16).

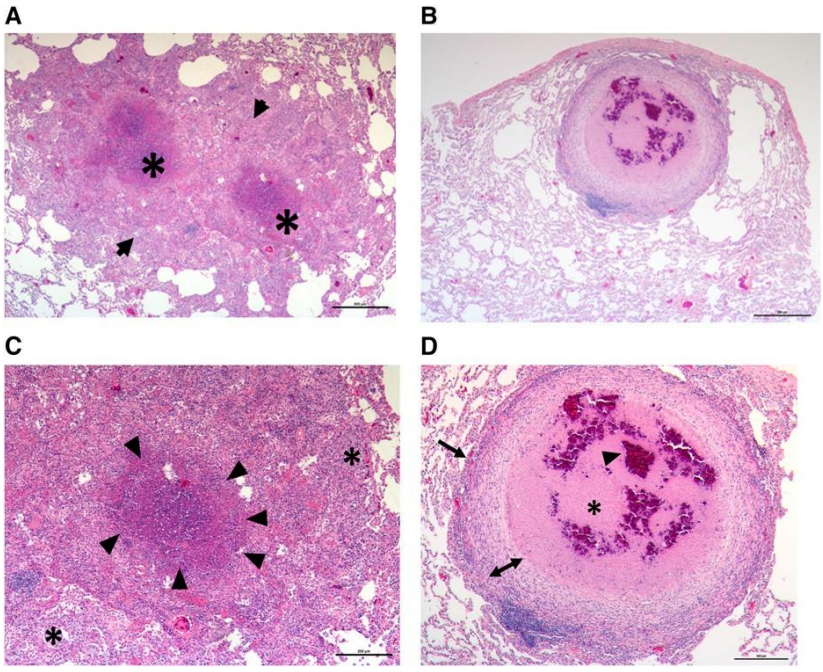

Figure 1: (*A* and *B*) Representative hematoxylin and eosin (H&E) image of active tuberculosis (ATB; DF30) lung. (*A*) A 325 magnification image of two coalescing granulomata, with extensive intervening and surrounding regions of inflammation. We termed this presentation as "representative pathology," which includes classical granulomata and associated caseum. *Arrows* define the two coalescing lung granulomas. (*B*) A 350 magnification image of an animal with ATB. (*C* and *D*) Representative H&E image of latent tuberculosis infection (LTBI) (FJ05) lung. (*C*) A 325 magnification image of a solitary granuloma surrounded by regions of normal lung. (*D*) A 350 magnification image of the same granuloma clearly describes the presence of a central necrotic region (the caseum). We termed such lesions as "classical granulomata." (*A*,*C*, and *D*) *Asterisks* correspond to necrotic-hypoxic centers within granulomas. (*C*) The *arrowheads* define the boundary between the necrotic center and the cellular layer to the outside. (*D*) The *arrows* define the boundary between the granuloma and the normal lung as well as between the myeloid and the lymphocytic layers. *Scale bars*: 500 mm.

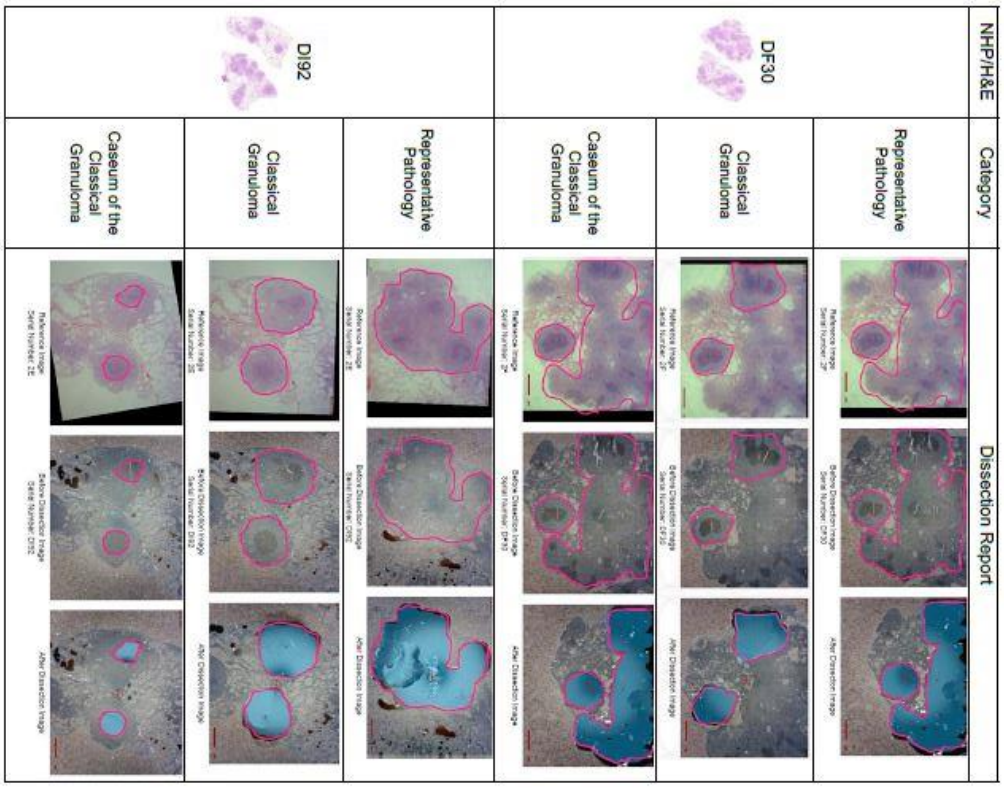

Figure 1. ATB granuloma H&E images and post microdissection reports.

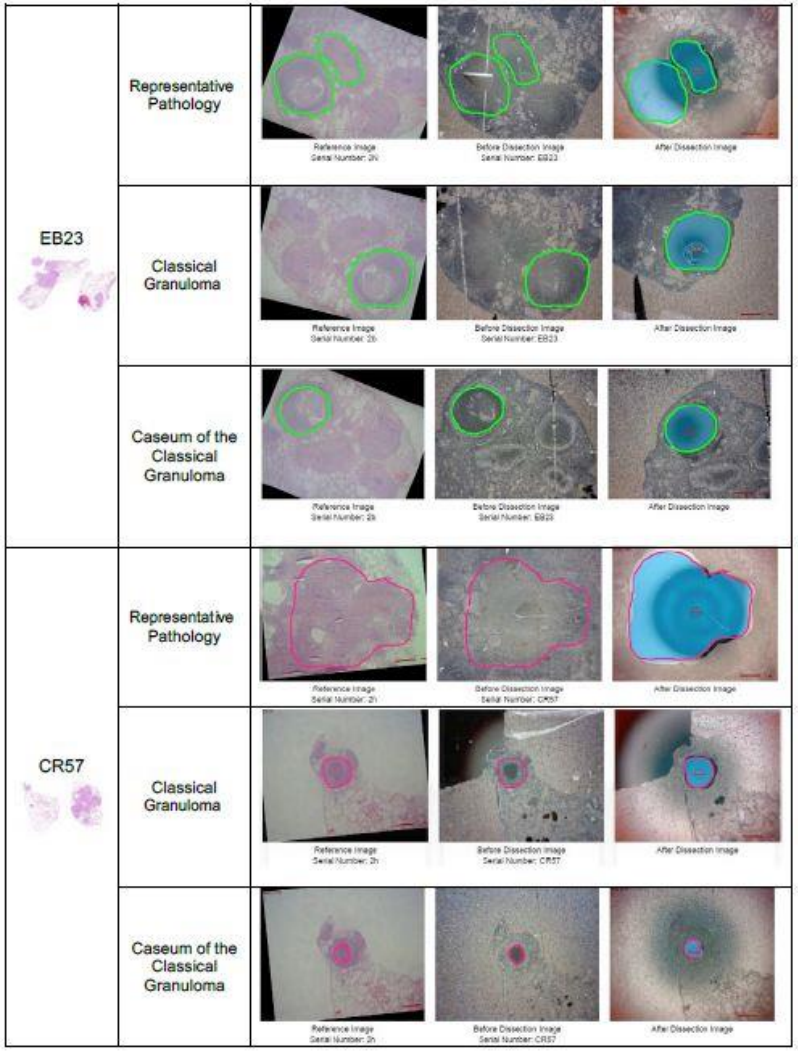
EB23
Representative Pathology
Classical Granuloma
Caseum of the Classical Granuloma
CR57
Representative Pathology
Classical Granuloma
Caseum of the Classical Granuloma

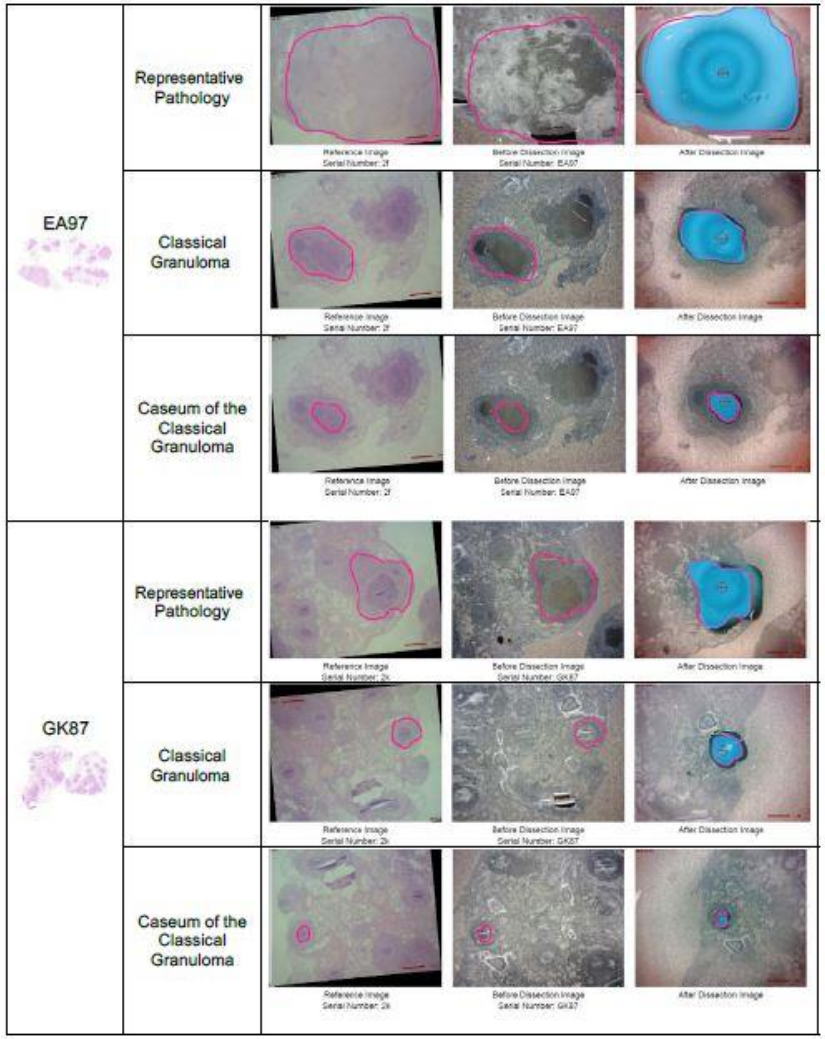
EA97
Representative Pathology
Classical Granuloma
Caseum of the Classical Granuloma
GK87
Representative Pathology
Classical Granuloma
Caseum of the Classical Granuloma

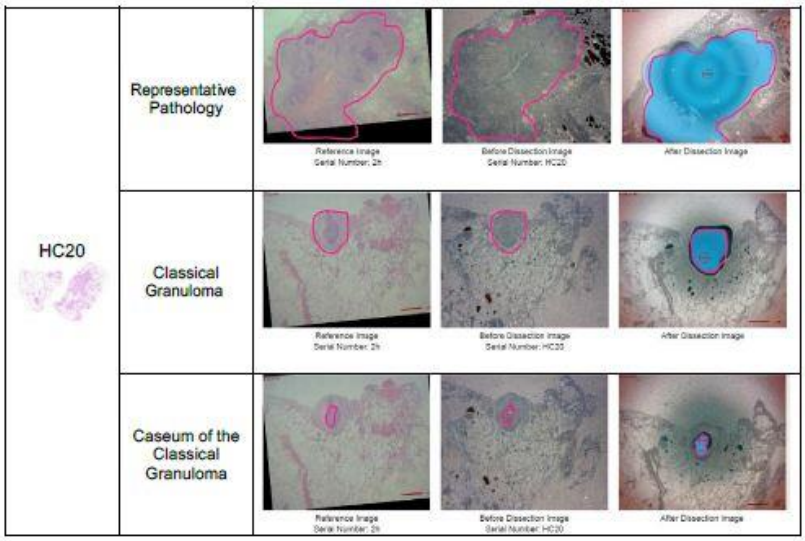

Supplementary Figure 1. ATB granuloma H&E images and post microdissection reports. H&E image from each ATB NHP FFPE slide utilized in study followed by dissection reports. The area to be dissected is outlined on both a reference image as well as an unstained slide. The post dissection image depicts the area dissected. Note that ATB included the following three dissection categories: representative pathology, classical granuloma and caseum of the classical granuloma.

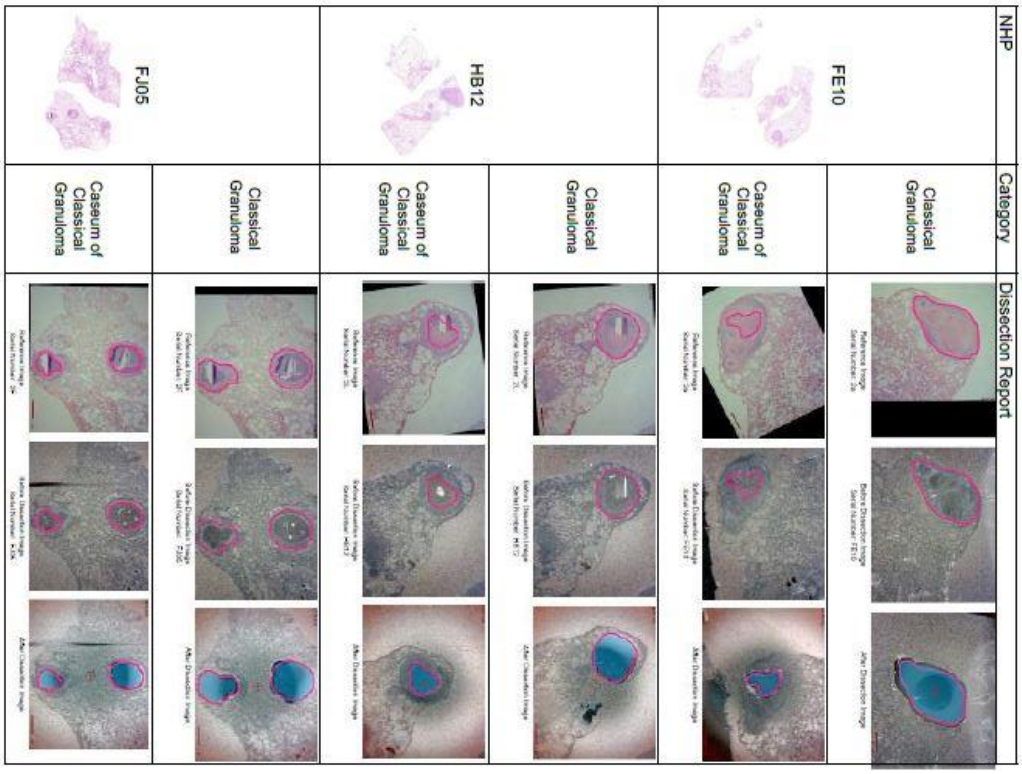

Figure 2. LTBI granuloma H&E images and post microdissection reports.

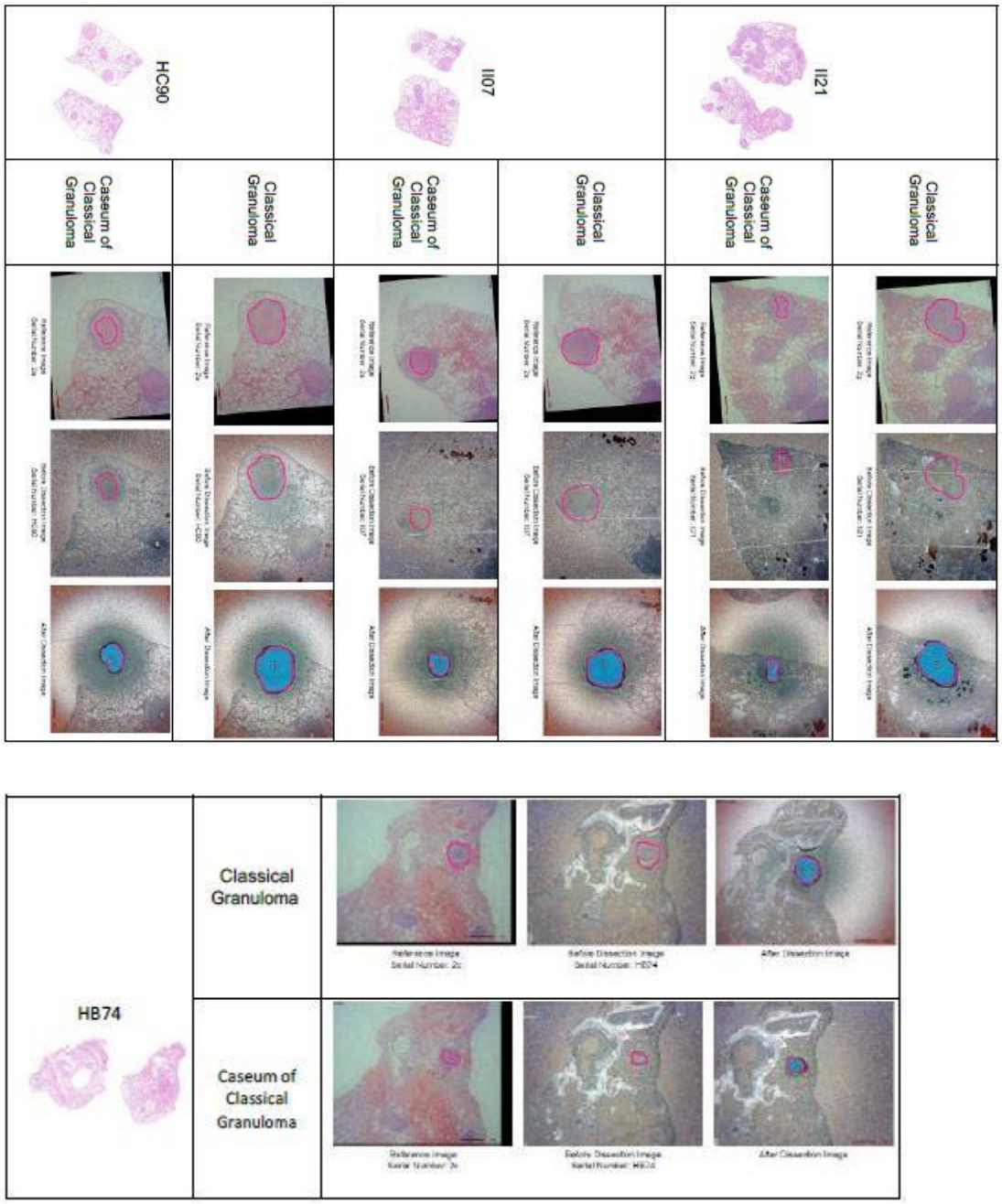

Supplementary figure 2: LTBI granuloma H&E images and post microdissection reports. H&E image from each LTBI NHP FFPE slide utilized in study followed by dissection reports. The area to be dissected is outlined on both a reference image as well as an unstained slide. The post dissection image depicts the area dissected. Note that LTBI included the following two categories: classical granuloma and caseum of the classical granuloma.

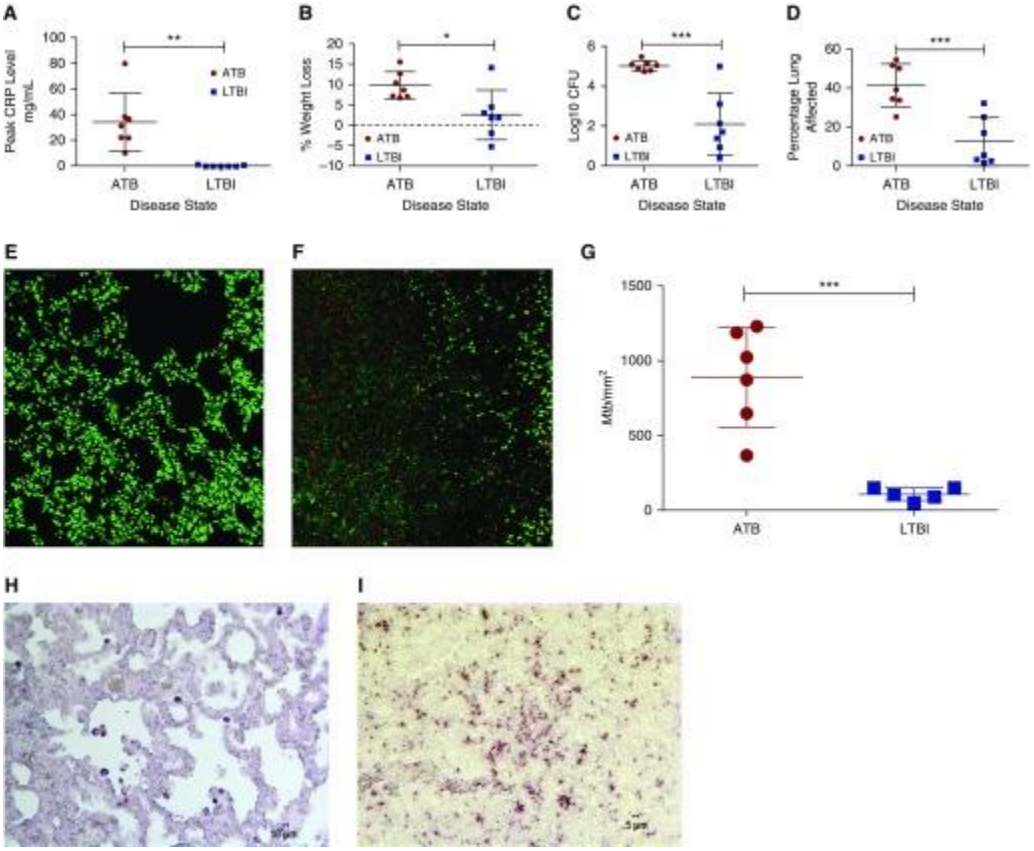

Figure 2. Clinical correlates of disease state and associated lung bacterial burdens and pathology. (a) Two groups of seven macaques were classified with either ATB (red) or LTBI (blue). Peak serum C-reactive protein (CRP)(mg/ml); **(b)** changes in body weight; **(c)** *Mtb* bacterial burden per gram of lung tissue post euthanasia; **(d)** percentage lung affected by TB pathology at necropsy and over course of infection; representative confocal staining of a section of lung with anti-*Mtb* antibody for an animal with LTBI **(e)** and ATB **(f)**. *Mtb* -**red**, To-Pro-3 -**green**; quantification of *Mtb*-positive signal over area (mm2) **(g)**; representative chromogen staining of a section of lung with anti-*Mtb* antibody for an animal with LTBI **(h)** and ATB **(i)**. *p<0.05, **p<0.01 and ***p<0.001 using unpaired student's t test.

Host specific hypoxia was assessed using Agilent Rhesus Macaque microarrays relative to normal lung tissue derived from uninfected macaques as baseline. Lesion hypoxia was assessed in tissues of animals injected with pimonidazole hydrochloride (PIMO, Hypoxyprobe) coupled to daylight red (16). A subset of 86 genes (5 housekeeping) was used

to validate microarray profiles using nCounter Analysis (23). Additionally, FFPE human lung blocks from patients with ATB were obtained from Hunter and Hwang, for validation of NHP gene expression profiles. A subset of bacillary genes with clearly defined expression profiles were used for real-time RT-PCR, performed as described earlier (4, 21, 24-30), for an additional level of validation of results. For this purpose, RNA isolated from *in-vitro* grown, log-phase (0.4 OD) *Mtb* cultures was used for comparison, and data were normalized using 16S gene as internal reference.

RESULTS:

Mesodissected samples from ATB and LTBI were used to identify *Mtb* genes that were expressed in a statistically significant manner *in-vivo*. Significance was defined as those whose expression level differed from that generated by the use of a discrete, constant amount of *Mtb* genomic DNA (control). The expression of approximately three-fourths of the entire *Mtb* genome could be detected in a statistically significant manner in all lesion types derived from NHPs with ATB, with 2909, 2848 and 2910 genes being detected in representative pathology, classical granuloma, and caseum of the classical granuloma, respectively (Supplementary Table 2-4). A similar analysis in lesions derived from animals with LTBI showed that 1874 genes exhibited expression in classical granulomas and 1872 in the caseum of the classical granuloma (Supplementary Tables 5-6).

Microarray sample inputs consisted of 3μg of either amplified lung derived mixed sample or *Mtb* control. Therefore, genes detected with a positive fold change in the mixed sample compared to the pure *Mtb* control reflect much larger actual fold changes. Given these limitations, we subsequently focused on statistically significant genes with a positive fold change. In ATB samples, 1344, 1328, and 1343 genes were detected with in a positive

manner in representative pathology, classical granuloma, and caseum of the classical granuloma, respectively (Fig. 3a, Supplementary Tables 2-4). In LTBI samples, the expression of 1082 and 891 genes with a positive fold change could be detected in classical granuloma and associated caseum (Fig. 3b, Supplementary Tables 5-6). The expression of a core group of 633 genes was induced in ATB, LTBI, and among all lesion types (Fig. 3c, Supplementary Table 7).

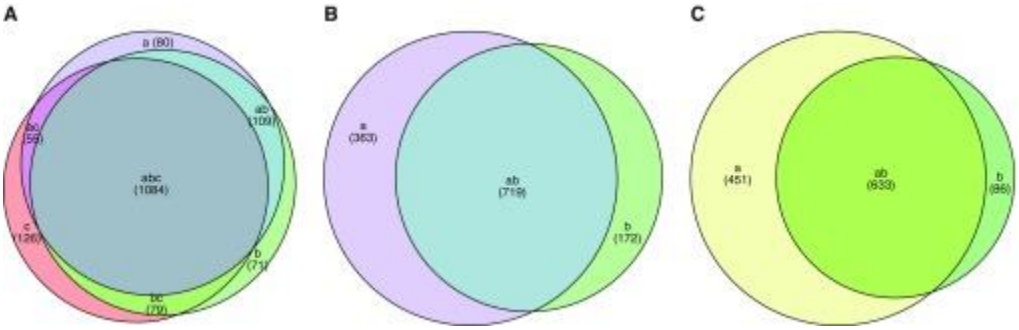

Figure 3: Transcriptome profiles. Statistically significant genes whose fold change expression is positively induced within nonhuman primate (NHP) lung in (*A*) ATB (a) classical granuloma, (b) caseum of classical granuloma, (c) representative pathology; and (*B*) LTBI (a) classical granuloma, (b) caseum of classical granuloma. (*C*) Corresponding genetic similarity among genes with induced expression in (a) all ATB granulomatous pathology, (b) all LTBI granulomatous pathology and (ab) genes with induced expression in all NHP-derived samples. $P < 0.05$ using linear models for microarray analysis and Bonferroni correction.

The *dos*R-regulon consists of 48 genes up-regulated during a multitude of *in-vitro* stress conditions that mimic the environment faced by *Mtb in-vivo*, including hypoxia (31). This regulon has generally been considered essential for *Mtb* dormancy, although conclusive evidence in this regard was lacking until recently (16). In ATB lesions, the expression of approximately 26%, 34%, and 32% of the genes within this regulon were found to be induced in a statistically significant manner in representative pathology, classical granuloma, and caseum of the classical granuloma (Supplementary Table 8). In LTBI samples,

approximately 30% of the genes within the regulon could be similarly detected in both classical granuloma and caseum of the classical granuloma. Additionally, 8 *dos*R-regulon members (Rv0080, Rv0081, Rv1736c, Rv1737c, Rv2032, Rv2625c, and Rv2630) were present in the core group common to all ATB and LTBI samples. We predicted that the expression of members of this regulon would occur at higher levels in animals progressing to LTBI. The greatest induction of genes of the *dos*R regulon occurred in the most hypoxic areas of the granuloma – e.g. the caseum derived from LTBI granulomas followed by entire LTBI classical granuloma and the caseum derived from ATB lesions (Fig. 4a).

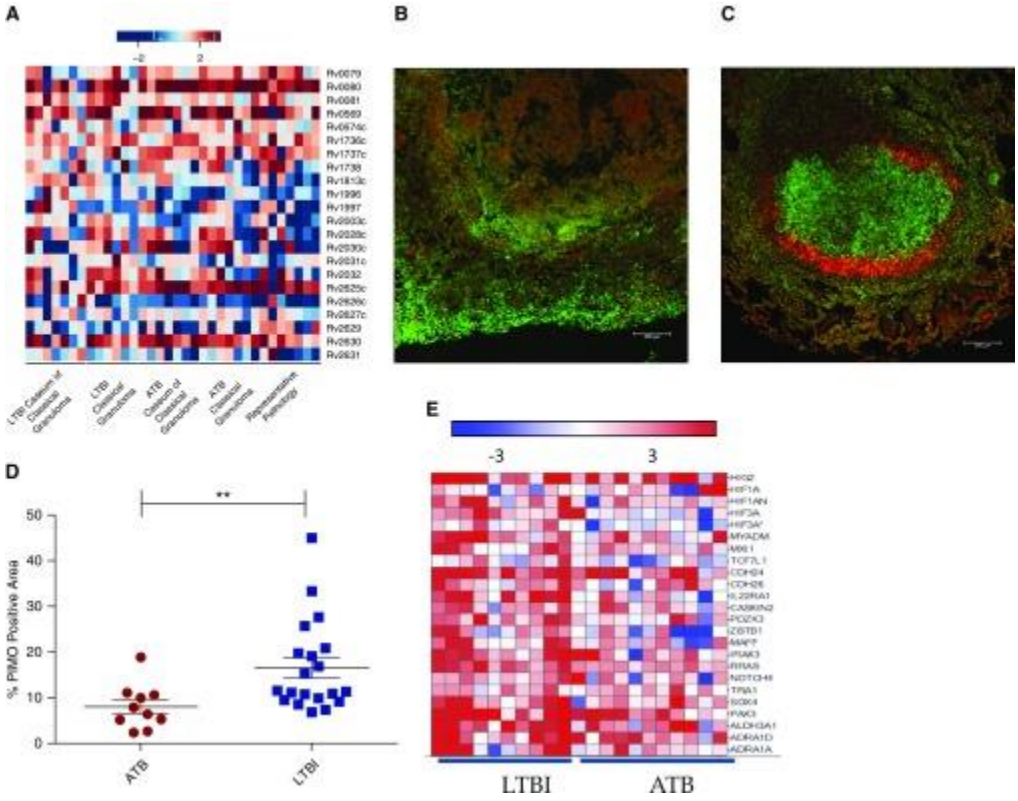

Figure 4. Expression of *Mtb dos*R regulon and detection of hypoxia in ATB and LTBI lung granulomas. (a) Comparison of genes within the *dos*R regulon with induced expression in all NHPs with either LTBI or ATB in each granuloma sample subset. For all heat maps included here, genes within the regulon or gene family of interest were included based upon published association and statistically significant positively induced expression within at least one granuloma category. The least induction is seen in ATB

representative pathology and the most in LTBI. **(b**). Confocal image of PIMO conjugated with Daylight-546 (**red**) with To-Pro-3 staining all nuclei (**green**). Signal in a representative ATB animal was much less than signal in a representative LTBI animal **(c)**. Additionally, PIMO signal within the lung as a percentage of total microscopic field was significantly greater in LTBI (**blue** squares) than ATB (**red** circles) (student's t test, p**<0.005) **(d)**. Lastly, heat map of genes associated with host hypoxic response showed greater response during LTBI as compared to ATB within NHP granulomas **(e)**.

Next, to further gauge the degree of hypoxia within the granuloma, we surveyed the amount of hypoxia within ATB and LTBI using PIMO (16) (Fig. 4b-c). TB lung lesions in both ATB and LTBI derived granulomas were positive for PIMO, indicating hypoxia. During ATB, PIMO was evident throughout granulomatous pathology (Fig. 4b). In contrast, in LTBI samples PIMO signal was predominately localized to the inner rim of the granuloma surrounding the caseum (Fig. 4c). PIMO signal was calculated as a percentage of lung and granuloma area within various microscopic fields (Fig. 4d). The highest levels of PIMO were observed in the classical granulomas of NHPs infected with LTBI (Fig. 4d). To determine if the expression of host genes known to be induced by hypoxia was correspondingly increased in LTBI compared to ATB, we screened a macaque transcriptome dataset of granuloma lesions isolated from 21 animals (LTBI (n=10) or ATB (n=11)), relative to normal lung tissue (SM, AAL, DK, manuscript in review), specifically focusing on host genes induced by hypoxia and regulated by the hypoxia-inducible factor 1 (HIF-1) (32) (Supplementary Table 9-10). These genes exhibited higher expression in lesions derived from both groups (Fig. 4b) with relatively higher expression of numerous hypoxia-sensitive genes in LTBI rather than ATB samples. These data suggest that the extent of the hypoxic environment is greater in lesions derived from animals with LTBI, strongly supporting our bacterial transcriptome data.

We detected the induced expression of a large number of genes that belong to the PE or PPE family of genes (Supplementary Table 11). We further assessed the expression of PE/PPE *in-vivo* by supervised clustering and observed increased induction in ATB samples (Fig. 5a). The PE/PPE family consists of more than 160 members unique to mycobacteria which have been implicated in antigenicity and associated with persister formation (33). We also investigated six known gene families and regulons for their intra-granulomatous expression, including sigma factors, TA systems, lipid metabolism, ESX1, enduring hypoxic response, and persisters. The expression of several TA genes, which potentially aid in the survival and persistence of *Mtb*, was highly induced (Supplementary Table 12). Although some differences existed between lesion types, which is expected, given the widely accepted concept of lesion heterogeneity we were able to detect approximately 26% of these genes in each of the granuloma types derived from animals with ATB (34). In animals with LTBI, we detected approximately 21% in the classical granuloma and 16 % in the caseum. TAs depicted greater induction in ATB than LTBI (Fig. 5b). The majority of the TAs expressed belonged to the largest TA family in the genome, the *vap*BC family. In total, we found the induction of 15 toxins and 14 antitoxins belonging to this family, including 4 pairs: *vap*BC19, *vap*BC21, *vap*BC33, and *vap*BC34, within granulomas.

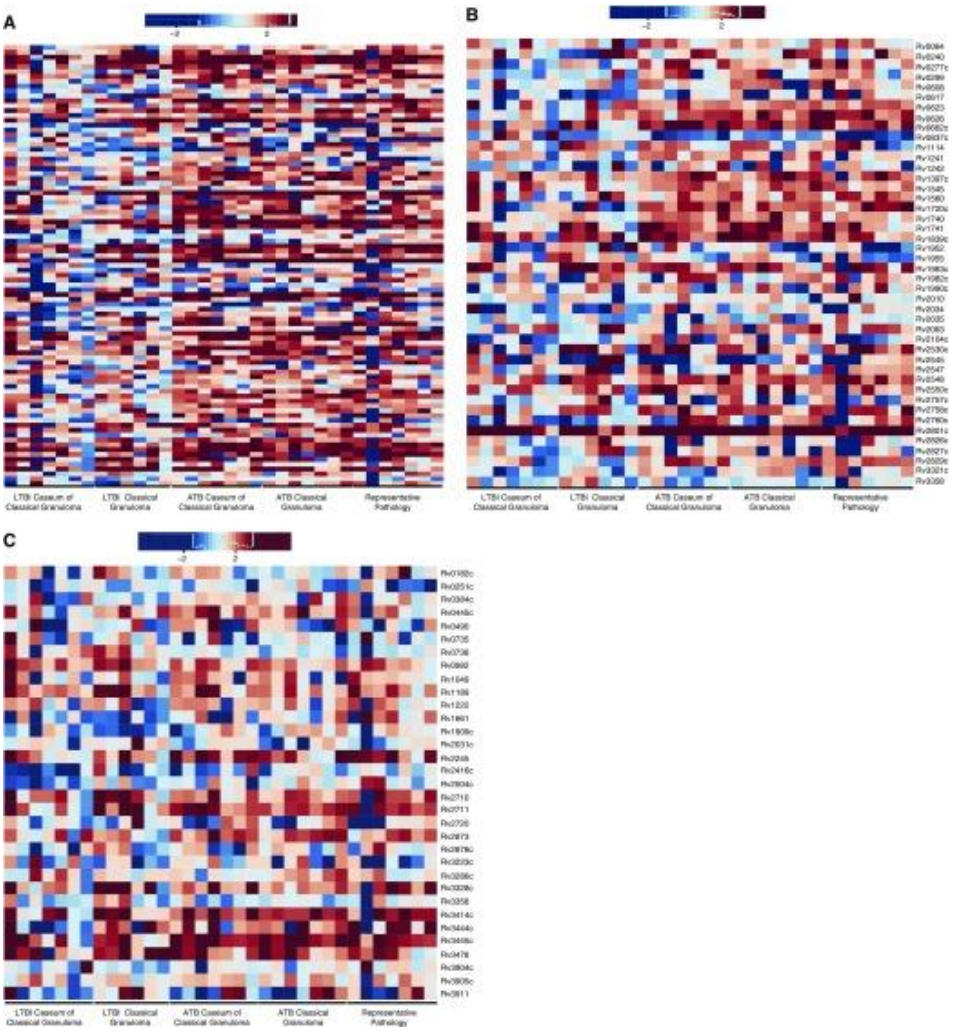

Figure 5: Mechanisms of persistence and validation. Comparison of genes within the (*A*) proline-glutamate/proline-proline-glutamate gene family, (*B*) toxin–antitoxin complexes, and (*C*) sigma factor family with induced expression in all NHPs with either LTBI or ATB in each granuloma sample subset.

To better assess the mechanisms of modulation of *Mtb* gene expression *in-vivo*, we assessed known sigma factors and their associated genes (Supplementary Table 13). We detected the following five in all samples: *sig*B, *sig*D, *sig*I, *sig*J, and *sig*F. We also detected the following factors within specific environments and disease states: LTBI – *sig*L and *sig*M (caseum) as well as *sig*K and *sig*G (granuloma); ATB – *sig*M, *sig*K, *sig*G (caseum), *sig*K (granuloma), *sig*G (representative pathology) and *sig*H (caseum). Overall, greater expression

was detected in ATB similarly to many of the aforementioned pathways (Fig. 5c). These results may suggest specific roles for each of these factors in facilitating the transition from ATB to LTBI. Thus, *sig*F and *sig*D have been shown to be required in the adaptation to stationary phase (35), while the induction of *sigJ*, *sigI* sigB, sigK, and *sigH* supports the importance of the oxidative stress on various bacterial components within the granuloma (35). These results point to a battery of alternate sigma factors being critically important for the survival of *Mtb in-vivo*, by modulating gene-expression in response to changing milieu.

We detected the up-regulation of 539 genes in a statistically significant manner common to all six granulomatous samples derived from patients with ATB (Supplementary Table 14). Additionally, 391 of the aforementioned genes were also detected in all NHP derived samples. Using a subset of 86 genes, we validated gene expression profiles via a microfluidic approach (Supplementary Fig. 4, Methods, Supplementary Table 15).

Supplemental Figure 4

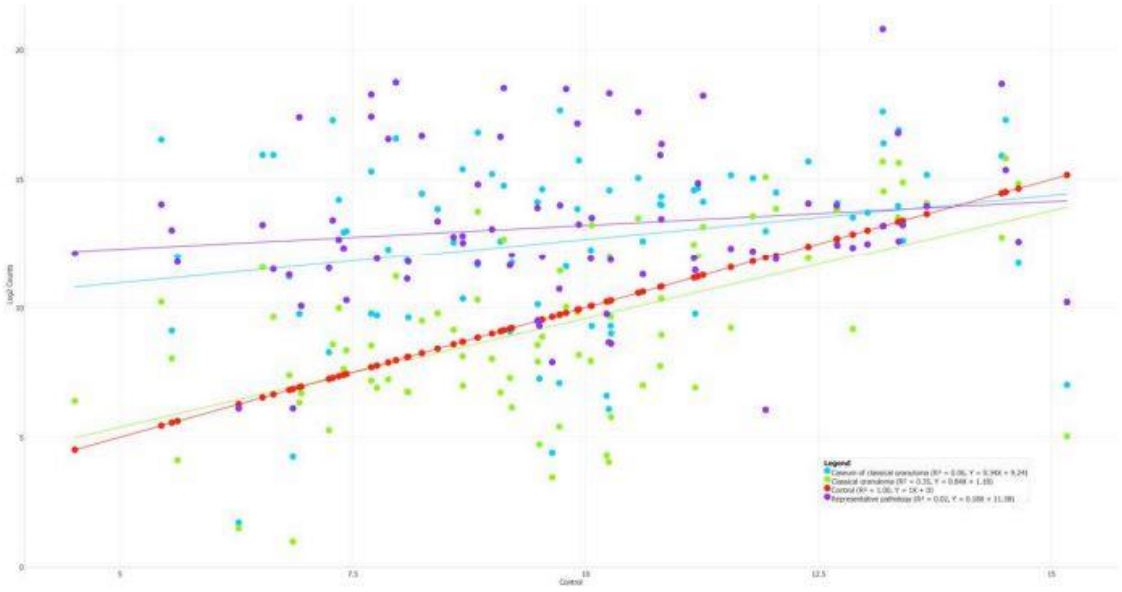

Supplementary Figure 4. Nanostring based validation of transcriptomics results. A defined subset of 86 genes including 5 housekeeping genes was used to validate RNA from microdissected ATB samples including: caseum of the classical granuloma (aqua, n=3, GK87, EA97, DI92), classical granuloma (green, n=4, DF30, CR57, EA97, DI91), representative pathology (purple, n=2, DI92, EB23) and control CDC1551 Mtb RNA (red) via NanoString Technology.

In addition, a small subset of genes with specific and interesting expression profiles were cherry-picked and transcriptome profiles validated by real-time RT-PCR in comparable classical granulomata derived from animals with ATB and LTBI (Fig 6). The expression of vapB21, an antitoxin of the TA system was validated to be induced ~100-fold in the classical lesions derived from animals with ATB, significantly higher than the expression in classical granulomata samples from animals with LTBI, where no induction was observed (Fig 6a). The expression of oxidative stress response factors *sigE* (12- vs. 0.1-fold) and *sigH* (~300- vs. 1.2-fold) was highly induced in lesions derived from ATB, relative to LTBI animals (Fig 6b-c). In the case of *sigH*, the difference approached statistical significance (P=0.0584). These results were comparable to those derived from whole-genome microarray analysis. The expression of the *dosR* gene was robustly detected in lesions derived from animals with both clinical outcomes, as was suggested by transcriptome and NanoString data (Fig 6d). The dosR levels were not statistically significantly different, but the overall expression was slightly higher in granulomata from animals with LTBI, relative to ATB.

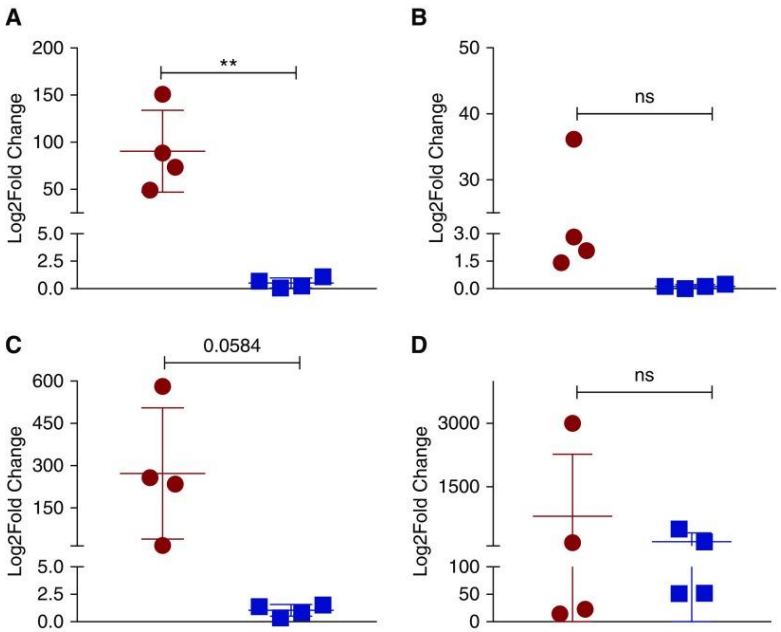

Figure 6: Real-time RT-PCR to validate macaque *Mtb* transcriptome results. Using cDNA derived from *in vitro*, log-phase–grown *Mtb*, and using the 16S gene as an internal reference, the fold changes of expression of *vapB21* (*A*), *sigE* (*B*), *sigH* (*C*), and *dos*R (*D*) was assessed in classical granulomata derived from animals with ATB (*red circles*) or LTBI (*blue squares*) (Student's *t* test, $^{**}P < 0.005$). ns, not significant.

We compared the genes expressed within granulomas to those previously essential for survival of the bacilli (Supplementary Fig. 5a) (4, 36-39). We found the greatest degree of similarity between intragranulomatous data described here to our previously conducted NHP mutant experiment where we identified 108 genes unable to survive in macaque lungs during active TB, implying that the genes whose expression was interrupted in these mutants were important for pathogenesis and likely expressed *in-vivo* (4) (Supplementary Table 16). An overwhelming number of genes overlapped in each disease state with 27% belonging to all ATB derived lesions, 18% to all LTBI derived lesions, and 17% to all NHP derived lesions (supplemental data). The next greatest degree of similarity was found with a computational prediction model (39), followed by the *in-vitro*/mouse TraSH (36), murine macrophage TraSH (38) and a mouse DeADMAn study (37) (Supplementary Tables 17-20). We detected

more essential genes in ATB presumably due to a higher burden of actively replicating bacteria. Pathway analysis of ATB and LTBI shows a high degree of known connection between essential genes defined by Dejesus et al (Supplementary Fig. 5b-c) (39). Interestingly, we detected 115 essential genes common to all ATB and LTBI NHP samples (Supplementary Fig. 5d) (39), ~50% of which function in intermediary metabolism and respiration, representing essential mechanisms *Mtb* employs to transition between active and latent disease. These results suggest the reprogramming of *Mtb* metabolism within lung lesions due to the varied availability of nutrients and metabolites.

Supplemental Figure 5.

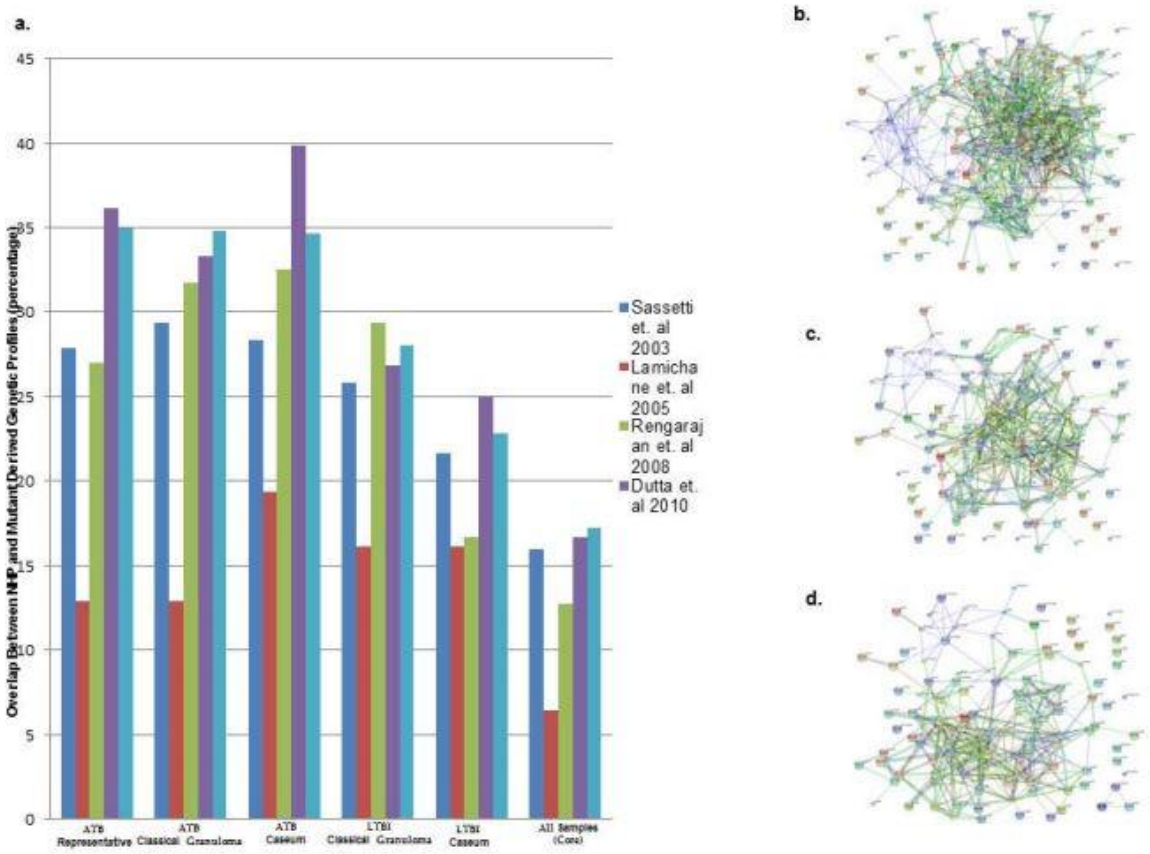

Supplementary Figure 5: Comparison of intragranulomatous gene profiles to previously determined gene essentiality profiles. (a) Genes, as a percentage of total mutant derived essential genes, found to be induced within the granuloma in-vivo that were previously deemed essential via either Sassetti (blue), Lamichane (red), Rengarajan (green), Dutta (purple) or DeJesus (aqua) et al. mutant based analysis; String pathway analysis of genes common to all (b) ATB derived granuloma samples; (c) LTBI derived granuloma samples; and (d) NHP derived samples and deemed essential by DeJesus et al.

DISCUSSION:

We assessed *Mtb* genes induced within defined micro-anatomic compartments of the TB lung in NHPs with ATB and LTB. Due to route of infection, pathologic, and disease spectrum similarities between NHPs and humans, especially in the context of TB, the NHP model is ideally suited to assess *in-vivo Mtb* gene expression. Lung samples utilized here reflect human TB disease because, like with human infection, NHPs were infected via aerosol. Additionally, NHP produce a spectrum of lesions most similar to those found in human TB patients as compared to other animal models; therefore, this is the best model for assessing specific granuloma microenvironments. This work extends beyond just assessing active disease transcriptome profiles, but also assesses the transition between LTBI and ATB. Like in humans, NHPs also develop LTBI. Unlike humans, it is possible to ethically obtain pulmonary endpoint samples from latently infected NHPs. Here we identified transcriptome profiles of both ATB and LTBI. Additionally, profiles were validated with lesions derived from human samples with active disease and comparable results obtained. Our results suggest that certain *Mtb* pathways are critical for the transition from LTBI to ATB disease.

Here we identify regulons associated with ATB, LTBI and the combination there of in representative ATB pathology, ATB and LTBI classical granulomas and their subsequent caseum. We identify a core group of genes common to all lesions indicating an underlying shared bacterial program to respond to the granulomatous environment, regardless of the clinical disease status. Our results conclusively demonstrate that the response of the bacillus to hypoxia is critical for the transition to latency. By finding the enhanced expression of hypoxia-responsive regulons, we provide the conclusive *in-vivo* evidence of its importance in maintaining *Mtb* in the chronic state of infection with the granuloma. By identifying genes and pathways involved in *Mtb* persistence, maintenance and growth *in-vivo* and coupling these findings to preexisting mutant based studies; this study provides critical information into genes that can be utilized in a potentially novel, targeted vaccine and therapeutic approaches.

Unsurprisingly; more genes were detected in a statistically significant manner in ATB than LTBI, since the latter is characterized by a greater bacterial burden as well as a higher magnitude of host response (5). The induced expression of a core group of 633 genes was identified in all intragranulomatous lesions representing a core group of genes essential for *Mtb* survival and persistence within the granuloma, suggesting these genes may be necessary for the transition from ATB to LTBI.

Stress is vitally important for *Mtb* gene regulation (40); consequently, we studied regulons known to respond to specific validated conditions with a primary focus on the expression of the hypoxia-sensing *dos*R gene and its regulon (31). While not required for initial infection, the *dos*R regulon is essential for the persistence of *Mtb* in human-like caseous granulomas (16). Further, the lack of *dos*R in *Mtb* allows the recruitment of stronger adaptive

immunity (16). A large number of *dosR*-dependent genes were expressed in every sample, disease state, and pathologic lesion studied. Importantly, intragranulomatous expression patterns of *dosR*-dependent genes circumvented our selection bias and strongly correlated with oxygenation patterns. Thus, the expression of the *dosR*-regulon was at the lowest level in the least hypoxic lesion type (ATB-representative pathology), while it was the greatest in the most hypoxic samples (LTBI-particularly caseum). This pattern was best exemplified by Rv1813c, which is co-regulated by both *dosR* and *mprAB* two component regulatory systems. It exhibited increased expression in LTBI, especially in the hypoxic caseum of the classical granuloma, demonstrating the ability of the bacillus to utilize multiple regulatory pathways concurrently to recognize, respond, and persist in specific environmental conditions.

At least two of the genes identified in this screen, Rv1996 and Rv2028c, are implicated in inducing greater T cell responses in patients with LTBI than ATB (41). Lastly, Rv2031c, which exhibited the highest induction in expression in LTBI and ATB caseum derived samples, is up regulated during latency. This gene has recently been implicated *in-silico* as an important regulator in cellular hypoxic stress response via its regulation of the Rv2028-Rv2031 operon. The higher induction of the *dosR* regulon in samples derived from macaques with LTBI was reinforced by increased hypoxia (PIMO) signal, as well as increased host HIF-1 expression, which is a known regulator of hypoxic responses (32). The expression of the downstream HIF-regulated host genes also occurred at much higher levels in LTBI, relative to ATB derived samples. Our study shows the critical importance of such mechanisms that allow the bacteria to alter its metabolism to favor survival in hostile conditions.

The expression of some *dosR*-dependent genes was high throughout granuloma types and disease states. This profile was exemplified by Rv0569, which encodes a signal transducer during hypoxia and by Rv2625c (*rip3)*, which encodes a mitochondrial reactive oxygen species induced in a TNF associated pathway (42). In conditions of excess TNF, ROS induces macrophage necrosis, allowing bacterial release into the extracellular environment, increasing host susceptibility (42). Since hypoxia was detected in all samples tested, our data strongly suggests that the induction of dormancy is critical in all granuloma stages, a result supported by observations that lesions of macaques with both ATB and LTBI contain levels hypoxia (Fig. 4b-d) (16). Our results are also supported by the recent evidence of *dosR* expression in the lungs of humans with TB (43). Overall, the pathogen's response to hypoxia is a critical component of its intragranulomatous physiology. While long suspected (44), we are only beginning to appreciate the importance of *dosR* and hypoxia in governing the transition from active to latent TB in classical lesions, and its impact on immunity.

Due to sustained *Mtb* replication, granulomata of different maturation levels can be observed in the same animal with ATB. These granulomata of varying pathologies provide an array of diverse environments to which the bacilli must respond to (45). Some of these lesions, especially the less mature ones, have not yet evolved to contain a fibrotic cuff on the exterior (Fig 1). As a result, these lesions are able to "breathe" and don't experience radically reduced oxygen tensions. On the contrary, virtually every LTBI lesion is highly ordered (Fig 1). Hence it is not surprising that the latter are more hypoxic and invoke a greater hypoxic response from both the host and the pathogen. It is believed that hypoxia within the LTBI lesions is the trigger that alters the physiology of the pathogen in a manner that bacilli acquire a dormant (or persistent) phenotype. There is support for our contention in

published literature. Thus, metronidazole is a drug that's only effective in hypoxic conditions, presumably against persisters. Treatment of LTBI but not ATB with metronidazole in this system prevents conversion to ATB (46).

Recent studies have in particular underlined the importance of the *dosR* regulon. T cells from humans with LTBI recognize *dosR*-regulated antigens, suggesting that these proteins are expressed and presented *in-vivo* during latency (47). Infection of macaques with *Mtb* mutants in the DosR regulon, causes nonpathogenic infection with enhanced adaptive immune responses recruited to the lung (16). Hence, the *dosR* response appears integral to *Mtb* pathogenesis and helps the pathogen manipulate immunity. Finally, an unbiased, system-wide proteomic approach found that upon in-vitro hypoxic stress, 20% of all *Mtb* protein mass is contributed by the <50 *dosR*-regulated genes (48). Moreover, the expression of this regulon was recently reported to be strongly induced in human TB and to significantly lower levels in patients with HIV (43). This suggests that the expression of DosR may promote more robust granulomas, a contention supported by data that expression of DosR by WhiB6 promotes granuloma stability in an environment of chronic oxidative/nitrosative stress (49). Thus, the notion that *dosR* is critical to the reprogramming of *Mtb* physiology in hypoxic conditions *in-vivo* is increasingly supported by experimental data (50). We propose that in macaque as well as human lesions, progressively increasing hypoxia elicits the expression of the DosR regulon. This results in the blockade of the highly cidal Th1 response from accessing the bacilli within the lesion through the expression of DosR-regulated antigens. The lesions characterized by high DosR expression are therefore likely robust granulomas that do not allow the bacilli to spread. The current study cements the role of the *dosR* regulon in *Mtb* persistence within human-like caseous lung granulomas by providing conclusive evidence for its deployment in this important niche (16). Since it is likely that

dosR-regulated antigens are expressed intragranulomatously, cognate *Mtb*-specific T cells could be effective in controlling or eradicating infection. By extension, our data suggests that the induction of *dosR* (or dormancy) results in the expression of numerous specific antigenic epitopes. Our results provide a compelling rationale to study responses specific to *dosR*-expressed antigens and suggest that vaccination approaches that induce CD4 and CD8 responses to these may be successful.

REFERENCES:

1. Russell DG, Barry CE, 3rd, Flynn JL. Tuberculosis: what we don't know can, and does, hurt us. Science. 2010;328(5980):852-6.

2. Foreman TW, Mehra S, LoBato DN, Malek A, Alvarez X, Golden NA, et al. CD4+ T-cell-independent mechanisms suppress reactivation of latent tuberculosis in a macaque model of HIV coinfection. Proceedings of the National Academy of Sciences of the United States of America. 2016.

3. Mehra S, Golden NA, Stuckey K, Didier PJ, Doyle LA, Russell-Lodrigue KE, et al. The Mycobacterium tuberculosis stress response factor SigH is required for bacterial burden as well as immunopathology in primate lungs. The Journal of infectious diseases. 2012;205(8):1203-13.

4. Dutta NK, Mehra S, Didier PJ, Roy CJ, Doyle LA, Alvarez X, et al. Genetic requirements for the survival of tubercle bacilli in primates. The Journal of infectious diseases. 2010;201(11):1743-52.

5. Mehra S, Pahar B, Dutta NK, Conerly CN, Philippi-Falkenstein K, Alvarez X, et al. Transcriptional reprogramming in nonhuman primate (rhesus macaque) tuberculosis granulomas. PloS one. 2010;5(8):e12266.

6. Mehra S, Golden NA, Dutta NK, Midkiff CC, Alvarez X, Doyle LA, et al. Reactivation of latent tuberculosis in rhesus macaques by coinfection with simian immunodeficiency virus. Journal of medical primatology. 2011;40(4):233-43.

7. Dutta NK, Mehra S, Martinez AN, Alvarez X, Renner NA, Morici LA, et al. The stress-response factor SigH modulates the interaction between Mycobacterium tuberculosis and host phagocytes. PloS one. 2012;7(1):e28958.

8. Kaushal D, Mehra S. Faithful Experimental Models of Human Infection. Mycobacterial diseases : tuberculosis & leprosy. 2012;2.

9. Kaushal D, Mehra S, Didier PJ, Lackner AA. The non-human primate model of tuberculosis. Journal of medical primatology. 2012;41(3):191-201.

10. Gopal R, Monin L, Torres D, Slight S, Mehra S, McKenna K, et al. S100A8/A9 Proteins Mediate Neutrophilic Inflammation and Lung Pathology during Tuberculosis. American journal of respiratory and critical care medicine. 2013.

11. Slight SR, Rangel-Moreno J, Gopal R, Lin Y, Fallert Junecko BA, Mehra S, et al. CXCR5(+) T helper cells mediate protective immunity against tuberculosis. The Journal of clinical investigation. 2013;123(2):712-26.

12. Darrah PA, Bolton DL, Lackner AA, Kaushal D, Aye PP, Mehra S, et al. Aerosol Vaccination with AERAS-402 Elicits Robust Cellular Immune Responses in the Lungs of

Rhesus Macaques but Fails To Protect against High-Dose Mycobacterium tuberculosis Challenge. J Immunol. 2014.

13. Luo Q, Mehra S, Golden NA, Kaushal D, Lacey MR. Identification of biomarkers for tuberculosis susceptibility via integrated analysis of gene expression and longitudinal clinical data. Frontiers in genetics. 2014;5:240.

14. Kaushal D, Foreman TW, Gautam US, Alvarez X, Adekambi T, Rangel-Moreno J, et al. Mucosal vaccination with attenuated Mycobacterium tuberculosis induces strong central memory responses and protects against tuberculosis. Nat Commun. 2015;6:8533.

15. Levine DM, Dutta NK, Eckels J, Scanga C, Stein C, Mehra S, et al. A tuberculosis ontology for host systems biology. Tuberculosis (Edinb). 2015.

16. Mehra S, Foreman TW, Didier PJ, Ahsan MH, Hudock TA, Kissee R, et al. The DosR Regulon Modulates Adaptive Immunity and is Essential for M. tuberculosis Persistence. American journal of respiratory and critical care medicine. 2015.

17. Mothe BR, Lindestam Arlehamn CS, Dow C, Dillon MB, Wiseman RW, Bohn P, et al. The TB-specific CD4 T cell immune repertoire in both cynomolgus and rhesus macaques largely overlap with humans. Tuberculosis (Edinb). 2015.

18. Phillips BL, Mehra S, Ahsan MH, Selman M, Khader SA, Kaushal D. LAG3 expression in active Mycobacterium tuberculosis infections. The American journal of pathology. 2015;185(3):820-33.

19. Mehra S, Alvarez X, Didier PJ, Doyle LA, Blanchard JL, Lackner AA, et al. Granuloma correlates of protection against tuberculosis and mechanisms of immune modulation by Mycobacterium tuberculosis. The Journal of infectious diseases. 2013;207(7):1115-27.

20. Dutta NK, McLachlan J, Mehra S, Kaushal D. Humoral and lung immune responses to Mycobacterium tuberculosis infection in a primate model of protection. Trials in vaccinology. 2014;3:47-51.

21. Hudock TA, Kaushal D. A novel microdissection approach to recovering mycobacterium tuberculosis specific transcripts from formalin fixed paraffin embedded lung granulomas. Journal of visualized experiments : JoVE. 2014(88).

22. Smyth GK. Linear models and empirical bayes methods for assessing differential expression in microarray experiments. Stat Appl Genet Mol Biol. 2004;3:Article3.

23. Kulkarni MM. Digital multiplexed gene expression analysis using the NanoString nCounter system. Curr Protoc Mol Biol. 2011;Chapter 25:Unit25B 10.

24. Mehra S, Kaushal D. Functional genomics reveals extended roles of the Mycobacterium tuberculosis stress response factor sigmaH. Journal of bacteriology. 2009;191(12):3965-80.

25. Dutta NK, Mehra S, Kaushal D. A Mycobacterium tuberculosis sigma factor network responds to cell-envelope damage by the promising anti-mycobacterial thioridazine. PloS one. 2010;5(4):e10069.

26. Mehra S, Dutta NK, Mollenkopf HJ, Kaushal D. Mycobacterium tuberculosis MT2816 encodes a key stress-response regulator. The Journal of infectious diseases. 2010;202(6):943-53.

27. Gautam US, McGillivray A, Mehra S, Didier PJ, Midkiff CC, Kissee RS, et al. DosS is Required for the Complete Virulence of Mycobacterium tuberculosis in Mice with Classical Granulomatous Lesions. American journal of respiratory cell and molecular biology. 2014.

28. McGillivray A, Golden NA, Gautam US, Mehra S, Kaushal D. The Mycobacterium tuberculosis Rv2745c Plays an Important Role in Responding to Redox Stress. PloS one. 2014;9(4):e93604.

29. Gautam US, Mehra S, Kaushal D. In-Vivo Gene Signatures of Mycobacterium tuberculosis in C3HeB/FeJ Mice. PloS one. 2015;10(8):e0135208.

30. McGillivray A, Golden NA, Kaushal D. The Mycobacterium tuberculosis Clp gene regulator is required for in vitro reactivation from hypoxia-induced dormancy. The Journal of biological chemistry. 2015;290(4):2351-67.

31. Boon C, Dick T. Mycobacterium bovis BCG response regulator essential for hypoxic dormancy. Journal of bacteriology. 2002;184(24):6760-7.

32. Semenza GL. HIF-1 mediates metabolic responses to intratumoral hypoxia and oncogenic mutations. The Journal of clinical investigation. 2013;123(9):3664-71.

33. Fishbein S, van Wyk N, Warren RM, Sampson SL. Phylogeny to function: PE/PPE protein evolution and impact on Mycobacterium tuberculosis pathogenicity. Molecular microbiology. 2015;96(5):901-16.

34. Lin PL, Ford CB, Coleman MT, Myers AJ, Gawande R, Ioerger T, et al. Sterilization of granulomas is common in active and latent tuberculosis despite within-host variability in bacterial killing. Nat Med. 2014;20(1):75-9.

35. Sachdeva P, Misra R, Tyagi AK, Singh Y. The sigma factors of Mycobacterium tuberculosis: regulation of the regulators. The FEBS journal. 2010;277(3):605-26.

36. Sassetti CM, Rubin EJ. Genetic requirements for mycobacterial survival during infection. Proceedings of the National Academy of Sciences of the United States of America. 2003;100(22):12989-94.

37. Lamichhane G, Tyagi S, Bishai WR. Designer arrays for defined mutant analysis to detect genes essential for survival of Mycobacterium tuberculosis in mouse lungs. Infection and immunity. 2005;73(4):2533-40.

38. Rengarajan J, Bloom BR, Rubin EJ. Genome-wide requirements for Mycobacterium tuberculosis adaptation and survival in macrophages. Proceedings of the National Academy of Sciences of the United States of America. 2005;102(23):8327-32.

39. DeJesus MA, Zhang YJ, Sassetti CM, Rubin EJ, Sacchettini JC, Ioerger TR. Bayesian analysis of gene essentiality based on sequencing of transposon insertion libraries. Bioinformatics. 2013;29(6):695-703.

40. Flentie K, Garner AL, Stallings CL. Mycobacterium tuberculosis Transcription Machinery: Ready To Respond to Host Attacks. Journal of bacteriology. 2016;198(9):1360-73.

41. Hozumi H, Tsujimura K, Yamamura Y, Seto S, Uchijima M, Nagata T, et al. Immunogenicity of dormancy-related antigens in individuals infected with Mycobacterium tuberculosis in Japan. Int J Tuberc Lung Dis. 2013;17(6):818-24.

42. Roca FJ, Ramakrishnan L. TNF dually mediates resistance and susceptibility to mycobacteria via mitochondrial reactive oxygen species. Cell. 2013;153(3):521-34.

43. Walter ND, de Jong BC, Garcia BJ, Dolganov GM, Worodria W, Byanyima P, et al. Adaptation of Mycobacterium tuberculosis to Impaired Host Immunity in HIV-Infected Patients. The Journal of infectious diseases. 2016;214(8):1205-11.

44. Boon C, Dick T. How Mycobacterium tuberculosis goes to sleep: the dormancy survival regulator DosR a decade later. Future microbiology. 2012;7(4):513-8.

45. Gengenbacher M, Kaufmann SH. Mycobacterium tuberculosis: success through dormancy. FEMS Microbiol Rev. 2012;36(3):514-32.

46. Lin PL, Dartois V, Johnston PJ, Janssen C, Via L, Goodwin MB, et al. Metronidazole prevents reactivation of latent Mycobacterium tuberculosis infection in macaques. Proceedings of the National Academy of Sciences of the United States of America. 2012;109(35):14188-93.

47. Lindestam Arlehamn CS, Gerasimova A, Mele F, Henderson R, Swann J, Greenbaum JA, et al. Memory T cells in latent Mycobacterium tuberculosis infection are directed against three antigenic islands and largely contained in a CXCR3+CCR6+ Th1 subset. PLoS pathogens. 2013;9(1):e1003130.

48. Schubert OT, Ludwig C, Kogadeeva M, Zimmermann M, Rosenberger G, Gengenbacher M, et al. Absolute Proteome Composition and Dynamics during Dormancy and Resuscitation of Mycobacterium tuberculosis. Cell host & microbe. 2015;18(1):96-108.

49. Chen Z, Hu Y, Cumming BM, Lu P, Feng L, Deng J, et al. Mycobacterial WhiB6 Differentially Regulates ESX-1 and the Dos Regulon to Modulate Granuloma Formation and Virulence in Zebrafish. Cell reports. 2016;16(9):2512-24.

50. Lipworth S, Hammond RJ, Baron VO, Hu Y, Coates A, Gillespie SH. Defining dormancy in mycobacterial disease. Tuberculosis (Edinb). 2016;99:131-42.

CHAPTER 6: NONPATHOLOGIC INFECTION OF MACAQUES BY AN ATTENUATED MYCOBACTERIAL VACCINE IS NOT REACTIVATED IN THE SETTING OF HIV CO-INFECTION

Summary of my contribution to the work:

Developed and applied my novel scoring system approach in a blinded fashion to assess pulmonary pathology for sections of all lung lobes for animals in this study, comparing wild type infection to attenuated vaccine strains. Performed chromagen immunohistochemical staining for lymphoid follicle identification. Wrote pathology portion of the manuscript, and took and edited pathology photomicrographs. Collaborated on preparing figures for publication. Edited manuscript prior to publication. The manuscript is provided below as it was published in the 2017 *American Journal of Pathology* 187(12): 2811-2820.

Short title: Attenuated TB vaccine is safe in lungs

Authors: Taylor Wayne Foreman[a,b], Ashley Victoria Veatch[a], Denae Nadine LoBato[a], Peter John Didier[a], Lara Angela Doyle-Meyers[a], Kasi Elizabeth Russell-Lodrigue[a], Andrew Alan

Lackner[a,b], Konstantin Gus Kousoulas[c,d], Shabaana Abdul Khader[e], Deepak Kaushal[a,b,2], and Smriti Mehra[a,c,d,2]

[a]Tulane National Primate Research Center, Covington, LA, 70471, USA; [b]Department of Microbiology and Immunology, Tulane University School of Medicine, New Orleans, LA, 70112, USA; [c]Center for Biomedical Research Excellence, Louisiana State University School of Veterinary Medicine, Baton Rouge, LA, 70803, USA; [d]Department of Pathobiological Sciences, Louisiana State University School of Veterinary Medicine, Baton Rouge, LA, 70803, USA; [e]Department of Molecular Microbiology, Washington University School of Medicine, St. Louis, Missouri, 63110, USA

[2]To whom correspondence may be addressed:

Smriti Mehra, Ph.D., Associate Professor of Microbiology, Louisiana University School of Veterinary Medicine, Baton Rouge, Louisiana, 70803, USA; Tel. 1-225-578-9695; smehra@lsu.edu AND Deepak Kaushal, Ph.D., Professor of Microbiology and Immunology, Tulane University School of Medicine and Tulane National Primate Research Center, 18703 Three Rivers Road, Covington, Louisiana, 70433, USA; Tel. 1-985-871-6254; dkaushal@tulane.edu

Abbreviations: ATB, active TB; BAL, bronchoalveolar lavage; BCG, bacille Calmette-Guérin; CRP, C-reactive protein; CXR, thoracic radiograph; iBALT, inducible bronchus-associated lymphoid tissue; LTBI, latent tuberculosis infection; *Mtb, Mycobacterium tuberculosis*;

NHPs, nonhuman primates; PBMC, peripheral blood mononuclear cell; TB, tuberculosis; TST, tuberculin skin test.

Funding: This research was supported by NIH awards to SM (R21AI127160, R21AI127222, P30GM110760) with additional support being provided by awards to DK (R01AI089323), SAK/DK (R01AI111914) and the TNPRC (P51OD011104, C06AI058609).

Disclosures: None declared

ABSTRACT:

Failure to replace BCG with efficacious anti-TB vaccines have prompted out-of-the-box thinking, including pulmonary vaccination in order to elicit local immunity. *MtbΔsigH*, a stress-response attenuated strain, protected against lethal TB when used to vaccinate macaques via inhalation. While live mycobacterial vaccines show promising efficacy, HIV co-infection and the resulting immunodeficiency prompts safety concerns about their use. We assessed the persistence and safety of *MtbΔsigH*, delivered directly to the lungs, in the setting of HIV coinfection. Macaques were aerosol vaccinated with *ΔsigH* and subsequently challenged with $SIV_{mac}239$. BAL and tissues were sampled for mycobacterial persistence, pathology and immune correlates. Only 35% and 3.5% lung samples were positive for live-bacilli and granulomas, respectively. Our results therefore suggest that the non-pathological infection of macaque lungs by *ΔsigH* was not reactivated by SIV, despite high viral titers and massive ablation of pulmonary $CD4^+$ T-cells. Protective pulmonary responses were retained, including

vaccine-induced bronchus associated lymphoid tissue (iBALT) and $CD8^+$ effector memory cells. Despite acute SIV infection, all animals remained asymptomatic of pulmonary TB. These findings highlight the efficacy of mucosal vaccination of this attenuated strain and will guide its further development to potentially combat TB in HIV endemic areas. Our results also suggest that lack of pulmonary pathology is a key correlate of safety for live mycobacterial vaccines.

INTRODUCTION:

Mucosal vaccination is being considered as a viable option to the systemic route (1), especially for lung pathogens like *Mtb*. Pulmonary mucosal vaccination can benefit from the unique physiology and the immune system in the lung. The respiratory system serves as the route of entry for numerous pathogens, which the lungs have evolved to contain by invoking rapid innate responses. Large surface area provides lungs with greater probability for interaction with the pathogen. Moreover, the mucosa in the airways and the parenchyma contain dendritic cells (DCs), which can phagocytose *Mtb* for efficient elicitation of adaptive responses via class I and II presentation (2). Antibodies are known to passively transfer through the lung epithelium into the alveoli. Furthermore, pulmonary immune cells can elicit the formation of local bronchus associated lymphoid tissue (BALT), the presence of which is strongly correlated with natural (3, 4) or vaccine-induced (5) immunity to TB, as well as to protection from development of HIV-induced reactivation of LTBI (6) in the human like macaque model (7, 8). Mucosal vaccination against agents of pulmonary infectious agents can result in the elicitation of local, antigen-specific, as well as broad-spectrum B- and T-cell responses, at the very site of the infection, resulting in more efficient protection.

Live attenuated mycobacterial vaccines demonstrate promising efficacy in protecting against TB (9). Due to the presence of a virtually complete array of antigens, such vaccines elicit a breadth of immune responses not obtained by vector or protein subunit strategies, increasing the likelihood of protection (10). Live vaccines can mimic natural infection through persistent antigenic stimulation, promoting stronger, long-lived immunity. However, a balance must exist between the pathogenicity and attenuation of the strain. Deletion various virulence pathways in *Mtb* is likely to result in a reduction of infectivity and arguably some of these mutations may generate the preferred combination of persistence, immunogenicity and nonpathogenicity (11-14). Human Immunodeficiency Virus (HIV), remains endemic to the regions of high TB incidence. Bacille Calmette-Guerin (BCG), a live attenuated mycobacterium that is one of the most widely used vaccines in the world, is efficacious against severe forms of TB. However, BCG is contraindicated in individuals with impaired immunity, including pregnant mothers and HIV infected individuals (15). The realization of a TB-free world is therefore contingent upon finding safe, novel, and efficacious replacements of BCG (16).

The World Health Organization recommends immunization with BCG as soon as possible after birth for infants born in endemic areas. Infants with symptomatic HIV disease are not immunized with BCG due to significantly increased rates of BCG-induced disease and the unknown efficacy of vaccinating HIV infected infants (17-19); however, infants who have not developed AIDS or will subsequently become HIV infected still get vaccinated. The risk of acquiring vaccine-induced disease poses a significant problem for the implementation of novel live attenuated mycobacterial vaccines; therefore, each vaccine candidate must be tested for persistence and safety upon subsequent HIV infection. There is currently only one new

live-attenuated mycobacterial vaccine in clinical trials (20), while there are multiple preclinical vaccines that have shown moderate to strong protection and varying immunogenicity. The *MtbΔsigH* mutant induced a nonpathogenic infection in macaques (21) and pulmonary vaccination with this strain protected significantly against subsequent lethal challenge with homologous *Mtb* (5). We previously demonstrated that this protection was strongly associated with recruitment of central memory T-cells to the lung and presence of vaccine-induced bronchus associated lymphoid tissue (BALT) (5). While these results were highly promising for clinical implementation of this live attenuated mycobacterial vaccine, safety concerns were noted due to the vaccine strain only containing a single gene deletion and possible persistence of the bacteria in the vaccinated individual.

In the current study, we aerosol vaccinated five macaques with *ΔsigH* and subsequently infected each macaque with SIV. We hypothesized that if *ΔsigH* was not adequately attenuated, some of the macaques could potentially develop signs of TB disease including dissemination of bacilli and uncontrolled bacterial replication in the lung, as has been replicated for BCG in this model (22).

MATERIALS AND METHODS:

Macaques.

Five mycobacteria-naive adult Indian rhesus macaques, bred and housed at the TNPRC that ranged from ~3-9 years in age and 4.0-11.6 kg in weight, were aerosol-vaccinated, as described earlier (for *Mtb*) (5, 6, 21, 23-29), to a high dose (~1000 CFU implanted) of *ΔsigH* isogenic deletion mutant in the *Mtb* CDC1551 background (5, 21, 30, 31). All macaques were exposed nine weeks post vaccination to 300 $TCID_{50}$ of $SIVmac_{239}$ administered intravenously in 1 mL saline, as described earlier (6, 24). All animal procedures were approved by the TNPRC

IACUC and performed in strict accordance with NIH guidelines. The TNPRC is accredited by the Association of Assessment and Accreditation of Laboratory Animal Care as well as by the United States Department of Agriculture (USDA). Criteria for euthanasia included presentation of four or more of the following conditions: i) body temperatures consistently greater than 2^0F above pre-infection values for three or more weeks in a row; ii) 15% or more loss in body weight; iii) serum CRP values higher than 10 mg/mL for three or more consecutive weeks; CRP is a marker for systemic inflammation that exhibits a high degree of correlation with active TB in macaques (8, 24); iv) CXR values higher than 2 on a scale of 0-4; v) dyspnea; vi) significant or complete loss of appetite, and vii) detectable bacilli in BAL samples.

NHP Sample Collection and Clinical Procedures

Samples were collected prior to and post vaccination, as well as post SIV infection. CXRs were acquired prior to and 3 weeks post-vaccination and 1 and 7 weeks post SIV infection, as previously described (5, 6, 24, 25, 27, 32, 33). The CXRs were scored by veterinary clinicians in a blinded fashion on a subjective scale of 0–4, with a score of 0 denoting normal lung and a score of 4 denoting severe tuberculous pneumonia, as previously described (5). Prior to vaccination, all 5 animals received a normal score of 0. Blood was drawn prior to vaccination and then weekly thereafter for measuring complete blood count (CBC) and serum chemistry (24, 25). Blood collected in EDTA tubes (Sarstedt AG & Co., Germany) was used for whole blood flow cytometry using the panels described earlier (5, 25, 27). BAL samples were obtained, as previously described, prior to vaccination, again at 3, 7, 11, and 14 weeks (24, 25), and then analyzed for CFUs and flow cytometry.

Bacterial Burden and Pulmonary Pathology

Humane endpoints were predefined in the animal use protocol and applied as a measure of reduction of discomfort (5). At necropsy, lung, spleen, and liver tissues were collected and processed, as previously described, using two sections of pulmonary tissue representing every lung lobe with at least one sample (5); CFU were determined per gram of tissue (3, 5, 6, 21, 24, 25, 27, 32, 33). Lung pathology at necropsy was determined as described earlier (6, 25). TB pathology was determined for multiple sections in each lung and averaged for each animal in the study. SIV-induced pathology was reported per section, with multiple sections analyzed per animal (6).

Flow cytometry.

Flow cytometry was performed on whole blood, BAL, lung and bronchial lymph node samples from all animals, as previously described (5, 6, 25, 27). Briefly, cells were stained for 25 minutes on ice with antibodies CD3 (SP34-2), CD4 (L200), CD8 (RPA-T8), CD28 (CD28.2), and CD95 (DX2) all from BD Biosciences, USA and washed twice with phosphate buffered saline containing 2% bovine serum albumin and 0.45% sodium azide then permebalized with BD Fix/Perm Kit and stained with Ki67 (B56) both from BD Biosciences, USA for 60 minutes on ice. Samples were fixed and acquired using a BD LSR Fortessa. Data was analyzed using FlowJo Software, version 10.3 (FlowJo, LLC, USA).

Immunohistochemistry.

Fluorescent immunohistochemistry, chromogenic staining, and *in situ* hybridization were performed on formalin-fixed, paraffin-embedded tissue as previously described (6, 34). Briefly, antigen retrieval was performed on tissue slides and stained with antibodies CD20

(L26), CD3 (polyclonal), CD68 (KP1) all from Agilent Technologies Dako, Denmark or CD163 (EDHu-1) from, Serotech, USA.

Statistical analyses

All statistical comparisons were performed using a one-way ANOVA, student's t-test, or peasrons correlation analysis in GraphPad Prism version 7.0b (GraphPad Software Inc., USA) as noted in figure legends as described earlier (5). All data is presented as mean ± SEM.

RESULTS:

Clinical/pulmonary correlates of mycobacterial infection in *ΔsigH* vaccination and SIV infection.

Direct aerosolization of *ΔsigH* into the lungs of macaques induced robust responses and impressive protection against lethal TB. Five macaques (Table 1) were therefore aerosol vaccinated with 1000 colony forming units (CFU) of *ΔsigH* to test the safety of this strain in the setting of HIV co-infection. This dose has been shown to produce a non-pathogenic infection in macaques and to induce superlative protection upon subsequent lethal challenge when used as a vaccine. The vaccinated animals were allowed to rest for nine weeks prior to high dose intravenous challenge with SIV. This dose and route of SIV challenge is commonly used in HIV research to study pathogenic infection in rhesus macaques. In our experiment, this dose/route combination modeled acute HIV infection resulting in the rapid ablation of $CD4^+$ T-cells and overall dysfunction of immune responses to *Mtb (6)*. For comparison purposes, rhesus macaques latently infected with a low dose (10^1 CFU) of *Mtb* CDC1551 and subsequently infected with the same dose/route of SIV at the same time (nine weeks after aerosol infection with *Mtb*) have been included in some graphs to demonstrate SIV-induced

reactivation of TB disease (Coinfected group shown in gray). The lower dose of *Mtb* in these reactivated animals, was chosen since 10^3 CFU of wild-type *Mtb* would lead to rapid death within 9 weeks. However, the low dose establishes latent infection in these animals and allows the study of reactivation by immunosuppression or SIV coinfection.

Table 1. Vaccinated Animals.

Animal	Age	Sex	Weight Pre-Vaccination	TST Pre-Vaccination
KH76	2.8	Male	4.0	-
KF62	2.9	Male	4.1	-
GB13	9.5	Female	8.4	-
IM63	5.4	Male	11.0	-
JG35	4.4	Male	11.6	-
Average ± SD	*5.0 ± 2.7*		*7.8 ± 3.6*	

Immediately post-vaccination, all animals maintained or gained weight (Fig. 1A) and maintained temperature (Fig. 1B) as shown as percent change compared to preinfection baseline weight and temperature. One out of five animals exhibited elevated CRP one-week post vaccination, which subsided by week 3, while the other four vaccinated animals showed no increase in CRP for the entire study (Fig. 1C). None of the animals had lung pathology as assessed by CXR three weeks post vaccination. Upon subsequent intravenous challenge with a high-dose of pathogenic SIV, all vaccinated animals remained devoid of TB disease as evidenced by lack of weight loss, minimal change in temperature, and no increase of CRP (Fig. 1A-C). Conversely, coinfected animals demonstrate reactivation disease as evidenced by progressive weight loss, extensive pyrexia, and significantly elevated CRP levels (Fig. 1).

Thoracic radiographs of these animals further validated the lack of pulmonary disease in vaccinated animals (Supplemental Fig. 1).

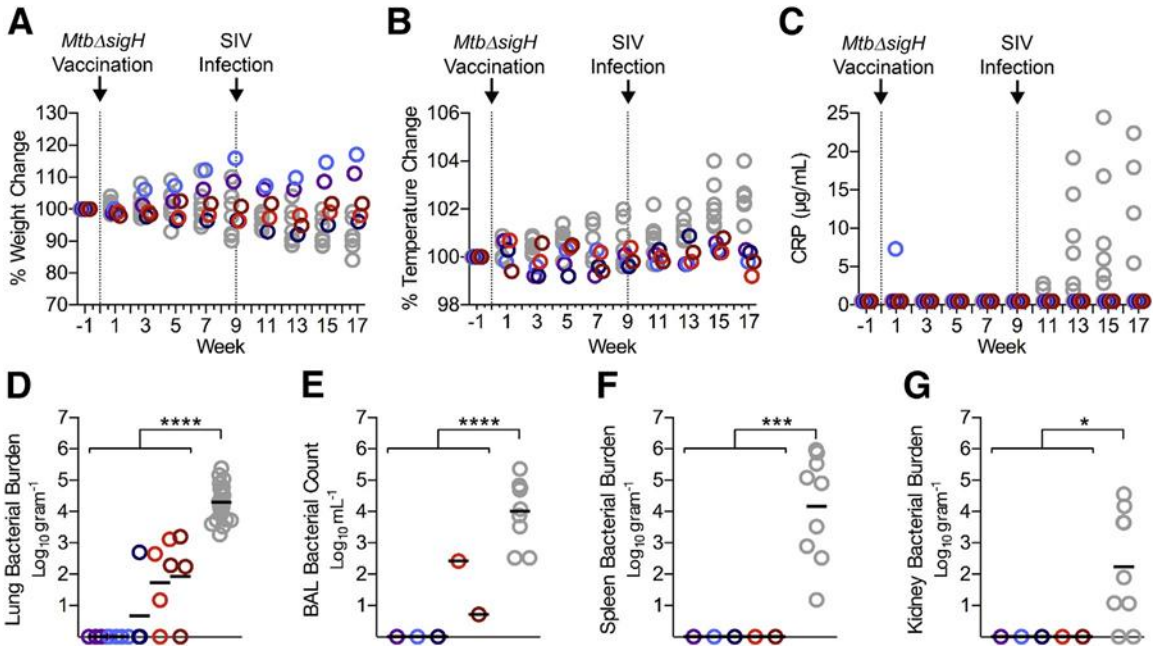

Figure 1: Clinical and bacteriologic correlates of *MtbΔsigH* vaccination and subsequent simian immunodeficiency virus (SIV) infection. Five Indian rhesus macaques were vaccinated with 1000 CFU of *MtbΔsigH* and challenged with a high dose of SIVmac239 at 9 weeks after vaccination. AeC: Comparisons of percent weight loss (A), percentage of temperature increases (B), and C-reactive protein (C) in *MtbΔsigH*-vaccinated animals (color) versus *Mtb*/SIV co- infected animals (gray). Dotted lines indicate day of vaccination or SIV challenge. D: *MtbΔsigH* bacilli present in the lung (in number per gram of tissue) at the time of euthanasia, with multiple lung sections sampled per animal. EeG: Vaccine bacilli present in bronchoalveolar lavage (E), spleen (F), and kidney (G). Data are expressed as means. $*P < 0.05$, $***P < 0.001$, and $****P < 0.0001$ using a *t*-test analyzing the mean values of all vaccinated animals versus *Mtb*/SIV-co-infected animals. CRP, C-reactive protein.

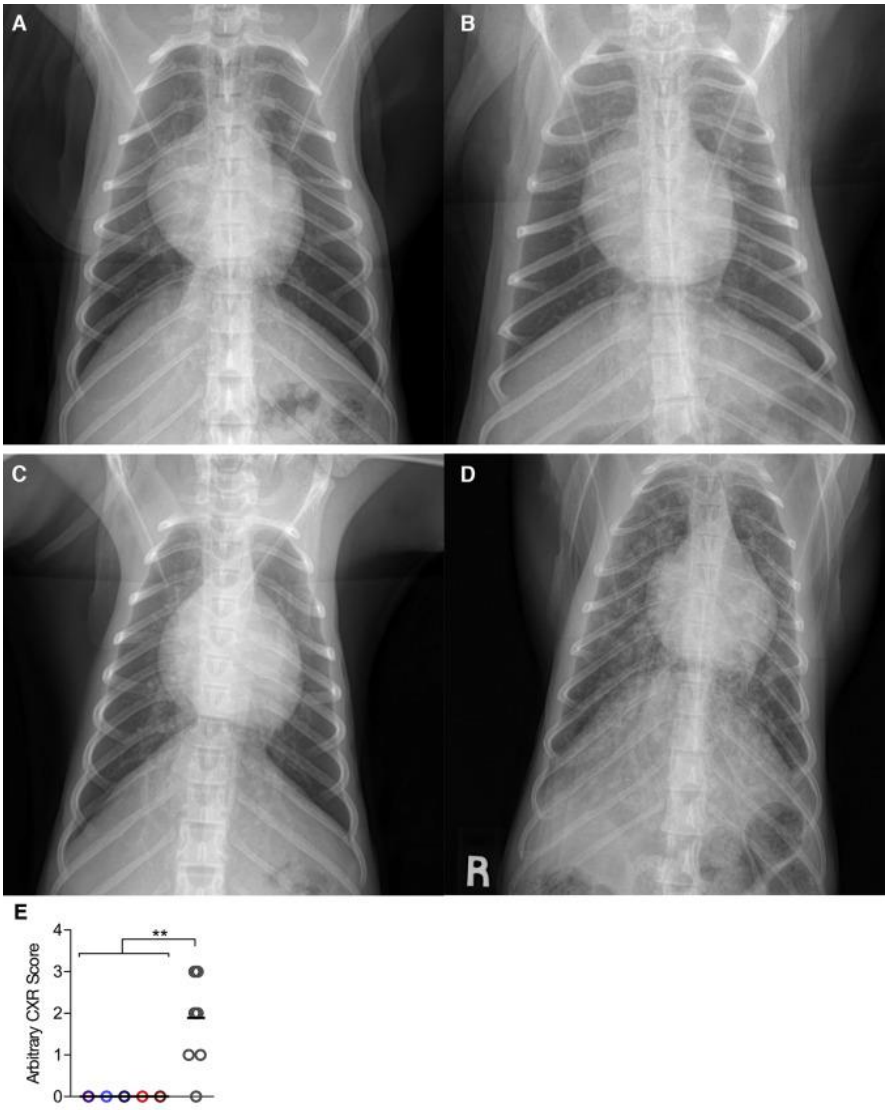

Supplementary Figure 1: Thoracic radiographs at euthanasia. **A–D:** Exemplary thoracic radiographs of three *Mtb*Δ*sigH*-vaccinated animals (**A–C**) in comparison to a *Mtb*/simian immunodeficiency virus (SIV)-co-infected animal (**D**) at the time of euthanasia, demonstrating a lack of pulmonary pathology. **E:** Quantitative analysis of radiographs scored in a single-blind fashion by a board-certified veterinarian (D.N.L.), on the following scale: 0 (null) to 4 (severe lung involvement). $^{**}P < 0.01$ using a *t*-test analyzing the mean values of all vaccinated animals versus *Mtb*/SIV–co-infected animals. R, lead marker used for identify right on the radiograph.

Lung bacterial burden after SIV infection. We next investigated whether *ΔsigH* persists in the lungs of vaccinated macaques and whether infection with SIV would permit uncontrolled bacterial replication. Nine weeks following SIV challenge, the animals were humanely euthanized and tissues were extensively assessed for bacterial burden. From the 5 vaccinated animals, 13 out of 20 lung sections tested were devoid of any detectable bacteria. Very low levels of *MtbΔsigH* could be cultured from the lungs of vaccinated animals ($10^{0.86}$, average 7 bacilli per gram of lung tissue) as compared to coinfected animals that had a significantly higher bacterial burden ($10^{4.3}$, ~20,000 bacilli) (Fig. 1D). To exclude potential skewing due to sterile lobes, the average bacterial burden of vaccinated animals with only culturable bacteria was $10^{2.47}$ or ~300 CFU. However, animals that are able to maintain control of infection in a latent state have been found to have upwards of $10^{3.5}$ CFU. Furthermore, an average of 4 bacilli ($10^{0.62}$) per mL of lavage fluid was recovered in bronchoalveolar lavage (BAL) while 3 animals had no detectable bacilli (Fig. 1E). In comparison, an average of 10,000 bacilli ($10^{4.0}$) was recovered from *Mtb*/SIV coinfected animals (6). These results are even more contrasting, since vaccinated animals received ~two-log (10^{3}) more *MtbΔsigH* bacilli than was used in *Mtb*/SIV coinfection (10^{1}) with wild-type *Mtb*. Coinfection of *Mtb* and HIV in humans and macaques is characterized by extensive dissemination to extra-thoracic organs. However, *ΔsigH* vaccinated animals had no detectable bacilli in spleen or kidney (Fig. 1F-G). These results demonstrate that while vaccination with *ΔsigH* is largely sterilized, very few bacilli persist and acute infection with SIV does not create a permissive environment for excessive bacterial replication.

Lung Pathology. As shown before, pathology induced by aerosol vaccination with *ΔsigH* remained insignificant as determined by both gross and histopathological examination. Despite infection with SIV, *ΔsigH* vaccinated macaques maintained minimal pathology (Supplemental Fig. 2). Out of 85 lung sections histopathologically examined, only three sections (3.5%) revealed evidence of granulomatous inflammation (Fig. 2A-E). Each of these few granulomas were well organized and lacked significant neutrophilic infiltrates. The severity of pulmonary pathology is increased in coinfected macaques versus only *Mtb*-infected animals, making macaques a good model of the synergy between HIV and TB during coinfection. In vaccinated animals, however, interstitial pulmonary pathology parameters—including vasculitis/lymphangitis (Fig. 2F-G), septal thickening, type II pneumocyte hyperplasia, accumulation of foamy alveolar macrophages, and lymphohistiocytic perivasculitis—were significantly reduced compared to coinfected animals (Supplemental Fig. 2), suggesting that SIV-induced pathology was not exacerbated in vaccinated animals.

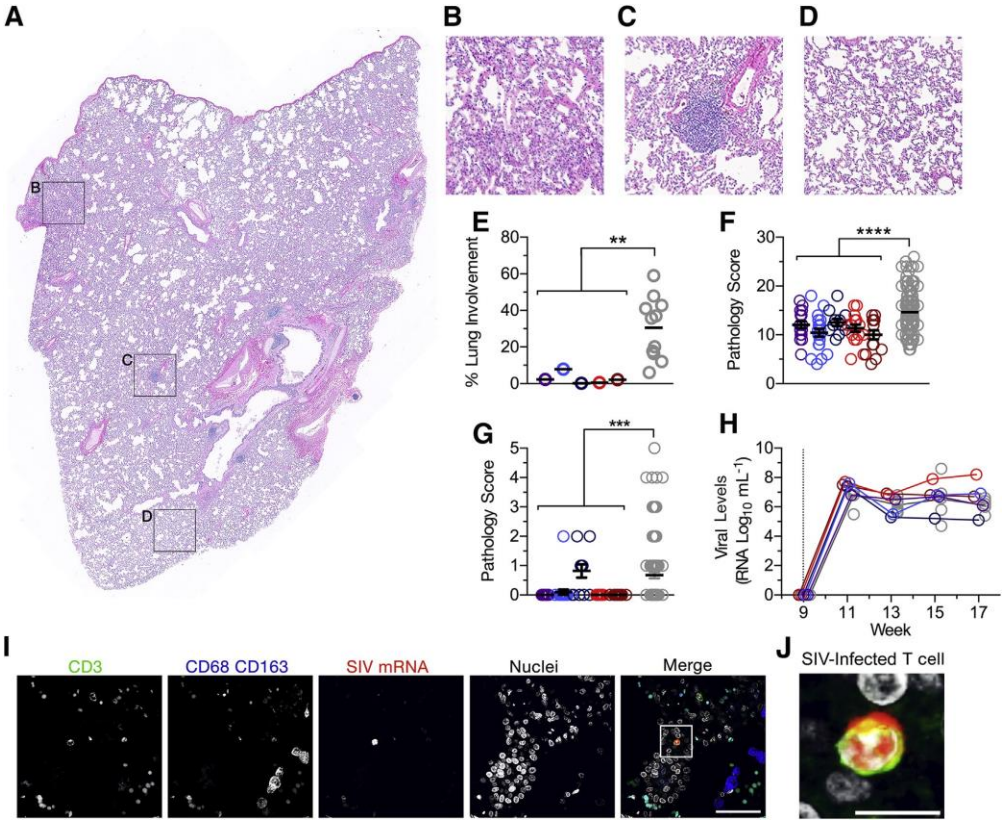

Figure 2: Pulmonary pathology after *Mtb*Δ*sig*H vaccination and simian immunodeficiency virus (SIV) infection. A–D: Hematoxylin and eosin staining of lung sections from a representative animal showing an entire lung section **(A),** with boxed areas in A shown as enlarged images of consolidation **(B),** vaccine-induced bronchus-associated lymphoid tissue (BALT) **(C),** and healthy lung tissue examples **(D)** corresponding to the boxed regions in A. E: Quantification of overall pathology as percentage of lung involvement. Multiple lung sections per animal were scored and quantitatively compared with those from *Mtb*/SIV–co-infected animals in total pathology score **(F)** and lymphangitis **(G). H:** Peripheral viral loads in vaccinated animals (color) and *Mtb*/SIV–co-infected animals (gray). Dotted line indicates the time of SIV infection. **I:** In situ hybridization demonstrating the presence of SIV-infected CD3+ T cells in the lungs of vaccinated animals. **J:** Enlarged inset image of an infected cell corresponding to the boxed area in **I**. Data are expressed as means ± SEM (E–H). $^{**}P < 0.01$, $^{***}P < 0.001$, and $^{****}P < 0.0001$ using a t-test analyzing the mean values of all vaccinated animals versus *Mtb*/SIV–co-infected animals. Scale bars: 100 um **(I);** 5 um **(J).**

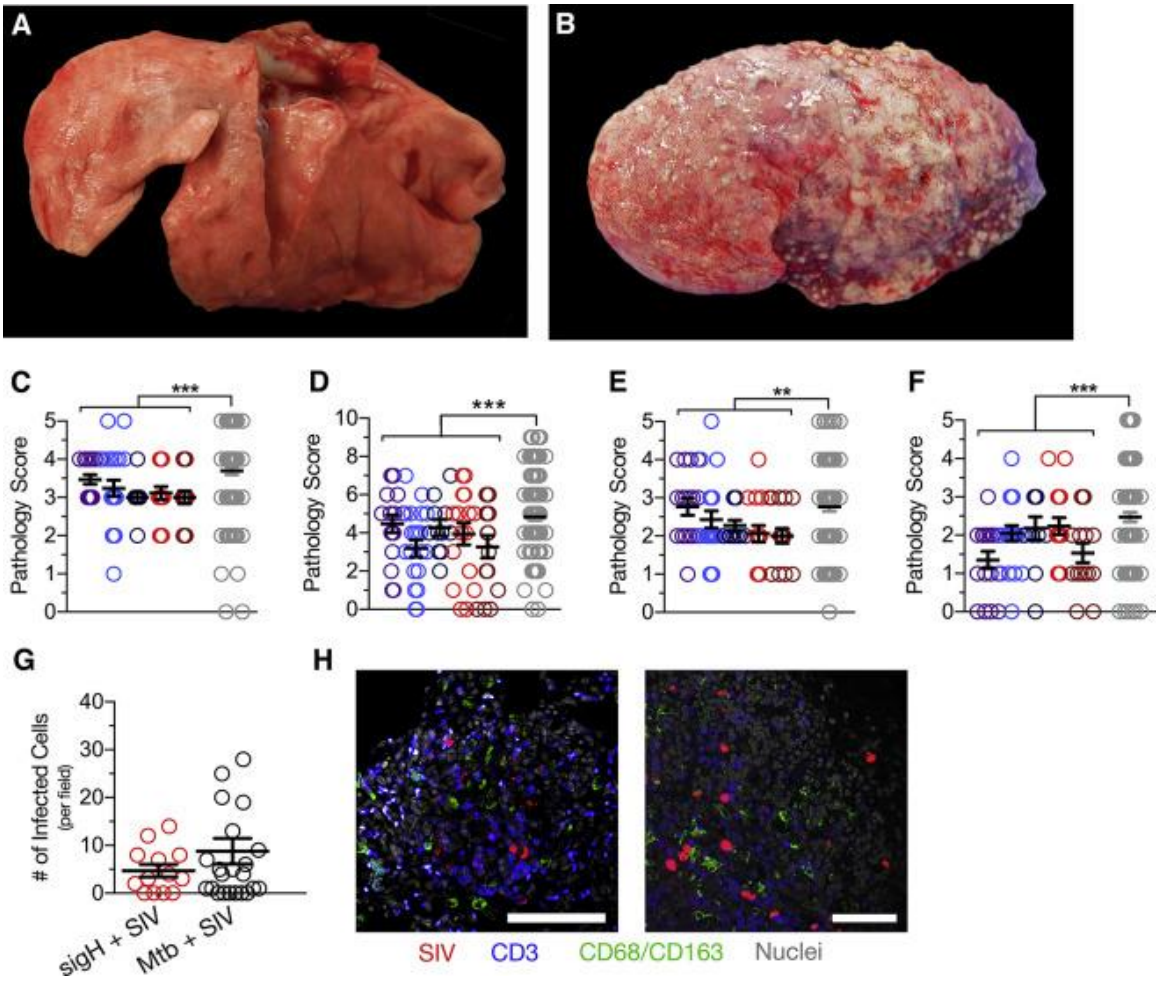

Supplemental Figure 2: Gross and histopathology in *Mtb*Δ sigH-vaccinated animals compared with *Mtb*/simian immunodeficiency virus (SIV)–co-infected animals. A and **B**: Gross pathology of a *Mtb*Δ sigH vaccinated animal **(A)** as compared to a *Mtb*/SIV–co-infected animal **(B). C–F:** Assessments of type II pneumocyte hyperplasia **(C)**, consolidation **(D)**, accumulation of alveolar macrophages **(E)**, and perivasculitis **(F). G** and **H**: Analysis of the number of SIV-infected cells for image field as compared to SIV-reactivated animals, with representative images demonstrating numerous SIV-infected cells at sites of inflammation (H). The merged cells appear purple. Data are expressed as means ± SEM (**C–G**). $^{**}P < 0.01$, $^{***}P < 0.001$ using a t-test analyzing the mean values of all vaccinated animals versus *Mtb*/SIV–co-infected animals. Scale bar = 100 μm.

Since diminished SIV replication could explain the lack of severe SIV-induced pathology and subsequent effects on the control of bacterial replication, we next assessed peripheral viral loads in plasma. While there were no distinct differences in peripheral viral loads during the entire study (Fig. 2H), differences in replication at the site of vaccination could explain the reduced pathology. *Mtb*/SIV coinfected animals with severe reactivation disease harbored SIV infected cells in the lung while animals that controlled reactivation were able to minimize viral replication in the lung. This indicates that viral replication at the site of infection or vaccination can act to inhibit immunity to the persistent bacteria. Permissive viral replication in the lungs of coinfected animals likely increased pathology and decreased immune control of latent TB in *Mtb*/SIV coinfected animals. Upon investigation, we observed that *MtbΔsigH* vaccinated animals harbored many SIV infected $CD3^+$ T-cells and a few $CD68^+CD163^+$ macrophages (Fig. 2I-J, Supplemental Fig. 2H). Hence, in terms of the presence of SIV in the lungs, the *MtbΔsigH* vaccinated animals resembled *Mtb*/SIV coinfected animals that could not control latent infection. However, despite the presence of large numbers of SIV-infected cells in the lungs, the *MtbΔsigH* vaccinated animals maintained minimal pathology and immune control of the attenuated bacterial vaccine despite productive viral replication in the lungs.

Systemic and lung immunity. We next studied the immune cells responding to both vaccination and SIV infection in both whole blood and in the lung via bronchoalveolar lavage fluid (BAL). Vaccination with *MtbΔsigH* resulted in the rapid accumulation of both $CD4^+$ and $CD8^+$ T-cells in BAL (Fig. 3A). We previously demonstrated that $CD4^+$ central memory (T_{CM}) cells rapidly respond to this vaccination and correlate with strong protection upon lethal challenge. As validation, there was a significant increase in the number of ($CD28^+CD95^+$) $CD4^+$ T_{CM} cells responding to vaccination at week 7 and also exhibited rapid proliferation post

vaccination as marked by Ki67 positivity (Fig. 3B-F). However, subsequent SIV infection resulted in the rapid ablation of pulmonary $CD4^+$ T-cells (Fig. 3A-B), resulting in a virtually complete loss $CD4^+$ T_{CM} cells (Fig. 3D). Furthermore, $CD8^+$ T-cells responding to vaccination persisted after SIV infection and demonstrated proliferation both after vaccination and subsequent infection (Fig. 3G-K). While these differences were apparent in BAL, comparison of $CD4^+$ and $CD8^+$ T-cells in whole blood showed no significant differences either after vaccination or SIV infection (Supplemental Fig. 3).

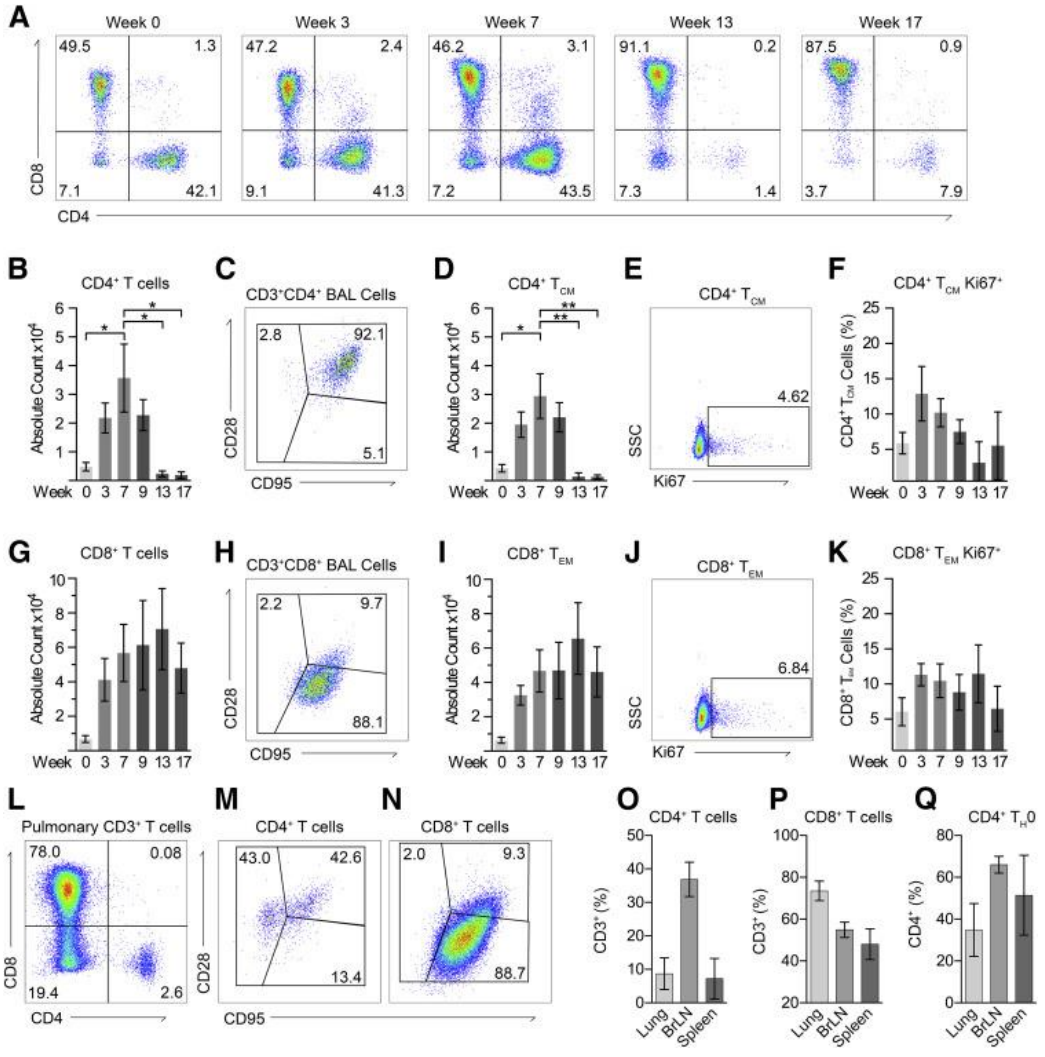

Figure 3: Correlates of cellular immune responses. A: Analysis of CD3+ lymphocytes found in bronchoalveolar lavage (BAL) throughout the study, demonstrating decline in CD4+ T cells after simian

immunodeficiency virus (SIV) infection at week 9. **B–D**: Absolute number of CD4+ T cells found in BAL (**B**), with example flow plot of memory status (**C**) and absolute count of CD4+ central memory T (TCM) cells (**D**). **E** and **F**: Ki67+-proliferating CD4+ TCM cells in BAL. Boxed areas indicate Ki67+ cells (**E**). **G–I**: CD8+ T cells found in BAL, with example flow plot of CD8+ T-cell memory status (**H**) and absolute count of CD8+ effector memory T (TEM) cells (**I**). **J** and **K**: Ki67+-proliferating CD8+ TEM cells in BAL. Boxed areas indicate Ki67+ cells (**J**). **L–N**: Representative flow plot of pulmonary lymphocytes at the time of euthanasia demonstrating depletion of effector and CD4+ TCM cells (**M**) and effector CD8+ T-cell retention (**N**). **O–Q**: Percentages of CD4+ T cells (**O**) and CD8+ T cells (**P**) in lung, bronchial lymph node (BrLN), and spleen, demonstrating the preservation of naïve (Th0) CD4+ T cells after SIV infection (**Q**). Data are expressed as means ± SEM (**B, D, F, G, I, K, O–Q**). ∗P < 0.05, ∗∗P < 0.01 using one-way analysis of variance with Šídák correction. SSC, side scatter.

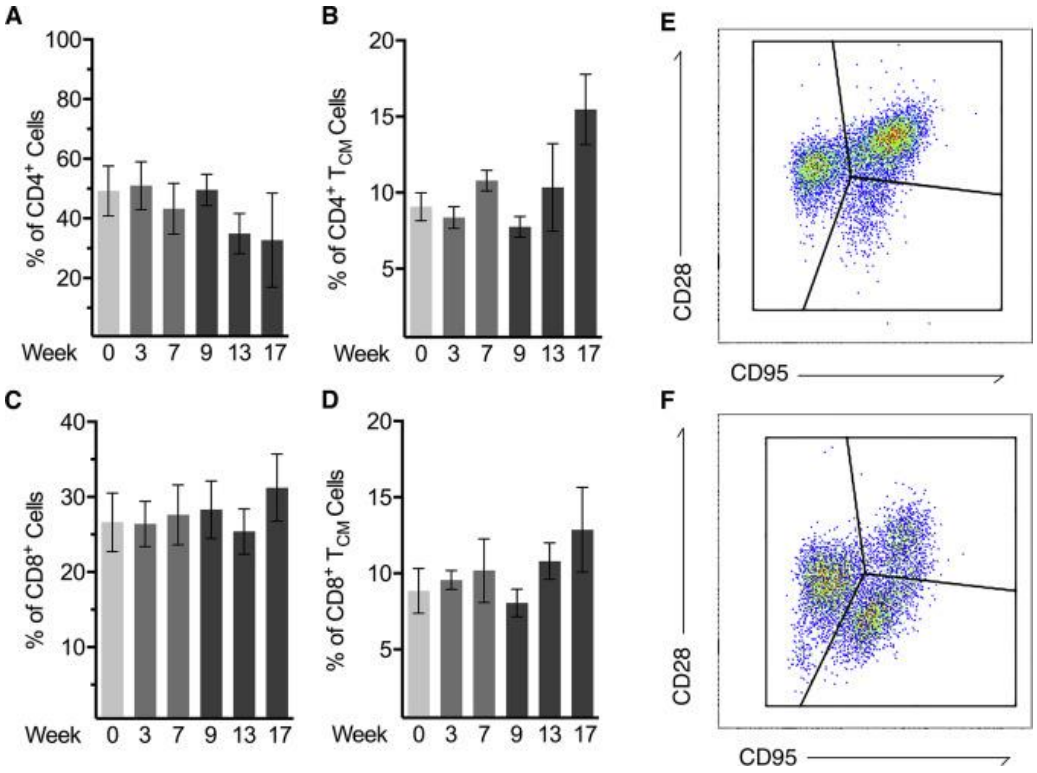

Supplemental Figure 3: Correlates of cellular immune responses. A and **B:** Analysis of CD4+ central memory T (TCM) cells found in whole blood throughout the study, demonstrating a modest decline after simian immunodeficiency virus (SIV) infection at week 9 (**A**), and the percentage of CD4+ TCM cells proliferating as marked by Ki67+ (**B**). **C**: Example flow plots showing gating for (CD28+CD95–)-naïve cells, (CD28+CD95+)

TCM cells, and (CD28−CD95+) effector memory T cells in CD4+ T cells. **D** and **E**: Analysis of CD8+ TCM cells in whole blood (**D**), with percent CD8+ TCM cells positive for Ki67 (**E**). **F**: Example flow plots showing gating for naïve cells, TCM cells, and CD8+ effector memory T cells. Data are expressed as means ± SEM **(A–D).**

We next assessed the level of $CD4^+$ T-cell depletion in tissues at the time of euthanasia (Fig. 3L-N). The extent of $CD4^+$ T-cell depletion in lung was comparable to BAL; however, relatively greater frequencies of $CD4^+$T-cells persisted in the bronchial lymph nodes (Fig. 3O-P). Examination of the memory status of the few remaining $CD4^+$ T-cells demonstrated that these cells were primarily T_{CM} or naïve (T_H0) cells (Fig. 3Q). $CD4^+$ cells that remained in the bronchial lymph nodes were also predominantly T_H0. The $CD8^+$ T-cells in lung were primarily ($CD28^-CD95^+$) effector memory (T_{EM}) cells, indicating that, $CD8^+$ T-cells likely compensate the absence of $CD4^+$ T-cells in order to facilitate the complete control of this avirulent *Mycobacterium* (Fig. 3P).

Persistence of Bronchus Associated Lymphoid Tissue. Presence of bronchus associated lymphoid tissue (BALT) strongly correlates with protection in *ΔsigH* vaccinated macaques after lethal challenge (5) and also correlates with protection from HIV-induced reactivation of latent TB (6). BALT is also associated with the natural control of *Mtb* infection in a latent state (4), whereas animals developing active disease coincidentally lose granuloma-associated BALT with neutrophilic influx (3). We therefore assessed the persistence of vaccine-induced BALT despite the very minimal bacterial burden and ablation of $CD4^+$ T-cells after SIV infection. While only 3.5% of the analyzed lung sections contained evidence of granulomatous pathology, 84% of lung sections contained BALT (Fig. 4). Chromogenic staining of lung sections with CD20 demonstrated large organized follicles persisted proximal to airways and the pulmonary vasculature (Fig. 4A). Further assessment of $CD3^+$ T-cells

demonstrated colocalization of T-cells in these lymphoid follicles (Fig. 4B). The scored level of BALT persistence strongly correlated with the amount of vaccine- and SIV-induced pathology as assessed by pathological scores for each lung section (Fig. 2F). The current findings support previous work demonstrating that induction of BALT by *ΔsigH* vaccination correlates with reduced overall pathology. Furthermore, the ability of BALT to persist for 17 weeks after vaccination, despite SIV infection and a lack of significant antigen stimulation, indicates that mucosal vaccination may drive long-lived tissue-specific immunity.

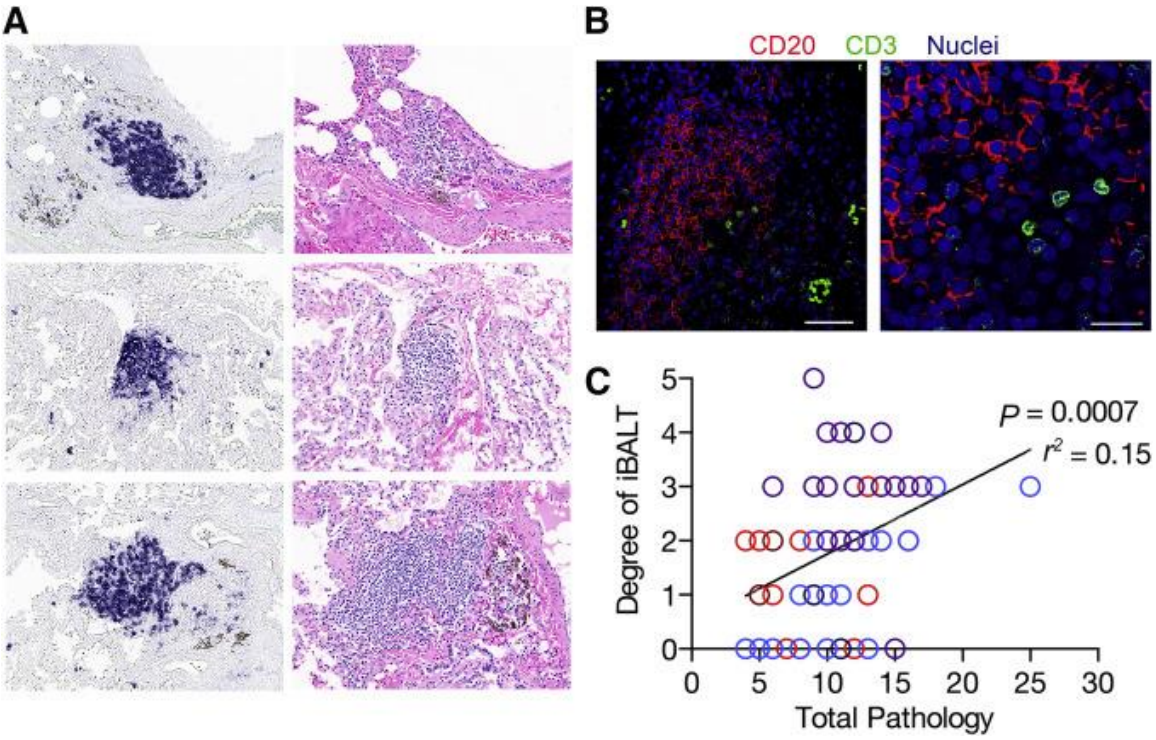

Figure 4: Persistent vaccine-induced bronchus-associated lymphoid tissue (BALT). A: Chromogenic staining with CD20 (left panels) and the respective hematoxylin and eosin staining (right panels) showing B-cell follicles in the lung at euthanasia. **B**: Immunohistochemistry analysis staining for CD20 B cells, CD3 T cells, and nuclei, showing that T cells remain in BALT. **C**: Correlation analysis of the degree of BALT formation and the overall pathology score for each lung section analyzed, demonstrating that BALT persists in areas of continued inflammation to maintain immune control of bacterial replication, analyzed using the Pearson r correlation analysis. Data are expressed as correlation values. Scale bars: 100 μm (B, right); 25 μm (B, left).

DISCUSSION:

Development of novel vaccination strategies for TB remains a high priority and significant endeavor (16). Correlates of natural immunity are incompletely defined due to the complex nature of *Mtb* infection and the breadth of antigenic responses elicited (35). Protection from active disease likely involves various arms of the immune system acting in synergy to control infection (6, 36, 37). This protection is seen in the approximately 90% of infected individuals able to maintain infection in a latent state. Therefore, a TB vaccine eliciting natural immunity through a resolved infection would be ideal. Live attenuated mycobacteria may protect better than either subunit or viral-vector based candidates due to their broader antigenic repertoires, which can elicit an array of immune responses mimicking natural immunity. Persistence of live attenuated mycobacteria likely drives long-lived memory immune responses through continual bacterial stimulation and an almost complete array of mycobacterial antigens. Mimicking natural infection may drive development of both conventional and unconventional T cells, natural killer cells and innate lymphocytes, and B cell responses that include antibody production. The key is to identify mutants unable to invoke pathogen-induced immunomodulatory pathways that hinder the ability of natural immunity to sterilize infection. *Mtb* is constantly exposed to various types of environmental stress during its life cycle and has become dependent on stress-response factors. SigH regulates a key stress-response module and the *ΔsigH* mutant, a poor scavenger of oxidative stress, protects against lethal TB. In this study, we sought to test the safety profile of this leading preclinical, live attenuated vaccine that is deficient in stress response that demonstrated significant protection upon lethal challenge.

It has been postulated that direct delivery of live-attenuated vaccines to the lung can elicit locally protective responses leading to a better control of infection (38-40). In addition, this route can permit co-delivery of adjuvants (41). Direct delivery of BCG to the pulmonary compartment improves protection against TB (40, 42), including in the macaque model (43). While vaccination with live attenuated mycobacterial vaccines has yielded promising results, the persistence that likely drives protective immune responses also raises safety concerns regarding the extent of attenuation. Despite the vast attenuation of the currently used vaccine, BCG cannot be given to infants with symptomatic HIV due to increased rates of dissemination. Recent data from Sharpe et al suggests that direct delivery of BCG to the lung may in fact elicit lesser pathology than the systemic intradermal route, thus alleviating concerns about the safety of mycobacterial vaccine strains delivered directly to the lung (44). More data is however required before such strains can be considered totally safe in lungs. The issues related to safety and the potential infectivity of the live-attenuated *Mtb* strains are only heightened by the choice of the pulmonary, relative to systemic delivery. Therefore, due to the persistence of the mycobacterial vaccine and the high endemicity of HIV in areas in desperate need of an efficacious TB vaccine, the attenuation of vaccine candidates must be tested in individuals who subsequently become infected with HIV and proven to be safe.

Using a macaque model of HIV co-infection (using SIV as a surrogate) (6, 24), we first aerosol vaccinated five nonhuman primates with the live mycobacterial strain *ΔsigH* and successively challenged them intravenously with pathogenic SIV. Animals were monitored throughout the study and euthanized at predetermined endpoints to determine if the bacterial vaccine strain persisted or disseminated to extrathoracic organs. Here we demonstrate that vaccinated macaques remain asymptomatic of tuberculous disease throughout the study despite severe depletion of $CD4^+$ T_{CM} cells and active replication of SIV in the lung. *Mtb*/SIV

coinfected macaques that reactivate latent TB disease were previously shown to have profound SIV-(6) and TB-associated pathology (8), contain SIV infected cells in pulmonary granulomas, and were characterized by a lack of BALT. If the mutant strain was not attenuated enough, we hypothesized that vaccinated macaques would develop symptoms comparable to *Mtb*/SIV coinfected macaques.

However, our results demonstrate that the infection of *ΔsigH*-vaccinated macaques with a high-dose of pathogenic SIV did not result in TB disease. None of these animals exhibited any clinical, microbiological, or pathological signs of disease characterized in *Mtb*/SIV coinfected macaques. A majority of *Mtb*/SIV coinfected macaques exhibit rapid reactivation of LTBI characterized by high bacterial burdens, significant extra-pulmonary dissemination, and severe granulomatous pathology (6). However, bacilli were barely detectable in the lungs and absent in extra-pulmonary tissues of *ΔsigH* vaccinated/SIV infected macaques. It is important that we report bacterial burden data generating by extensive sampling of the lung compartment, and from every animal individually, and not as a whole group, which would have averaged and masked some of the heterogeneity observed in our experiments. While we could not include a BCG/SIV co-infection experiment in our study design due to some limitations, prior data indicates that BCG infection in rhesus macaques can be reactivated by SIV co-infection (22). While the studies were performed at different times/sites and used different (intradermal vs. aerosol) routes, it appears that *ΔsigH* may be more attenuated than BCG in rhesus macaques. Another consideration is that rhesus macaques are highly susceptible to mycobacteria, and far more than Chinese cynomolgus, and yet, *ΔsigH* could not be reactivated.

Despite the significant ablation of $CD4^+$ T cells caused by SIV infection, vaccinated macaques were able to maintain control of bacterial replication. As seen in *Mtb*/SIV coinfected macaques, both $CD8^+$ T cells and B cells contribute to improved clinical outcomes. Here we demonstrate that in the absence of effective $CD4^+$ T cell responses, $CD8^+$ T cells and B cells are able to persist in the lungs and maintain control of *ΔsigH* replication after SIV infection. The current results reinforce the notion that protective immunity to *Mtb* infection is composed of multiple layers, with $CD8^+$ and B cell responses playing critical roles in the absence of $CD4^+$ responses. A key feature of reactivation of latent *Mtb* infection was the presence of SIV infected cells within pulmonary granulomas, whereas animals that retained control of infection were completely devoid of the virus. Here, we report that substantial quantities of the virus could be detected in the lungs of *ΔsigH* vaccinated animals and yet the control of mycobacterial infection did not diminish.

Differential induction of immune responses to *ΔsigH* as compared to wild-type *Mtb* demonstrates that modulation of key aspects of immunity occur in a SigH-dependent manner. BCG may also modulate some aspects of host immunity; however, it lacks the genomic segment RD1, which encompasses highly immunogenic *Mtb* antigens ESAT-6 and CFP-10, and do not induce long-lived immunity (45). Vaccination with BCG and subsequent SIV infection in cynomolgus macaques resulted in a number of animals developing tuberculous disease (22). In contrast, our results demonstrate that *ΔsigH* vaccination does not induce tuberculous disease upon acute viral challenge. The virtual absence of disease in immunocompromised macaques highlights that *ΔsigH* may be more attenuated than BCG, yet retains a complete array of *Mtb* antigens and could serve as a better anti-TB vaccine vector. It therefore appears that the inability to sequester thiol-oxidative stress in the absence of the

SigH regulon drastically attenuates the bacillus so that it is rendered nonpathogenic to such an extent that a primary immunodeficiency does not hinder immune control. It remains to be seen whether *ΔsigH* vaccinated/SIV infected animals will develop TB disease if subsequently infected with *Mtb*. This will be a telling experiment, and if protection by *ΔsigH* solely depends on B cells/iBALT then it is possible that coinfected macaques will still be protected. On the contrary, if high levels of T_{CM} $CD4^+$s and T_{CM}/T_{EM} $CD8^+$s recruited to the lungs following *ΔsigH* vaccination play a key role in mediating protection, and if such cells are depleted and unable to proliferate following SIV co-infection, then protection may be compromised.

BCG remains the most widely used vaccine in the world yet is contraindicated in a large population that are in most need an efficacious TB vaccine. Vaccination with live attenuated mycobacterial vaccines results in superlative protection as compared to subunit or viral vector-based candidates. However, live attenuated vaccines should not be used in HIV endemic areas until each candidate vaccine can be proven safe in individuals with primary immunodeficiencies. Vaccination with *ΔsigH* resulted in protection comparable to or better than natural immunity, and results from this current study demonstrate that *ΔsigH* is also safe in immunocompromised macaques. Our results suggest that live attenuated mycobacterial vaccines based on the *ΔsigH* vehicle are likely to be both safe and efficacious.

ACKNOWLEDGMENTS. We thank the TNPRC flow cytometry and confocal microscopy core facilities for their assistance. This paper is dedicated to the memory of Dr. Andrew A. Lackner, DVM, PhD, DACVP, long-serving director of the TNPRC who passed away after the submission of the initial version of the manuscript.

Author Contributions. T.W.F. carried out the experiments, analyzed the results, and participated in manuscript preparation; D.N.L. performed histopathology, analyzed results, and contributed to manuscript preparation; P.J.D. analyzed results and performed veterinary pathology; L.A.D. and K.E.R-L. provided veterinary assistance**;** S.A.K. provided funding and analyzed the results; A.A.L. performed veterinary pathology and participated in manuscript preparation; D.K. and S.M. provided funding, advised on the experimental design**,** analyzed the results, and participated in manuscript preparation. All authors reviewed the manuscript before submission

REFERENCES

1. Tonnis WF, Kersten GF, Frijlink HW, Hinrichs WL, de Boer AH, Amorij JP. Pulmonary vaccine delivery: a realistic approach? J Aerosol Med Pulm Drug Deliv. 2012;25(5):249-60. PubMed PMID: 22856876.

2. Sou T, Meeusen EN, de Veer M, Morton DA, Kaminskas LM, McIntosh MP. New developments in dry powder pulmonary vaccine delivery. Trends Biotechnol. 2011;29(4):191-8. PubMed PMID: 21255854.

3. Gopal R, Monin L, Torres D, Slight S, Mehra S, McKenna K, Fallert Junecko BA, Reinhart TA, Kolls J, Baez-Saldana R, Cruz-Lagunas A, Rodriguez-Reyna TS, Kumar NP, Tessier P, Roth J, Selman M, Becerril-Villanueva E, Baquera-Heredia J, Cumming B, Kasprowicz VO, Steyn AJ, Babu S, Kaushal D, Zuniga J, Vogl T, Rangel-Moreno J, Khader SA. S100A8/A9 Proteins Mediate Neutrophilic Inflammation and Lung Pathology during Tuberculosis. Am J Respir Crit Care Med. 2013. Epub 2013/09/21. PubMed PMID: 24047412.

4. Slight SR, Rangel-Moreno J, Gopal R, Lin Y, Fallert Junecko BA, Mehra S, Selman M, Becerril-Villanueva E, Baquera-Heredia J, Pavon L, Kaushal D, Reinhart TA, Randall TD, Khader SA. CXCR5(+) T helper cells mediate protective immunity against tuberculosis. J Clin Invest. 2013;123(2):712-26. Epub 2013/01/03. PubMed PMID: 23281399; PMCID: 3561804.

5. Kaushal D, Foreman TW, Gautam US, Alvarez X, Adekambi T, Rangel-Moreno J, Golden NA, Johnson AM, Phillips BL, Ahsan MH, Russell-Lodrigue KE, Doyle LA, Roy CJ, Didier PJ, Blanchard JL, Rengarajan J, Lackner AA, Khader SA, Mehra S. Mucosal vaccination with attenuated Mycobacterium tuberculosis induces strong central memory responses and protects against tuberculosis. Nat Commun. 2015;6:8533. PMCID: PMC4608260.

6. Foreman TW, Mehra S, LoBato DN, Malek A, Alvarez X, Golden NA, Bucsan AN, Didier PJ, Doyle-Meyers LA, Russell-Lodrigue KE, Roy CJ, Blanchard J, Kuroda MJ, Lackner AA, Chan J, Khader SA, Jacobs WR, Jr., Kaushal D. CD4+ T-cell-independent mechanisms suppress reactivation of latent tuberculosis in a macaque model of HIV coinfection. Proc Natl Acad Sci U S A. 2016. PubMed PMID: 27601645.

7. Kaushal D, Mehra S. Faithful Experimental Models of Human Infection. Mycobact Dis. 2012;2. Epub 2012/02/20. PubMed PMID: 24490123; PMCID: 3908825.

8. Kaushal D, Mehra S, Didier PJ, Lackner AA. The non-human primate model of tuberculosis. J Med Primatol. 2012;41(3):191-201. Epub 2012/03/21. PubMed PMID: 22429048.

9. Ottenhoff TH, Kaufmann SH. Vaccines against tuberculosis: where are we and where do we need to go? PLoS Pathog. 2012;8(5):e1002607. PubMed PMID: 22589713; PMCID: PMC3349743.

10. Sampson SL, Mansfield KG, Carville A, Magee DM, Quitugua T, Howerth EW, Bloom BR, Hondalus MK. Extended safety and efficacy studies of a live attenuated double leucine and pantothenate auxotroph of Mycobacterium tuberculosis as a vaccine candidate. Vaccine. 2011;29(29-30):4839-47. Epub 2011/05/10. PubMed PMID: 21549795; PMCID: 3146342.

11. Sampson SL, Dascher CC, Sambandamurthy VK, Russell RG, Jacobs WR, Jr., Bloom BR, Hondalus MK. Protection elicited by a double leucine and pantothenate auxotroph of Mycobacterium tuberculosis in guinea pigs. Infect Immun. 2004;72(5):3031-7. PubMed PMID: 15102816; PMCID: PMC387862.

12. Larsen MH, Biermann K, Chen B, Hsu T, Sambandamurthy VK, Lackner AA, Aye PP, Didier P, Huang D, Shao L, Wei H, Letvin NL, Frothingham R, Haynes BF, Chen ZW, Jacobs WR, Jr. Efficacy and safety of live attenuated persistent and rapidly cleared Mycobacterium tuberculosis vaccine candidates in non-human primates. Vaccine. 2009;27(34):4709-17. Epub 2009/06/09. PubMed PMID: 19500524; PMCID: 3512200.

13. Sambandamurthy VK, Derrick SC, Hsu T, Chen B, Larsen MH, Jalapathy KV, Chen M, Kim J, Porcelli SA, Chan J, Morris SL, Jacobs WR, Jr. Mycobacterium tuberculosis DeltaRD1 DeltapanCD: a safe and limited replicating mutant strain that protects immunocompetent and immunocompromised mice against experimental tuberculosis. Vaccine. 2006;24(37-39):6309-20. PubMed PMID: 16860907.

14. Sambandamurthy VK, Wang X, Chen B, Russell RG, Derrick S, Collins FM, Morris SL, Jacobs WR, Jr. A pantothenate auxotroph of Mycobacterium tuberculosis is highly attenuated and protects mice against tuberculosis. Nat Med. 2002;8(10):1171-4. PubMed PMID: 12219086.

15. Eibl MM, Wolf HM. Vaccination in patients with primary immune deficiency, secondary immune deficiency and autoimmunity with immune regulatory abnormalities. Immunotherapy. 2015;7(12):1273-92. PubMed PMID: 26289364.

16. McShane H, Jacobs WR, Fine PE, Reed SG, McMurray DN, Behr M, Williams A, Orme IM. BCG: myths, realities, and the need for alternative vaccine strategies. Tuberculosis (Edinb). 2012;92(3):283-8. Epub 2012/02/22. PubMed PMID: 22349516.

17. Hesseling AC, Cotton MF, Marais BJ, Gie RP, Schaaf HS, Beyers N, Fine PE, Abrams EJ, Godfrey-Faussett P, Kuhn L. BCG and HIV reconsidered: moving the research agenda forward. Vaccine. 2007;25(36):6565-8. PubMed PMID: 17659816.

18. Hesseling AC, Marais BJ, Gie RP, Schaaf HS, Fine PE, Godfrey-Faussett P, Beyers N. The risk of disseminated Bacille Calmette-Guerin (BCG) disease in HIV-infected children. Vaccine. 2007;25(1):14-8. PubMed PMID: 16959383.

19. Hesseling AC, Rabie H, Marais BJ, Manders M, Lips M, Schaaf HS, Gie RP, Cotton MF, van Helden PD, Warren RM, Beyers N. Bacille Calmette-Guerin vaccine-induced disease in HIV-infected and HIV-uninfected children. Clin Infect Dis. 2006;42(4):548-58. PubMed PMID: 16421800.

20. Spertini F, Audran R, Chakour R, Karoui O, Steiner-Monard V, Thierry AC, Mayor CE, Rettby N, Jaton K, Vallotton L, Lazor-Blanchet C, Doce J, Puentes E, Marinova D, Aguilo N, Martin C. Safety of human immunisation with a live-attenuated Mycobacterium tuberculosis vaccine: a randomised, double-blind, controlled phase I trial. Lancet Respir Med. 2015;3(12):953-62. PubMed PMID: 26598141.

21. Mehra S, Golden NA, Stuckey K, Didier PJ, Doyle LA, Russell-Lodrigue KE, Sugimoto C, Hasegawa A, Sivasubramani SK, Roy CJ, Alvarez X, Kuroda MJ, Blanchard JL, Lackner AA, Kaushal D. The Mycobacterium tuberculosis stress response factor SigH is required for bacterial burden as well as immunopathology in primate lungs. J Infect Dis. 2012;205(8):1203-13. Epub 2012/03/10. PubMed PMID: 22402035; PMCID: 3308902.

22. Chen ZW, Zhou D, Chalifoux L, Lee-Parritz D, Mansfield K, Lord CI, Letvin NL. Disseminated granulomatous disease in a simian immunodeficiency virus- and bacille Calmette-Guerin-infected rhesus monkey. AIDS. 1997;11(2):266-7. PubMed PMID: 9030386.

23. Mehra S, Pahar B, Dutta NK, Conerly CN, Philippi-Falkenstein K, Alvarez X, Kaushal D. Transcriptional reprogramming in nonhuman primate (rhesus macaque) tuberculosis granulomas. PLoS One. 2010;5(8):e12266. Epub 2010/09/09. PubMed PMID: 20824205; PMCID: 2930844.

24. Mehra S, Golden NA, Dutta NK, Midkiff CC, Alvarez X, Doyle LA, Asher M, Russell-Lodrigue K, Monjure C, Roy CJ, Blanchard JL, Didier PJ, Veazey RS, Lackner AA, Kaushal D. Reactivation of latent tuberculosis in rhesus macaques by coinfection with simian immunodeficiency virus. J Med Primatol. 2011;40(4):233-43. Epub 2011/07/26. PubMed PMID: 21781131; PMCID: 3227019.

25. Mehra S, Foreman TW, Didier PJ, Ahsan MH, Hudock TA, Kissee R, Golden NA, Gautam US, Johnson AM, Alvarez X, Russell-Lodrigue KE, Doyle LA, Roy CJ, Niu T, Blanchard JL, Khader SA, Lackner AA, Sherman DR, Kaushal D. The DosR Regulon Modulates Adaptive Immunity and is Essential for M. tuberculosis Persistence. Am J Respir Crit Care Med. 2015. PubMed PMID: 25730547.

26. Dutta NK, Mehra S, Didier PJ, Roy CJ, Doyle LA, Alvarez X, Ratterree M, Be NA, Lamichhane G, Jain SK, Lacey MR, Lackner AA, Kaushal D. Genetic requirements for the survival of tubercle bacilli in primates. J Infect Dis. 2010;201(11):1743-52. Epub 2010/04/17. PubMed PMID: 20394526; PMCID: 2862080.

27. Phillips BL, Mehra S, Ahsan MH, Selman M, Khader SA, Kaushal D. LAG3 expression in active Mycobacterium tuberculosis infections. Am J Pathol. 2015;185(3):820-33. PubMed PMID: 25549835; PMCID: 4348466.

28. Mothe BR, Lindestam Arlehamn CS, Dow C, Dillon MB, Wiseman RW, Bohn P, Karl J, Golden NA, Gilpin T, Foreman TW, Rodgers MA, Mehra S, Scriba TJ, Flynn JL, Kaushal D, O'Connor DH, Sette A. The TB-specific CD4 T cell immune repertoire in both cynomolgus and rhesus macaques largely overlap with humans. Tuberculosis (Edinb). 2015. PubMed PMID: 26526557.

29. Levine DM, Dutta NK, Eckels J, Scanga C, Stein C, Mehra S, Kaushal D, Karakousis PC, Salamon H. A tuberculosis ontology for host systems biology. Tuberculosis (Edinb). 2015. PubMed PMID: 26190839.

30. Kaushal D, Schroeder BG, Tyagi S, Yoshimatsu T, Scott C, Ko C, Carpenter L, Mehrotra J, Manabe YC, Fleischmann RD, Bishai WR. Reduced immunopathology and mortality despite tissue persistence in a Mycobacterium tuberculosis mutant lacking alternative sigma factor, SigH. Proc Natl Acad Sci U S A. 2002;99(12):8330-5. Epub 2002/06/13. PubMed PMID: 12060776; PMCID: 123067.

31. Mehra S, Kaushal D. Functional genomics reveals extended roles of the Mycobacterium tuberculosis stress response factor sigmaH. J Bacteriol. 2009;191(12):3965-80. Epub 2009/04/21. PubMed PMID: 19376862; PMCID: 2698404.

32. Darrah PA, Bolton DL, Lackner AA, Kaushal D, Aye PP, Mehra S, Blanchard JL, Didier PJ, Roy CJ, Rao SS, Hokey DA, Scanga CA, Sizemore DR, Sadoff JC, Roederer M, Seder RA. Aerosol Vaccination with AERAS-402 Elicits Robust Cellular Immune Responses in the Lungs of Rhesus Macaques but Fails To Protect against High-Dose Mycobacterium tuberculosis Challenge. J Immunol. 2014. Epub 2014/07/16. PubMed PMID: 25024382.

33. Mehra S, Alvarez X, Didier PJ, Doyle LA, Blanchard JL, Lackner AA, Kaushal D. Granuloma correlates of protection against tuberculosis and mechanisms of immune modulation by Mycobacterium tuberculosis. J Infect Dis. 2013;207(7):1115-27. Epub 2012/12/21. PubMed PMID: 23255564; PMCID: 3633457.

34. Li Q, Skinner PJ, Duan L, Haase AT. A technique to simultaneously visualize virus-specific CD8+ T cells and virus-infected cells in situ. Journal of visualized experiments : JoVE. 2009(30). PubMed PMID: 19684569; PMCID: 3149910.

35. Fletcher HA. Correlates of immune protection from tuberculosis. Current molecular medicine. 2007;7(3):319-25. PubMed PMID: 17504116.

36. Woodworth JS, Behar SM. Mycobacterium tuberculosis-specific CD8+ T cells and their role in immunity. Crit Rev Immunol. 2006;26(4):317-52. Epub 2006/11/01. PubMed PMID: 17073557; PMCID: 3134450.

37. Lu LL, Chung AW, Rosebrock TR, Ghebremichael M, Yu WH, Grace PS, Schoen MK, Tafesse F, Martin C, Leung V, Mahan AE, Sips M, Kumar MP, Tedesco J, Robinson H, Tkachenko E, Draghi M, Freedberg KJ, Streeck H, Suscovich TJ, Lauffenburger DA, Restrepo BI, Day C, Fortune SM, Alter G. A Functional Role for Antibodies in Tuberculosis. Cell. 2016. PubMed PMID: 27667685.

38. Lu D, Hickey AJ. Pulmonary vaccine delivery. Expert Rev Vaccines. 2007;6(2):213-26. Epub 2007/04/06. PubMed PMID: 17408371.

39. Fiegel J, Garcia-Contreras L, Thomas M, VerBerkmoes J, Elbert K, Hickey A, Edwards D. Preparation and in vivo evaluation of a dry powder for inhalation of capreomycin. Pharm Res. 2008;25(4):805-11. Epub 2007/07/28. PubMed PMID: 17657592.

40. Garcia-Contreras L, Wong YL, Muttil P, Padilla D, Sadoff J, Derousse J, Germishuizen WA, Goonesekera S, Elbert K, Bloom BR, Miller R, Fourie PB, Hickey A, Edwards D. Immunization by a bacterial aerosol. Proc Natl Acad Sci U S A. 2008;105(12):4656-60. Epub 2008/03/18. PubMed PMID: 18344320; PMCID: 2290758.

41. Manjaly Thomas ZR, McShane H. Aerosol immunisation for TB: matching route of vaccination to route of infection. Trans R Soc Trop Med Hyg. 2015;109(3):175-81. PubMed PMID: 25636950; PMCID: 4321022.

42. Derrick SC, Kolibab K, Yang A, Morris SL. Intranasal administration of Mycobacterium bovis BCG induces superior protection against aerosol infection with Mycobacterium tuberculosis in mice. Clinical and vaccine immunology : CVI. 2014;21(10):1443-51. PubMed PMID: 25143340; PMCID: PMC4266354.

43. Barclay WR, Busey WM, Dalgard DW, Good RC, Janicki BW, Kasik JE, Ribi E, Ulrich CE, Wolinsky E. Protection of monkeys against airborne tuberculosis by aerosol vaccination with bacillus Calmette-Guerin. Am Rev Respir Dis. 1973;107(3):351-8. PubMed PMID: 4632221.

44. Sharpe S, White A, Sarfas C, Sibley L, Gleeson F, McIntyre A, Basaraba R, Clark S, Hall G, Rayner E, Williams A, Marsh PD, Dennis M. Alternative BCG delivery strategies improve protection against Mycobacterium tuberculosis in non-human primates: Protection associated with mycobacterial antigen-specific CD4 effector memory T-cell populations. Tuberculosis (Edinb). 2016;101:174-90. PubMed PMID: 27865390; PMCID: PMC5120991.

45. Andersen P, Doherty TM. The success and failure of BCG - implications for a novel tuberculosis vaccine. Nature Reviews Microbiology. 2005;3(8):656-62. PubMed PMID: WOS:000230879700016.

CHAPTER 7: DISCUSSION, LIMITATIONS, AND FUTURE DIRECTIONS

Efforts to understand TB pathogenesis, and thus to develop more effective interventional strategies, are likely to continue for decades. Even with the progress that has been made in the last several hundreds of years in our understanding of Mycobacterial diseases, it truly remains the prime example of the evolutionary arms race between host and pathogen. And while we most strongly associated *Mtb* with Robert Koch's discovery in the 1800's, some have suggested that that the genus may have originated as long as 150 million years ago (Barberis et al., 2017). With that in mind, and given the number of other mycobacterial diseases that cause both human and animal disease, it is unlikely that it will be eliminated overnight. However, with the advent of new and emerging approaches to vaccine and drug development, in combination with ever-increasing understanding of pathophysiologic mechanisms at the host and pathogen level, we may get closer to a world free of *Mycobacterium tuberculosis*.

Part of moving towards that goal, however, is to more accurately understand the true pathologic differences in infected animals and humans. And prior to this point, we really have not progressed much beyond the early days of TB in that regard. The development and use of this histopathologic scoring system—in combination with the approaches already established for gross and imaging-based assessment of pathologic burden—may help to gain a better understanding of the host response to disease burden, and may elucidate

mechanisms heretofore not understood in regards to disease progression. While likely that adjustments will need to be made, this scoring system represents an important first step in establishing a standardized approach for evaluation of pulmonary pathology in the NHP model of tuberculosis.

Sharpe et al. (2017) in an aerosol challenge of TB in Mauritian cynomolgus macaques used MRI assessment of TB burden as by (Sharpe et al., 2016) and assessments of gross pathology as by (Lin et al., 2009) but largely limited selection of samples histopathologic examination to grossly visible lesions. This approach has been widely used by many researchers in the examination of pulmonary pathology in TB, and may be part of the contributing factor leading to prevention of distinguishing differentiating lesions. Part of the benefit of our study approach is that the TNPRC employs a wider standardized stereologic sampling approach which ensures that more of the lung is routinely sampled, which allowed for a wider portion of the pulmonary parenchyma to be examined in this retrospective study. This is particularly important as the pattern of pulmonary TB can differ widely between individuals. Even with MRI as an adjunctive method for assessment of disease burden, the limit of detection for pulmonary nodules varies and depends on several factors—including the capacity of a patient to hold their breath, something not feasible for veterinary patients. While the sensitivity of MRI machines is improving, the estimates of detection based on one study reported the overall sensitivity for detection of pulmonary nodules (in humans) at 57.1% for nodules ≤4mm, 75% for nodules >4-6mm, 87.5% for nodules >6-8mm and 100% for nodules >8mm (Cieszanowski et al., 2016). Considering that many of the observed histologic granulomas in our animals were less than 1 mm, they would be considered well below these limits of MRI detection, and could lead to incomplete information if these

methods were the sole or main parameters used to determine disease burden and classification; histopathologic assessment is thus an important component to any NHP TB research project if the goal is to gain a complete picture of disease. Indeed, in the same study by Sharpe et al. (2017) they noted that in one of their animals, "an atypical combination of mature mild lesions with very numerous small miliary lesions were noted." Similarly, loose nodular aggregates of infected macrophages have been described in early stages of TB in other studies prior to development of caseous granulomas (Lin et al., 2006). It is these small lesions, many of which will only be visible microscopically, that may be missed with other methods of surveillance, and that may provide important keys to understand disease progression. It is also important to note that in many of the studies in which these gross and image based scoring systems have been applied to distinguish between disease burden and progression in TB infected macaques, they have most often been done in cynomolgus macaques. As mentioned earlier, Rhesus macaques are more sensitive to *Mtb* infection than either Chinese or Mauritius origin cynomolgus macaques, with more rapid onsent of clinical signs and disease progression (Foreman et al., 2017; Gardner and Luciw, 2008; Kaushal et al., 2012; Maiello et al., 2018; O'Toole, 2010), and it may thus be of even more importance to account for the presence of smaller granulomas in experimentally-infected Rhesus macaques as these granulomas may represent earlier manifestations of disease (Lin et al., 2006).

Because so much NHP tuberculosis work is done in cynomolgus macaques, it would be ideal to either acquire slides from previous studies for application of this scoring system, or to have veterinary pathologists working with cynomolgus macaques being used for TB studies apply these scoring paramaters to their own work to determine if this system remains

validated for use in that species, or if there are parameters that must be adjusted for its application.

One area not explored in this work that is ripe for future exploration would be a systematic approach to the granuloma burden in *Mtb* infected animals. In these studies, with the exception of the Hudock et al., 2017, paper, granulomas were merely counted as present or absent as the focus of this work was truly on the non-granulomatous pulmonary pathology. However, in the course of scoring system development, in addition to my numerous other collaborative activities within the lab, several observations in regards to TB granulomas have become clear. Rhesus macaques experimentally infected with *Mtb* truly display a range of granulomatous pathology, ranging from the classic well-developed caseous and even cavitating granulomas, to solid-type granulomas characterized by nodular accumulations of epithelioid macrophages, to confluent aggregates of macrophages and lymphocytes with little clear structure (Gormus et al., 2004; Hudock et al., 2017; Lin et al., 2006; Scanga and Flynn, 2014). There is opportunity for future studies, still utilizing retrospective samples to characterize granuloma subtype and percentage of lung sections affected, which could best be accomplished with the aid of specialized digital imaging software. Immunohistochemistry for cytokeratin expression as in (van Leeuwen et al., 2015) and immunofluorescence to evaluate differential expression of tryptophan and IDO in these various granuloma subtypes may help to gain a more complete picture of the role that granuloma subtypes may play in disease progression. Prospective studies could also be utilized to address differential cytokine expression and bacterial burden within granulomas from animals in different disease categories to gain more information about the pathologic basis of changes associated with the granuloma.

Previous work has demonstrated differential cytokine expression in granulomas over time in Rhesus macaques in early and late stages of TB infection, with higher expression of pro-inflammatory cytokines including IL-6, TNF-alpha, JAK, STAT and C-C/C-X-C chemokines in animals euthanized 4 weeks following *Mtb* infection in comparison to animals euthanized at 13 weeks following infection (Mehra et al., 2010). Animals selected for the scoring system development and validation component of this work were euthanized between 8.7 and 25.9 weeks following *Mtb* infection. However, it would be interesting to assess the cytokine expression in these animals to determine whether systemic or local perturbations in pro-inflammatory cytokines may be related to the development of vascular associated pathology in particular.

As with the majority of NHP studies, one of the greatest challenges of these studies is the limitation of sample size. However, p values were strongly significant for all examined categories despite these low sample sizes, and application more broadly, with multi-institutional adoption could help to increase the strength and validity of the associations. The limitations of sample size were felt most acutely in regards to teasing out the additive effects of SIV infection on some of the pathology parameters in development and validation of the wider scoring system. While it was clear that SIV seemed to be having an effect, that effect was obscured when viewed in the predictive model which struggled to distinguish between co-infected LTBI-SIV animals and ATBI animals. Practically, this distinction would be unlikely to be significant as it is likely that researchers and pathologists will know whether or not an animal is co-infected, but inclusion of more animals would likely help to make those distinctions more clear and increase the predictive strength of the model from an epidemiologic standpoint.

Because drug resistance is such a vital concern with tuberculosis currently, with the emergence of both multi- and extremely drug-resistant strains—and concern for untreatable tuberculosis on the rise (Centers for Disease Control and Prevention (CDC), 2009; Dheda et al., 2014), it would be useful to examine the effect of drug treatment on pulmonary pathology scores in these animals. We have already used a similar scoring system approach with success in a previous study looking at a potential vaccine candidate (Foreman et al., 2017b), which illustrates its usefulness in this context. Given the failure of the currently used BCG vaccine to control and prevent spread of TB worldwide, with the most recent estimates from the World Health Organization of one quarter of the world's population infected with TB and 10 million new cases in 2017 alone, our collective need for development and implementation of safe and effective control strategies for this disease, founded on a more holistic understanding of its pathophysiology, must remain a paramount concern.

REFERENCES

Barberis, I., Bragazzi, N.L., Galluzzo, L., and Martini, M. (2017). The history of tuberculosis: from the first historical records to the isolation of Koch's bacillus. J. Prev. Med. Hyg. *58*, E9–E12.

Centers for Disease Control and Prevention (CDC) (2009). Plan to combat extensively drug-resistant tuberculosis: recommendations of the Federal Tuberculosis Task Force. MMWR Recomm. Rep. Morb. Mortal. Wkly. Rep. Recomm. Rep. *58*, 1–43.

Cieszanowski, A., Lisowska, A., Dabrowska, M., Korczynski, P., Zukowska, M., Grudzinski, I.P., Pacho, R., Rowinski, O., and Krenke, R. (2016). MR Imaging of Pulmonary Nodules: Detection Rate and Accuracy of Size Estimation in Comparison to Computed Tomography. PLoS ONE *11*.

Dheda, K., Gumbo, T., Gandhi, N.R., Murray, M., Theron, G., Udwadia, Z., Migliori, G.B., and Warren, R. (2014). Global control of tuberculosis: from extensively drug-resistant to untreatable tuberculosis. Lancet Respir. Med. *2*, 321–338.

Foreman, T.W., Mehra, S., Lackner, A.A., and Kaushal, D. (2017a). Translational Research in the Nonhuman Primate Model of Tuberculosis. ILAR J. *58*, 151–159.

Foreman, T.W., Veatch, A.V., LoBato, D.N., Didier, P.J., Doyle-Meyers, L.A., Russell-Lodrigue, K.E., Lackner, A.A., Kousoulas, K.G., Khader, S.A., Kaushal, D., et al. (2017b). Nonpathologic Infection of Macaques by an Attenuated Mycobacterial Vaccine Is Not Reactivated in the Setting of HIV Co-Infection. Am. J. Pathol. *187*, 2811–2820.

Gardner, M.B., and Luciw, P.A. (2008). Macaque Models of Human Infectious Disease. ILAR J. *49*, 220–255.

Gormus, B.J., Blanchard, J.L., Alvarez, X.H., and Didier, P.J. (2004). Evidence for a rhesus monkey model of asymptomatic tuberculosis. J. Med. Primatol. *33*, 134–145.

Hudock, T.A., Foreman, T.W., Bandyopadhyay, N., Gautam, U.S., Veatch, A.V., LoBato, D.N., Gentry, K.M., Golden, N.A., Cavigli, A., Mueller, M., et al. (2017). Hypoxia Sensing and Persistence Genes Are Expressed during the Intragranulomatous Survival of Mycobacterium tuberculosis. Am. J. Respir. Cell Mol. Biol. *56*, 637–647.

Kaushal, D., Mehra, S., Didier, P.J., and Lackner, A.A. (2012). The non-human primate model of tuberculosis. J. Med. Primatol. *41*, 191–201.

van Leeuwen, L.M., van der Sar, A.M., and Bitter, W. (2015). Animal Models of Tuberculosis: Zebrafish. Cold Spring Harb. Perspect. Med. *5*.

Lin, P.L., Pawar, S., Myers, A., Pegu, A., Fuhrman, C., Reinhart, T.A., Capuano, S.V., Klein, E., and Flynn, J.L. (2006). Early events in Mycobacterium tuberculosis infection in cynomolgus macaques. Infect. Immun. *74*, 3790–3803.

Lin, P.L., Rodgers, M., Smith, L., Bigbee, M., Myers, A., Bigbee, C., Chiosea, I., Capuano, S.V., Fuhrman, C., Klein, E., et al. (2009). Quantitative Comparison of Active and Latent Tuberculosis in the Cynomolgus Macaque Model. Infect. Immun. *77*, 4631–4642.

Mehra, S., Pahar, B., Dutta, N.K., Conerly, C.N., Philippi-Falkenstein, K., Alvarez, X., and Kaushal, D. (2010). Transcriptional reprogramming in nonhuman primate (rhesus macaque) tuberculosis granulomas. PloS One *5*, e12266.

O'Toole, R. (2010). Chapter 3 - Experimental Models Used to Study Human Tuberculosis. In Advances in Applied Microbiology, (Academic Press), pp. 75–89.

Scanga, C.A., and Flynn, J.L. (2014). Modeling Tuberculosis in Nonhuman Primates. Cold Spring Harb. Perspect. Med. *4*.

Sharpe, S., White, A., Gleeson, F., McIntyre, A., Smyth, D., Clark, S., Sarfas, C., Laddy, D., Rayner, E., Hall, G., et al. (2016). Ultra low dose aerosol challenge with Mycobacterium tuberculosis leads to divergent outcomes in rhesus and cynomolgus macaques. Tuberculosis *96*, 1–12.

Sharpe, S.A., White, A.D., Sibley, L., Gleeson, F., Hall, G.A., Basaraba, R.J., McIntyre, A., Clark, S.O., Gooch, K., Marsh, P.D., et al. (2017). An aerosol challenge model of tuberculosis in Mauritian cynomolgus macaques. PloS One *12*, e0171906.